COMPUTATIONAL MODELING AND SIMULATION OF THROMBUS FORMATION

A Dissertation

Presented to the Faculty of the Graduate School

of Cornell University

in Partial Fulfillment of the Requirements for the Degree of

Doctor of Philosophy

by

Deyan Luan

August 2009

COMPUTATIONAL MODELING AND SIMULATION OF THROMBUS FORMATION

Deyan Luan, Ph.D.

Cornell University 2009

Thrombosis is a serious medical complication because excessive thrombus formation could lead to obstruction of blood vessels, resulting in tissue ischemia or death. This study is aimed to understand the cell-biology and biophysics, at the molecular level, of thrombosis in a blood vessel. We first review the biology underlying thrombosis and the previous mathematical models of thrombus formation (Chapter 1). In Chapter 2, mathematical modeling and sensitivity analysis were used to explore the mechanistic model of thrombus formation; the results support our working hypothesis that computationally derived points of fragility of human relevant cascades could be used as a rational basis for target selection despite model uncertainty. Chapter 3 focuses on the impact of parametric sampling strategies of Monte-Carlo sensitivity analysis and network structural uncertainty upon the assessment of the qualitative importance of molecular interactions in the coagulation network. While parametric uncertainty can be partially overcome by sampling feasible parameter regions using one of several strategies, structural uncertainty remains a critical determinant of our ability to classify mechanisms as fragile or robust in networks relevant to human health. The mathematical model was further extended to describe platelet activation by other agonists besides thrombin and the intrinsic pathway in Chapter 4. An ensemble of probable parameter sets were estimated using nine experimental data sets from a cell-based model and then used to

predict the thrombin generation in experiments using patient-derived plasma for coronary artery and hemophilia A patients. In Chapter 5, analysis of the sensitivity results discloses that the intrinsic protease factor XI could be an excellent therapeutic target for thrombosis treatment with the advantage of not affecting hemostasis. Chapter 6 describes the effect of flow on the initiation of arterial clotting under conditions of exposed tissue factor (TF). Thresholds in shear rates or TF patch sizes were observed for the initiation of clot formation; the balance between the generation of active factors and the removal of those factors by flow was possibly the reason for the threshold phenomena.

BIOGRAPHICAL SKETCH

Deyan Luan graduated from Beijing University of Aeronautics and Astronautics, School of Materials Science and Engineering, Beijing, the People's Republic of China, in 2002 (B.Eng.). After that, she was offered a scholarship for studying in the National University of Singapore (NUS). She graduated for the School of Chemical and Biomolecular Engineering, NUS, Singapore, with a Master's degree in 2004. She worked as a QA/MSL (Quality Assurance/Materials Science Lab) Engineer at Hitachi Global Storage Technologies (HitachiGST) in Singapore before she joined the PhD program in the School of Chemical and Biomolecular Engineering at at Cornell University in August 2005. Her PhD research focused on the computational modeling and simulation of thrombus formation.

This document is dedicated to my beloved family.

ACKNOWLEDGEMENTS

I would like to express my gratitude to all those who gave me the possibility to complete this dissertation. I want to thank Professor Jeffrey D. Varner, who is my advisor, for his continuous guidance during past four years. He is very kind, patient, encouraging, open-minded and has great passion for science. I am obliged to Professor Yong L. Joo, who is my co-advisor, for his help, stimulating suggestions and encouragement in all the time. I am grateful to Professor William L. Olbricht for his enlightening discussions, and for serving as one of my committee members.

Special appreciations to the entire Varner and Joo group members, especially Dr. Sang Ok Song, Satyaprakash Nayak, Tom Mansell, Ryan Tasseff, Anirikh Chakrabarti, Michael Zai and Damien Kudela, for the timely and instructive comments, and for broadening my research horizons; to all support staff, especially Shelby Clark-Shevalier and Carol Casler, for their help which allow me to complete this project on schedule.

In addition to the technical assistance above, I received equally important assistance from family and friends. My husband, Xiongwen (David) Lou, provided on-going support throughout the process of my PhD study; my parents, Mingyuan Luan and Lizhi Shao, instilled in me, from an early age, the desire and skills to obtain the advanced degrees.

Lastly but not the least, I would like to thank the Cornell University, the Weill Cornell Medical Collage for the research scholarships awarded to me.

TABLE OF CONTENTS

LIST OF TABLES

LIST OF FIGURES

CHAPTER 1

INTRODUCTION

Cardiovascular diseases are predicted as the leading cause of death for the future two decades by the World Health Organization in 2008 [1]. Central to cardiovascular diseases is Arteriosclerosis, the thickening or hardening of the arteries. Arteriosclerosis is caused by aging, high blood pressure, cigarette smoke, and high cholesterol levels. One particular kind of arteriosclerosis that contributes to cardiovascular diseases is Atherosclerosis, which is characterized by a buildup of plaque within the arteries. Plaque, which is formed from fatty substances, cholesterol, cellular waste, calcium, and fibrin, may partially or totally block blood flow through arteries leading to chronic conditions, e.g., cardiovascular diseases. However, plaques are also linked with acute events such as Myocardial Infarction (MI) or Ischemic Stroke (IS); plaques become fragile and can rupture leading to clot or thrombus formation [2, 3, 4].

MI is a thrombotic event triggered by atherosclerosis plaque rupture. The exposed procoagulant materials, e.g. collagen, tissue factor (TF), etc, following plaque rupture lead to the activation of platelets and the formation of thrombin, resulting in thrombosis or thrombus formation. Thrombosis is a serious medical complication because excessive thrombus formation can lead to obstruction of blood vessels, resulting in tissue ischemia or death. In addition to occluding the blood vessel where it was formed, it is also possible for a thrombus to break free (embolize) and lodge somewhere downstream in the microcirculation, the most deleterious possibility being a brain infarction if it finds its way into a cerebral artery or being a heart attack if it blocks a coronary artery. The *specific aims* of this study are to understand the cell-biology and biophysics, at the molecular

level, of thrombosis in a blood vessel. In particular, we will focus upon the processes underlying thrombus formation in ruptured plaques: thrombin generation, platelet adhesion, activation and aggregation in the absence or presence of an arterial flow field. We will employ tools from Systems Biology, Computational Fluid Dynamics (CFD) and High-Performance Computing (HPC) to construct and validate a *first-principles* mathematical model of disease progression which can be employed in a treatment planning context to improve the effectiveness of current therapies in community practice, to better understand primary and secondary prevention issues and to *computationally screen* novel therapeutic strategies at a molecular level. It is hoped that this will one day lead to improved computational design strategies for understanding the mechanisms and the development of new drugs for thrombosis.

1.1 Thrombus formation

Although unraveling the many complex and intertwined chemical and biological processes that lead to thrombus formation is a continuing challenge for modern medical research, the primary factors governing thrombosis were identified nearly 150 years ago by the German pathologist Rudolf Virchow (1821-1902) [5]. Decades following his death, a consensus was reached proposing that thrombosis is the result of "abnormalities of blood constituents", "abnormalities of blood vessel wall", and "abnormalities of blood flow", which are the three elements of the well-know "Virchow's triad" [6]. The contributions of each element of the triad to the thrombotic process are described below.

1.1.1 The constitution of the blood

The constituents of the blood are many and varied, but soluble coagulation factors, such as factor I (fI or fibrinogen) and factor II (fII or prothrombin), and cells, such as platelets, are clearly important [6]. The blood elements primarily responsible for coagulation are the coagulation factors, typically identified by Roman numerals I – XIII. Most of the coagulation factors are synthesized in the liver. In addition, factor VIII (fVIII) is synthesized in a large number of other tissue. Other important factors in the coagulation process include prothrombin, factor VII (fVII), factor IX (fIX), factor X (fX) and factor XI (fXI); these proteins are synthesized in precursor form, which are biochemically termed as zymogens. These zymogens are precursor enzymes that are converted to active enzymes by the cleavage of one or in some instances two peptide bonds during blood coagulation. There are two protein cofactors, factor V (fV) and fVIII, that also play an important role in blood coagulation by binding to activated platelets surface and forming a focal point for the organization of certain protein complexes. The corresponding active forms of these proteins are denoted as FVa, FVIIa, FVIIIa, FIXa, FXa and FXIa, respectively.

Blood coagulation cascades

Clotting can be achieved via either of two coagulation cascades, or via platelet aggregation and deposition. However, all three feed into and depend upon one another, meaning none usually occurs independent of the others. What follows is a brief overview of these complex processes. More detail can be obtained from any basic physiology text, e.g. Guyton & Hall [7], and the references therein. Upon plaque ruptures, the exposed collagen is one of the most thrombogenic

materials because it supports platelet adhesion and it is a strong platelet agonist. The collagen-activated platelet membranes expose receptors which bind circulating fibrinogen to their surfaces. An aggregation of platelets and fibrinogen build up to form a soft plug. This is often called primary hemostasis, which is normally short lived. If flow is allowed to increase, the soft plug could be sheared from the injured surface, possibly creating emboli. Secondary hemostasis or blood coagulation is responsible for stabilizing the soft clot and maintaining vasoconstriction. The soft plug is solidified through complex interactions that bring about the generation of thrombin and the formation of fibrin from fibrinogen. Thrombin cleaves fibrinogen into fibrin monomers and these fibrin monomers polymerized to form fibrin mesh on and between the soft plug, resulting in the formation of the stable fibrin clot [8, 9].

The intrinsic and the extrinsic pathways of coagulation are involved in the generation of thrombin; each is activated by a different trigger, although they share many steps in the course of thrombin generation. It is generally believed that the extrinsic pathway is the main mechanism *in vivo*. The extrinsic blood coagulation cascade is thought to be triggered when tissue factor (TF) is exposed as a consequence of vascular damage or plaque rupture. TF activates fVII to activated FVIIa, and with which it forms an enzymatic complex TF-FVIIa. TF-FVIIa complex activates fX and fIX. FIXa in complex with its cofactor, FVIIIa, activates fX at an $\approx$50-fold higher rate than the factor TF-FVIIa complex [10]. FXa and FVa in turn form a complex on the surface of activated platelets which converts prothrombin (fII) to thrombin (FIIa). The terminal protease thrombin plays a key role in the activation of upstream factors and platelets [8, 9, 11]. The intrinsic or contact pathway of coagulation consists of a group of plasma proteins which are activated by interaction with exogenous negatively charged

surfaces such as glass or kaolin. This pathway has been described as a series of enzymatic reactions which starts with the formation of activated factor XIIa (FXIIa). FXIIa activates fXI to FXIa, which could cleave fIX to FIXa. The intrinsic pathway of coagulation joins with the extrinsic at this point. The reactions of this pathway have been well characterized *in vitro*; however, the physiologic activator of fXII has not been identified. Furthermore, individuals with fXII deficiencies have developed no significant bleeding diathesis; however, individuals have been identified with fXI deficiencies do have significant episodes of bleeding complications associated with surgical challenges [12]. Some investigators have reported that FXIa could also be activated by thrombin as complement to the extrinsic pathway when the extrinsic pathway is shut down by inhibitors [13, 14, 15, 16, 17, 18, 19].

To maintain normal hemostasis, it is necessary to have the appropriate balance between pro- and anti-coagulant constituents in the blood. There are three major anti-coagulants in the blood that sever as control points in the cascade to inhibit thrombin formation. Tissue Factor Pathway Inhibitor (TFPI) down-regulates FXa formation catalyzed by TF-FVIIa by sequestering free FXa and the TF-FVIIa-FXa complex. Antithrombin III (ATIII) neutralizes all serine proteases generated during the coagulation response, making it perhaps the most powerful control element in the cascade. Thrombin itself plays an inadvertent role in its own inhibition by binding to thrombomodulin which is constitutively expressed on normal vasculature. The binding of thrombin with thrombomodulin in turn activates Protein C (PC) to activated PC (APC) which attenuates the coagulation response by the proteolytic cleavage of fV/FVa and fVIII/FVIIIa [20, 21, 22, 23].

Hemophiliacs

Defects in the balance of blood constituents can result in either thrombotic of bleeding tendencies. Some genetic deficiencies in the sex-linked, X chromosomes may lower blood plasma clotting factor levels of coagulation factors needed for a normal clotting process and result in bleeding disorders [24]. Hemophilia is a group of hereditary genetic disorders that impair the body's ability to control blood clotting or coagulation. In its most common forms, hemophilia A and B are congenital bleeding disorders caused by deficiencies of the coagulation factors fVIII and fIX, respectively [24]. Hemophilia A occurs in about 1 in 5,000-10,000 male births, while hemophilia B occurs at about 1 in about 35,000-50,000 male births [25]. Hemophilia C, caused by deficiency in fXI, is a mild form of hemophilia affecting both sexes. In the USA it is thought to affect 1 in 100,000 of the adult population, making it 10% as common as hemophilia A [26]. The concept of mild bleeding disorders has evolved in contrast to severe hemophilia A and B to indicate less severe disorders [27]. A hemophilia patient do not bleed more intensely than a normal person, but for a much longer amount of time. In severe hemophiliacs even a minor injury could result in blood loss lasting days, weeks, or not ever healing completely. The critical risk here is with normally small injuries which, due to missing coagulation factors, take long times to heal. In areas such as the brain or inside joints this can be fatal or permanently debilitating. The bleeding with external injury is normal, but incidence of late re-bleeding and internal bleeding is increased, especially into muscles, joints, or bleeding into closed spaces. Major complications include hemarthrosis, hemorrhage, gastrointestinal bleeding, and menorrhagia.

Though there is no cure for hemophilia, it can be controlled with regu-

lar infusions of the deficient clotting factor, i.e. fVIII in hemophilia A or fIX in hemophilia B. Replacement therapy markedly improves the management of bleeding of most patients with hemophilia. However, fVIII and fIX inhibitors have developed in 18-32% and 2-3% of hemophiliacs A and B in response to fVIII and fIX, respectively [28] and those inhibitors make the subsequent management of patient, using coagulation factor concentrates, difficult. In the 1980s, activated prothrombin complex concentrates (APCCs) from pooled plasma were developed for hemophiliacs with inhibitors, assuring 'fVIII bypassing activity' [29, 30]. However, APCCs induce disseminated intravascular coagulation syndromes or acute MI [31]. Recently, recombinant factor VIIa (rFVIIa) was developed as a new bypassing agent, and its clinical efficacy and safety have been established [32, 33]. However, because of its short half-life, therapy with rFVIIa requires frequent administration (at intervals of 2-3 h) to achieve hemostasis [28]. Therefore, the search for a novel therapeutic agent for hemophilia with inhibitors is still ongoing.

Fibrinolysis

Fibrinolysis is the process wherein a fibrin clot, the product of coagulation, is broken down. The set of enzymatic reactions that constitute fibrinolysis is initiated when thrombin and fibrin, formed during coagulation, activate endothelial cells resulting in enhanced production of tissue plasminogen activator (tPA) or urokinase-like plasminogen activator (uPA) [9]. tPA and uPA catalyze the transformation of plasminogen into the active form plasmin, which cuts the fibrin mesh at various places, leading to the production of circulating fragments that are cleared by other proteases or by the kidney and liver. Plasminogen con-

tains secondary structure motifs known as kringles, which bind specifically to lysine and arginine residues on fibrin(ogen). When converted from plasminogen into plasmin, it functions as a serine protease, cutting C-terminal to these lysine and arginine residues. tPA and uPA are themselves inhibited by plasminogen activator inhibitor-1 and plasminogen activator inhibitor-2 (PAI-1and PAI-2) [34]. Plasmin activity is also reduced by thrombin-activatable fibrinolysis inhibitor (TAFI), which modifies fibrin to make a less potent cofactor for the tPA-mediated plasminogen [35].

1.1.2 Quality of the vessel wall

Blood vessels are lined with endothelial cells which, in their normal state, express anticoagulant activity and do not support platelet adhesion [36]. Exposure of the subendothelial surface by injury, however, initiates coagulation. This is due both to exposure of tissue factor, which activates the extrinsic cascade, and to the presence of collagen, which not only activates platelets, but also avidly supports their adhesion [9]. In addition, biomaterial-induced blood coagulation remains a major impediment to the successful use of implantable and peripheral medical devices [37]. When the blood-contacting surface is a foreign material, the interactions are mediated by blood proteins. Within seconds of blood contact, proteins begin to adsorb to the foreign surface. Once adsorbed, the proteins can change their conformations to interact more strongly (or in some cases, weakly) with cells and platelets than their bulk counterparts do [38]. In terms of thrombosis, adsorption of high-molecular-weight kininogen (HMWK) can lead to activation of fXII and initiation of the intrinsic coagulation cascade, while adsorption of fibrinogen or von Willebrand factor (vWF) will support platelet

adhesion via the GpIIbIIIa and GpIb receptors, respectively, with aggregation and thrombus formation following thereafter [39, 40].

1.1.3 Nature of the blood flow

The last leg of the triad is the one that ties everything together. Clearly, in order for platelets and coagulation factors to reach an artificial surface or the site of an injury, they must be transported there. Hemostasis, atherogenesis and thrombosis are processes which occur in flowing blood. Hence, the flow behaviour of blood may partly explain the localisation and morphology of arterial, intracardiac and venous thrombi within the human circulation [41]. Furthermore, it may partly explain why increases in hematocrit, fibrinogen and other macromolecules and rigid blood cells may increase the risk of ischaemic events [42].

The rheological behavior of normal whole blood is dominated by red blood cells (RBCs), which typically account for about 40% of the total blood volume and 99% of the volume of particulate matter [43]. Largely due to their deformability, an excess of RBCs develops in the central core of a steady tube flow, while an RBC-depleted layer develops near the wall; this is the well-known "Fahraeus effect" [44]. Due to the crowding of RBCs in the center of the vessel, platelets are expelled to the near-wall region, where an excess which has been observed to be as high as nine times the bulk concentration can develop [45]. RBC collisions and rotational motions also enhance mixing and transport of platelets near the vessel wall, where they are strategically placed for adhesion and activation. In streamline (laminar) flow, shear stresses are maximal at the vessel wall, and affect endothelial cell morphology and function. Endothelial cells

elongate and align in the direction of flow. Furthermore, high shear forces at the vessel wall may activate platelets and increase their vWF-induced adhesion to exposed subendothelium. However, high wall shear forces also increase removal of platelet aggregates, thrombin and fibrin monomer; hence stasis (induced by internal or external pressure) is required to allow fibrin formation and secondary hemostasis.

Atherogenesis occurs preferentially at arterial bifurcations and bends, at which sites flow separation results in areas of low-flow, low-shear recirculation of blood cells and proteins, in contact with the vessel wall [41, 42]. Such flow conditions may favour adhesion of platelets and monocytes, as well as infiltration of plasma components such as low density lipoprotein (LDL) cholesterol and fibrinogen. Rheological variables such as wall shear stress, and blood viscosity and its determinants (hematocrit, fibrinogen, LDL) have been correlated with the extent of ultrasonic carotid artery intima-media thickening (IMT) [46]. This may partly account for the predictive value of blood viscosity for stroke in the same study [46]. Blood viscosity has also been associated with the extent of coronary and peripheral atherosclerosis.

Arterial thrombosis usually follows rupture of atherosclerotic plaques, and is the commonest pathophysiological process in acute coronary syndromes, MI or IS. High intra-stenotic shear stresses may be one factor promoting arterial plaque rupture, and through high-shear activation of blood platelets they may also promote the initial platelet-rich "white head" of arterial thrombi. Distal to the atherothrombotic stenosis, low-shear stresses may promote the subsequent, fibrin-and red-cell-rich "red tail" [3]. Low post-stenotic perfusion pressure may also promote the ability of blood viscosity (which increases under low shear

conditions, due to red cell aggregation), platelet microemboli, and activated leucocytes to reduce microcirculatory blood flow, promoting infarction. These rheological mechanisms may explain the associations of blood and plasma viscosity, hematocrit, erythrocyte sedimentation rate (ESR; which reflects red cell aggregation), white cell count, fibrinogen and von Willebrand factor with the risk and the outcome of myocardial, cerebral and limb infarction [47].

1.2 Previous mathematical models

Complexity of blood coagulation and flow has been an obstacle and a simulating challenging factor for theoretical research in hemostasis and thrombosis for decades. Recent decades witnessed an explosion of mathematical modeling and computer-simulation-based research in all areas of biochemistry and biology, including coagulation. Two possible reasons could be suggested to explain the popularity of theoretical methods. First, efficient theoretical analysis is possible only when a sufficient amount of empirical information is collected. Second, the complexity of biochemical objects makes analysis of mathematical models extremely complicated without computer simulation. Thus the role of mathematical and computer modeling gradually becomes more and more important in the selection of the most effective experimental approaches, and blood coagulation is not an exception in this sense.

The function of the complex reaction network of coagulation is to provide thrombin where and when it is needed to form the fibrin. Understanding the roles of the system components (feedback loops, inhibitors, platelets functions, etc) in this regulation is important for a therapeutic control of thrombotic and

bleeding disorders. Initial theoretical studies of the system structure were stimulated by the hypothesis that reactions of coagulation form a cascade [48]. The study of Levine [49] analyzed the kinetics of a simple enzymatic cascade consisting of second-order reactions, with each enzyme being inhibited in a first-order reaction. The system response (kinetics of the bottom enzyme of the cascade) was a pulse with an amplitude proportional to the degree of stimulation, and the steepness of the initial kinetics increased with the increase of the number of stages in the cascade. Thus, the amplification role of the cascade was demonstrated. Later, rapidly increasing volume of experimental knowledge about the coagulation system induced modifications of this model. Models of greater complexity, which brought together the kinetics of various sets of reactions and included feedback loops and inhibitors under different reaction conditions (like flow, extent of stimulus, etc.), emerged towards the late 1980s [50, 51]. Jones and Mann [52] presented an early large scale model for thrombin generation via the extrinsic pathway, and extended it to include the role of inhibitors [53]. Leipold and coworkers [54] developed a linear system of ordinary differential equations (ODEs) to simulate the generation of thrombin and compared with published experimental results without the adjustment of any parameter value.

Within the context of this historical trend, individual research groups have focused on certain important questions related to the coagulation response. Beltrami and Jesty [55] focused on the threshold response of simple representative systems of the enzyme cascade, and found that the activation threshold of these systems was affected by flow rate, the size of the patch/injury, initial concentrations of active enzymes, etc. Basmadjian and coworkers investigated the possible steady states of their models, and also studied the regulation of the activation threshold by flow rate, surface area (of injury), and the type of sur-

face [56, 57, 58]. Khanin and coworkers presented one of the earliest models of thrombin generation in plasma that integrated five zymogen conversion reactions, and investigated the regulation of the activation threshold by levels of stimulation of VII and XII [50], and the sensitivity of clotting time to concentrations of zymogens [59]. These models primarily described spatially homogenous systems, i.e., ODEs were used. Kuharsky and Fogelson [60] also reported a threshold manner to changes in the availability of binding sites for surface bound enzyme complexes. They included the role of bulk flow in controlling the mass transfer of reactants to and from a thin shell where they were well mixed and also with different levels of binding site densities; such study eliminated the role that convection and diffusion may in all probability play in clot formation and, especially, clot dissolution but remain significant in view of the insight into the coagulation pathway that they offer.

In addition, numerous empirical studies have shown [61, 62], platelet aggregation [63] and clot formation can be highly spatially variable, especially when flow disturbances or highly reactive surfaces are present. Predicting such variations may be important if one is to accurately determine where clinically significant thrombi will form [64]. Studies on the growth of clots upon the activation of a series of enzymatic reactions, chosen to represent various features of the coagulation pathway, have emerged since late 1980s. Basmadjian used classical fluid dynamical correlations to estimate critical ranges of thrombus height and fluid shear rate which predisposed to embolization [65]. He also predicted that thrombus porosity and fluid inertial effects have relatively less effect on thrombus stability than drag forces. Ataullakhanov and coworkers studied the growth and termination of clot formation in spatially inhomogenous unstirred systems primarily due to contact activation (intrinsic pathway) by means of a mathemat-

ical model [66, 67]. Post-activation, the growth of the fibrin clot into the blood zone was studied in one spatial dimension. In a similar study, Ataullakhanov *et al.* [68] described and corroborated a slightly improved version of this model, and again investigated the spatial growth of a clot on a segment. Sorensen *et al.* [69, 70] proposed a set of coupled convection-reaction-diffusion equations to govern 6 components that the authors believed were crucial to the processes governing platelet activation and deposition in flowing human blood. They, however, incorporated these reactions as taking place in a Newtonian (Navier-Stokes) fluid, and solved the equations governing the platelets and platelet agonists while ignoring the effect of the growing thrombus on the flow field. Similar models which specifically attempt to predict spatially varying platelet deposition in the presence of two-dimensional disturbed flow have been published by David et al. [71], who consider stagnation-point flow, and Wootton et al. [72], who simulated axisymmetric stenoses. Both models used steady-state two-dimensional convection-diffusion equations to model platelet transport, with adhesion simulated by a non-saturating surface-flux boundary condition whose rate constant was the only adjustable parameter in the model. And surprisingly, both models showed the poorest agreement between predicted and experimental results in the downstream, fully-developed-flow regions of their geometries, rather than in the disturbed flow regions.

While in almost all the mathematical models that have been published thus far decoupled the complex reactions in the coagulation cascade from the rheological aspects of the local environment. In these studies, the coagulation network was either simplified or only activities of platelets were considered in the flowing blood. In addition, scant attention has been paid to the role of the fibrinolytic mechanisms or shear stresses in clot formation, growth and dissolu-

tion [9]. Thus in this study, we developed, to the best of our knowledge, the most detailed model of thrombus formation in both normal and pathological conditions; we further studied the effect of flow and wall shear stresses on the formation and dissolution of thrombi.

1.3 Computational systems biology and sensitivity analysis

Computational systems biology, a term coined by Kitano in 2002 [73], is a field that aims at a system-level understanding by analyzing biological data using computational techniques [74]. As the need for a complete quantitative part list in biology is recognized, the understanding develops that living systems, e.g., cells, tissues, and organisms, cannot be understood by studying just individual parts. Under the guiding vision of systems biology, sophisticated computational methods, e.g. mathematical modeling and sensitivity analysis, are currently being developed to analyze the data generated by this new technology in a systematic fashion.

1.3.1 Computational systems biology

These days it is well recognized that the many mechanisms involved in the proliferation of complex diseases such as cancer cannot be understood solely on the basis of knowing all of their molecular components. However, a lack of system-level understanding of cellular dynamics has prevented any substantial increase in the number of new drugs available to the public and any increase in drug efficacy or eradication of any specific diseases. In contrast, pharma-

ceutical companies are currently lacking criteria for selecting the most valuable targets, research-and-development expenses skyrocket, and new drugs rarely hit the market and often fail in clinical trial, while physicians face an increasing wealth of information that needs to be interpreted intelligently and holistically [75]. Analysis of this dilemma reveals primary difficulties due to the enormous biomolecular complexity, structural and functional unknowns in a large portion of gene products, and a lack of understanding of how the concert of molecular activities transfers into physiological alterations and disease.

We are at a very important turning point in biology, in that the ever-increasing quality and quantity of molecular data now provides the basis for building mathematical models of biological processes with increasing complexity. The general focus of biomedical research needs to change from a primarily steady-state analysis at the molecular level to a systems biology level capturing the characteristic dynamic behavior. Such concepts will likely transform current diagnostic and therapeutic approaches to medicine [75]. Assmus *et al.* and others maintained that analysis of the dynamics of human relevant networks using predictive computer models and high-throughput data generation would play an increasingly important role in medical research and the elucidation of disease mechanisms [76, 77].

The multitude of computational tools needed for systems biology research can roughly be classified into two categories [78]: system identification and behavior analysis. Once the system has been identified and a model constructed, the system behavior can be studied, for instance, by numerical integration or sensitivity analysis against external perturbations. In molecular biology, system identification amounts to identifying the regulatory relationships between

genes, proteins, and small molecules, as well as their inherent dynamics hidden in the specific kinetic and binding parameters. System identification is arguably one of the most complicated problems in science. Whereas behavior analysis is solely performed on a model, model construction is a process tightly connected to reality.

1.3.2 Sensitivity analysis

Sensitivity analysis is an essential part of analyses for complex systems [79]. Specifically, sensitivity analysis refers to the determination of the contributions of individual uncertain analysis inputs to the uncertainty in analysis results. A number of approaches to sensitivity analysis have been developed, including differential analysis [79], Monte Carlo analysis [80], and variance decomposition procedures [81]. Overviews of these approaches are available in several reviews [82, 83]. The focus of this study is on Monte Carlo (i.e., sampling-based) approach to sensitivity analysis, which is both effective and widely used [82, 80]. Analyses of this type involve the generation and exploration of a mapping from uncertain analysis inputs to uncertain analysis results. The underlying idea is that analysis results y(x) are functions of uncertain analysis inputs x. This leads to the question: How important are the individual elements of x with respect to the uncertainty in y(x)? The goal of sensitivity analysis is to answer the question.

Sensitivity analysis has also been used to explore the robustness and fragility of metabolic and signaling networks. Robustness, the ability to maintain system performance in the face of perturbation and uncertainty, is a desirable feature

in both biological as well as man-made networks, machines and systems [84]. Conversely, fragility, i.e., extreme sensitivity to small perturbations, is a very undesirable trait that could lead to catastrophic system failure following seemingly innocuous perturbations, e.g., a Boeing 777 crashing because of minor software failures or microscopic alterations in a few integrated chips [85]. Stelling *et al.* reviewed several examples of robustness in biological networks [84], while Leibler first computationally predicted and later experimentally verified robust features of chemotaxis control networks [86, 87]. Bullinger and coworkers explored the robustness of models of programmed cell death or apoptosis [88], while Stelling *et al.* computationally identified points of robustness and fragility, using Monte Carlo sensitivity analysis and overall state sensitivity coefficients, in models of circadian rhythm [89]. In this study, the sensitivity analysis was used to extract qualitative information about the critical elements, i.e., sensitive mechanisms, in the process of blood clotting, and these mechanisms could serve as a rational basis for therapeutic target selection.

CHAPTER 2

COMPUTATIONALLY DERIVED POINTS OF FRAGILITY OF A HUMAN CASCADE ARE CONSISTENT WITH CURRENT THERAPEUTIC STRATEGIES [1]

2.1 Abstract

The role that mechanistic mathematical modeling and systems biology will play in molecular medicine and clinical development remains uncertain. In this study, mathematical modeling and sensitivity analysis were used to explore the working hypothesis that mechanistic models of human cascades, despite model uncertainty, can be computationally screened for points of fragility, and that these sensitive mechanisms could serve as therapeutic targets. We tested our working hypothesis by screening a model of the well-studied coagulation cascade, developed and validated from literature. The predicted sensitive mechanisms were then compared with treatment literature. The model, composed of 92 proteins and 148 protein-protein interactions, was validated using 21 published datasets generated from two different quiescent *in-vitro* coagulation models. Simulated platelet activation and thrombin generation profiles in the presence and absence of natural anticoagulants were consistent with measured values, with a mean correlation of 0.87 across all trials. Overall state sensitivity coefficients, which measure the robustness or fragility of a given mechanism, were calculated using a Monte Carlo strategy. In the absence of anticoagulants, fluid and surface phase factor X/activated factor X (fX/FXa) activity and thrombin-mediated platelet activation were found to be fragile, while fIX/FIXa

[1] Deyan Luan, Michael Zai and Jeffrey D. Varner, PLOS Computational Biology, 2007 3(7), 1347-1359. Open Access: No permission is required from the authors or the publishers.

and fVIII/FVIIIa activation and activity were robust. Both anti-fX/FXa and direct thrombin inhibitors are important classes of anticoagulants; for example, anti-fX/FXa inhibitors have FDA approval for the prevention of venous thromboembolism following surgical intervention and as an initial treatment for deep venous thrombosis and pulmonary embolism. Both *in-vitro* and *in-vivo* experimental evidence is reviewed supporting the prediction that fIX/FIXa activity is robust. When taken together, these results support our working hypothesis that computationally derived points of fragility of human relevant cascades could be used as a rational basis for target selection despite model uncertainty.

2.2 Introduction

The role that mechanistic mathematical modeling and systems biology will play in molecular medicine and clinical development remains uncertain. Kitano suggested that understanding of critical questions in biology required the integration of experimental and computational research [73]. Assmus *et al.* and others maintained that analysis of the dynamics of human relevant networks using predictive computer models and high-throughput data generation would play an increasingly important role in medical research and the elucidation of disease mechanisms [76, 77]. However, parametric and structural uncertainty remains an open challenge to mechanistic modeling in medicine.

Strategies that integrate experimental and computational techniques have had success at elucidating network structures. Arm and Arkin reviewed experimental and computational techniques to uncover molecular interaction networks [90]. The central experimental advancements in the area of protein-

protein network identification have been the yeast two-hybrid system [91, 92] and quantitative mass spectrometry proteomic techniques to determine protein complexes [93, 94]. Young and coworkers explored proteinDNA interactions using the chromatin immunoprecipitation technique [95] where likely transcription factor binding sites were determined using a combination of chromatin immunoprecipitation chips and DNA microarrays. Time-lagged correlation matrices [96, 97], genetic programming techniques [98], and network decomposition strategies have also been used with time-series concentration measurements to estimate reaction network structures [99].

Sensitivity analysis has been used to integrate model identification and discrimination with optimal experimental design and knowledge discovery. Cho *et al.* used sensitivity analysis to study TNF-αmediated NF-κB signalling where parametric uncertainty was addressed using Monte Carlo sensitivity analysis; using the best-guess parameter set, a family of random parameter sets was generated where sensitivity coefficients were calculated for each member of the random family [80]. Cho *et al.* went on to develop a unifying framework, building upon the earlier work of Kholodenko *et al.* and Sontag *et al.* to unravel the functional interactions in biomolecular networks using a stimulus-response strategy and metabolic control analysis [100, 101, 102]. Kremling *et al.* investigated the benchmark problem of growth of a microorganism in a continuous bioreactor subject to feed shifts using sensitivity-based model identification and discrimination strategies; they determined optimal experimental design and perturbation strategies to identify and discriminate between rival model formulations [103]. Gadkar *et al.* identified signal transduction models from time-course measurements using a nonlinear scheme to estimate missing protein measurements from measured values [104]. They went further and proposed strategies to cal-

culate D-optimal experimental designs that maximized the experimental information used to identify signal transduction models as well as an iterative strategy to explore model structure [104, 105]. Sensitivity analysis has also been used to explore the robustness and fragility of metabolic and signaling networks. Robustness, the ability to maintain system performance in the face of perturbation and uncertainty, is a desirable feature in both biological as well as man-made networks, machines and systems [84]. Conversely, fragility, i.e., extreme sensitivity to small perturbations, is a very undesirable trait that could lead to catastrophic system failure following seemingly innocuous perturbations, e.g., a Boeing 777 crashing because of minor software failures or microscopic alterations in a few integrated chips [85]. Stelling *et al.* reviewed several examples of robustness in biological networks [84], while Leibler first computationally predicted and later experimentally verified robust features of chemotaxis control networks [86, 87]. Bullinger and coworkers explored the robustness of models of programmed cell death or apoptosis [88], while Stelling *et al.* computationally identified points of robustness and fragility, using Monte Carlo sensitivity analysis and overall state sensitivity coefficients, in models of circadian rhythm [89].

In this study, we use tools from systems biology, namely mathematical modeling and sensitivity analysis, to explore the working hypothesis that mechanistic models of human relevant cascades, despite model uncertainty, can be computationally screened for points of fragility, i.e., sensitive mechanisms, and that these mechanisms could serve as a rational basis for therapeutic target selection. We test our working hypothesis by computationally screening a mechanistic model of the well-studied coagulation cascade developed and validated from literature sources. After model validation, using 21 published datasets

generated from two different quiescent in vitro coagulation models, we use Monte Carlo sensitivity analysis to computationally screen the model for sensitive mechanisms in the presence and absence of natural anticoagulants. We then contrast the predicted fragile mechanisms with literature to determine if they are consistent with experimental investigation, thereby proving or disproving our working hypothesis. While the current development is restricted to coagulation, the broader strategy is general and could be applied to an arbitrary network.

2.2.1 A review of the coagulation cascade

Coagulation, mediated by a family of serine proteases (factors) and a key group of blood cells (platelets), both of which are normally inactive in the circulation, is directly relevant to human health and has been suggested by Somogyi and Greller to be an ideal candidate for in silico drug discovery [106]. Insufficient coagulation is manifested in disorders such as hemophilia A (1 in 5,000 live births), hemophilia B (1 in 30,000 live births), or von Willebrand disease (1 in 1,000 live births) [107, 24]. Conversely, unwanted clotting can be a serious complication following surgical intervention and is directly involved in coronary artery diseases, which collectively account for 38% of all deaths in North America [4].

The salient features of the coagulation cascade included in our model, shown schematically in Figure 2.2.1 and presented in detail in Appendix A Table A.3, are reviewed here. Several extensive reviews of the underlying biochemistry and cell biology of coagulation can be found elsewhere [108, 109, 110, 111].

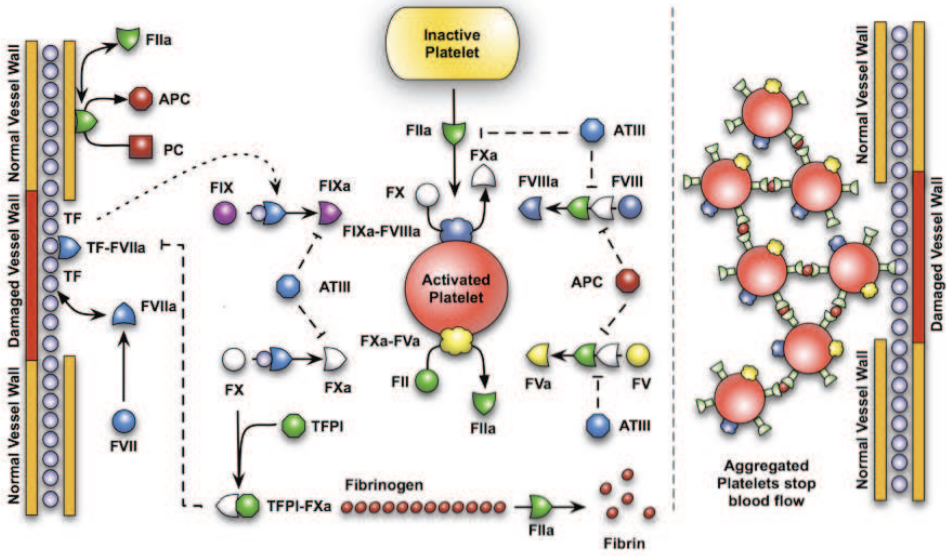

Figure 2.1: Schematic of the coagulation cascade. (A) Upstream coagulation factors are activated by substances exposed because of vessel injury; chief among these factors is TF. Activated upstream coagulation factors initiate a cascade of events that culminate in the activation of platelets and the key protease thrombin (FIIa). Thrombin forms an amplification loop by activating itself and other coagulation factors as well as platelets. (B) Activated platelets then aggregate to form platelet plugs, which serve as scaffolds for fibrin clots.

There are two pathways that lead to activation of the master protease thrombin and eventually to a clotthe intrinsic and extrinsic cascades. It is generally believed that the extrinsic cascade is the main mechanism of thrombinogenesis in the blood [110, 111, 22]. Upstream coagulation factors are activated by materials exposed because of vessel injury chief among these tissue factors (TFs) [112]; TF and activated factor VIIa (FVIIa) present in the blood form a complex that activates factor X (fX) and fIX. FXa activates downstream factors, including fV, fVIII, and fIX. FXa can also, along with FVa, form a complex on the surface of activated platelets that converts prothrombin (fII) to thrombin (FIIa). TF-FVIIa is not the only mechanism to activate fX; FIXa and FVIIIa can complex on the

surface of activated platelets and catalyze the formation of FXa. Platelet localization at the wound site occurs through specific interactions between the platelet and the subendothelium, primarily through recognition of exposed materials such as collagen, fibronectin, and von Willebrand factor. Localized platelets are activated by external signals such as adenosine diphosphate and thrombin. Thrombin irreversibly activates platelets through a family of transmembrane receptors on the platelet surface called protease-activated receptors [113, 114]. Thrombin, in addition to playing a key role in platelet activation, catalyzes the conversion of fibrinogen (secreted by activated platelets from internal stores) to fibrin. Fibrin, with the help of FVIIIa, forms a cross-linked mesh inside the platelet plug that stops blood flow. Thrombin also activates upstream coagulation factors, thereby forming a strong positive feedback that ensures rapid activation. Three control points that inhibit thrombin formation are considered in the model. TF pathway inhibitor (TFPI) downregulates FXa formation and activity by sequestering free FXa and TF-FVIIa in an FXa-dependent manner. Antithrombin III (ATIII) neutralizes all serine proteases generated during the coagulation response, making it perhaps the most powerful control element in the cascade. Thrombin itself plays an inadvertent role in its own inhibition by binding the surface protein thrombomodulin (TM), expressed on normal vasculature [23]. The FIIaTM complex catalyzes the conversion of protein C (PC) to activated PC (APC); APC attenuates the coagulation response by the proteolytic cleavage of fV/FVa and fVIII/FVIIIa [23].

2.3 Results

Simulations of TF-FVIIa initiated coagulation in the presence and absence of anticoagulants were compared with 21 published datasets from two different in vitro coagulation models [108, 115, 116]. The model parameters used in the validation simulations (unless otherwise noted) were compiled from literature and are shown in Appendix A Table A.3. Initial conditions for the validation simulations are given in the Appendix A Table A.2. To gauge the robustness and fragility of each interaction in the cascade, overall state sensitivity coefficients (OSSCs) were calculated for each of the 148 model parameters over a family of random parameter sets (see Methods and Materials). Simulation results are shown in Figure reffig-sim-results, and error quantification is reported in Table 2.1. With the exception of PC and one TFPI case, the model explained the time-resolved thrombin generation profile following TF-FVIIa addition to quiescent synthetic plasma. Platelet activation was assumed to be instantaneous for the synthetic plasma simulations. To test the ability of the model to simultaneously describe platelet activation and thrombin formation, simulations of TF-FVIIa initiated coagulation were compared with the *in vitro* cell-based assay of Roberts and coworkers [115] (Figure 2.2F); both platelet activation and thrombin generation profiles were consistent with the cell-based assay after adjusting three parameters used in the synthetic plasma simulations. Analysis of the sensitivity results for the control (no inhibitors) revealed that thrombin formation is controlled by both initiation and amplification mechanisms; the 25 most fragile mechanisms for the control are reported in Table 2.2, and the rank-ordered fragility results for 100 random parameter sets for the control, TFPI, and ATIII cases are shown in Figure 2.3.2AC. Mechanisms involving fluid and surface

phase fX/FXa and thrombin were found to be the most sensitive, while mechanisms involving fIX/FIXa and fVIII/FVIIIa were found to be robust. Binding interactions were found to be the most sensitive group of interactions. Analysis of the significant shifts in the overall state sensitivity coefficients (see Methods and Materials) revealed both additive and synergistic effects when compared to the control (Figure 2.3.2).

2.3.1 Thrombin activation in synthetic plasma in the presence and absence of natural anticoagulants.

The predicted thrombin concentration profiles following the addition of TF-FVIIa to synthetic plasma were quantitatively consistent with in vitro observations (Figure 2.2E). The fraction of variation explained by the model (Table 2.1) was found to be inversely proportional to TF-FVIIa input strength. In the absence of inhibitor, thrombin generation was characterized by two regimes; at first, FXa generated thrombin in the bulk fluid, and then subsequently, the thrombin signal was amplified by activity of FVa-FXa surface complex (prothrombinase). Decreasing the TF-FVIIa input prolonged the initiation phase as it slowed the rate of generation of FXa and thrombin in the bulk. However, TF-FVIIa input strength did not influence the maximal rate of thrombin formation because this is surface dominated; this was observed by comparing the slope or total net rate of thrombin generation across the TF-FVIIa cases.

TFPI and ATIII influenced both the initiation and amplification of the FIIa signal (Figure 2.2A and 2.2B). Increased TFPI concentration lead to a longer initiation delay and a decreased rate of FIIa amplification (Figure 2.2A). TFPI

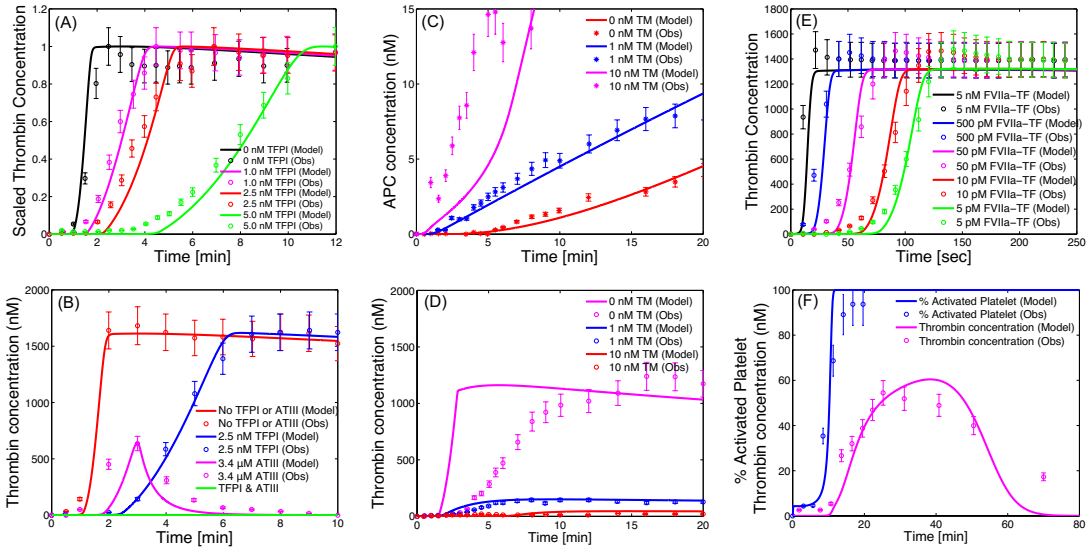

Figure 2.2: Model validation using published *in-vitro* datasets. (A) Thrombin concentration versus time as a function of TFPI concentration following the addition of 1.25pM TF-FVIIa to synthetic plasma. (B) Thrombin concentration versus time for different combinations of TFPI and ATIII following the addition of 1.25pM TF-FVIIa to synthetic plasma. (C) APC concentration versus time as a function of TM concentration following the addition of 1.25pM TF-FVIIa to synthetic plasma. (D) Thrombin concentration as a function of time as a function of TM concentration following the addition of 1.25pM TF-FVIIa to synthetic plasma. (E) Thrombin concentration versus time as a function of TF-FVIIa initation strenght in synthetic plasma. (F) Fraction of activated platelets and thrombin concentration as a function of time in the cell-based assay. The synthetic plasma assay cases were reproduced from Mann and coworkers [108, 116, 117], while the platelet activation data (panel F) was reproduced from Roberts *et al.* [115]. The GraphClick software (Arizona Software, www.arizona-software.ch) was used for data extraction where a coefficient of variation (CV) of ±10 was added to the data to account for extraction and experimental error. The initial conditions are shown in the Appendix A Table A.2.

delayed initiation through interaction with free FXa and TF-FVIIa in an FXa-dependent manner; sequestering FXa reduced flux through the initial FXa-dependent route of FIIa generation. Thrombin amplification was negatively impacted by TFPI by reducing free FXa available for the formation of the FVaFXa surface complex. On average, the model explained 95% of the TFPI dynamics; one exception was the 2.5 nM TFPI case (Figure 2.2B), where the correlation between model and experiment was 0.90. In contrast, ATIII reversibly binds FIXa, FXa, and TF-FVIIa, and irreversibly inactivates FIIa. ATIII produced a different thrombin generation profile when compared with TFPI (Figure 2.2B). ATIII influenced FIIa initiation by sequestering FXa (a mechanism similar to TFPI) and inactivated FIXa, thereby decreasing the rate of formation of the FVIIIaFIXa surface complex. However, unlike TFPI, ATIII directly inactivated FIIa, leading to the decreasing FIIa concentration observed experimentally. While the model captured the qualitative features of ATIII (3.4 μM) activity, the correlation between the model and experiment was 0.68, indicating that slightly more than half of the FIIa dynamics were correctly described. The combination of TFPI (2.5 nM) and ATIII (3.4 μM), consistent with the experiment, completely quenched FIIa formation following TF-FVIIa addition.

Simulations of APC generation and inhibition of thrombin formation in the presence and absence of TM were qualitatively consistent with in vitro data (Figure 2.2C and 2.2D). APC was generated from PC via TM-dependent and -independent routes; the TM-dependent route catalyzes the conversion of PC to APC at a rate 400-fold greater than the thrombin route alone [116]. Three different TM concentrations were simulated, and the time course of APC and FIIa were compared with published data [116]. The correlation between model and experimental data for APC was approximately 96% for TM values 1 nM. How-

Table 2.1: Quantification of model error.

Simulation	Normalized Standard Error	Correlation r^2
FVIIa-TF Simulations		
5 nM	0.12	0.80
500 pM	0.08	0.93
50 pM	0.08	0.96
10 pM	0.07	0.97
5 pM	0.06	0.98
TFPI Simulations		
0 nM	0.07	0.96
1.0 nM	0.06	0.98
2.5 nM	0.13	0.90
5.0 nM	0.06	0.96
ATIII and TFPI Simulations		
No TFPI + No ATIII	0.03	0.99
2.5 nM TFPI + No ATIII	0.03	0.99
3.4 μM ATIII	0.21	0.68
2.5 nM TFPI + 3.4 μM ATIII	ND	ND
APC+TM Simulations		
0 nM TM (APC)	0.07	0.95
1 nM TM (APC)	0.06	0.97
10 nM TM (APC)	0.29	0.49
0 nM TM (FIIa)	0.45	0.51
1 nM TM (FIIa)	0.19	0.82
10 nM TM (FIIa)	0.69	0.57
Platelet Activation and Thrombin Simulations		
Platelet Activation	0.12	0.94
Thrombin	0.15	0.89

ever, the average correlation between the predicted and measured FIIa profile for TM 1 nM was 67%. Simulations of the TM 10 nM case failed to quantitatively capture both APC and FIIa formation; the correlation between model and experiment for APC in the presence of 10 nM TM was 49%, while 57% of the FIIa dynamics were correctly described.

In-vivo, amplification of the thrombin signal requires the surface of activated platelets. Preliminary simulations of simultaneous platelet activation and thrombin formation (Figure 2.2F) were found to be consistent with the results of the cell-based coagulation assay of Roberts and coworkers [115]. The correlations between the measured and the simulated fraction of activated platelets and thrombin were 0.94 and 0.89, respectively. In contrast with coagulation in synthetic plasma, lag periods were observed for platelet activation and thrombin generation. Following the initial lag, the activated platelet concentration increases rapidly to a plateau of ≈100% activation. The thrombin concentration reaches a maximum of 55 nM at 30 min and then decreases to 0 nM at 70 min because of ATIII activity. Three parameter values were changed in the cell-based assay simulations compared with synthetic plasma; the rate constant controlling the activation of subendothelial bound platelets by thrombin was changed from $9.0 \times 10^{-3}\ s^{-1}$ to $4.5\ s^{-1}$, the activation of prothrombin by prothrombinase was changed from $30\ s^{-1}$ to $6\ s^{-1}$, and the binding of ATIII to thrombin was changed from $1.5 \times 10^{-5}\ nM^{-1}s^{-1}$ to $4.8 \times 10^{-5}\ nM^{-1}s^{-1}$.

2.3.2 The fragility and robustness of the coagulation architecture.

Overall state sensitivity coefficients were calculated for treatment cases AD shown in Table 2.3. The top 25 fragile mechanisms for the control (case A) are shown in Table 2.2; four of the top five fragile mechanisms involve the binding or activation of fX/FXa, with the fifth being platelet activation by FIIa. Other sensitive mechanisms include the formation of the FVaFXa surface complex, the activation of thrombin by the FVaFXa complex, and the activation of surface or fluid phase fIX and fV. Fragility is spread across initiation and amplification mechanisms; 14 of 25 fragile mechanisms were upstream of the FVaFXa or FVIIIaFIXa surface complexes, while the remaining 11 involved platelet activation, FVaFXa activity, and FIIa inactivation. Binding interactions were found to be the majority of fragile mechanisms; 21of 25 of the top fragile points were binding interactions. Six paired binding interactions were found to be sensitive, indicating affinity was controlling in these cases; the exception was the TF-FVIIaX and VaP5sXaP10s complexes, where on rate, catalytic turnover, and off rate were all found to be sensitive. Of the predicted robust mechanisms, the most nonintuitive were the formation and activity of the FVIIIaFIXa surface complex responsible for FXa amplification.

Statistically significant changes in overall sensitivity coefficients relative to the control were used to gauge the importance of mechanisms in each treatment case. For example, if the sensitivity of a binding interaction increased relative to

[2]A family of random parameter sets ($N = 100$) was generated by perturbing the nominal parameter by up ±50%. OSSCs were calculated for each random family member where the resulting OSSC values for each parameter were scaled by the maximum OSSC. Statitics of the population of scaled OSSC values were computed and the mean OSSC value (μ) ± one standard deviation (σ) is reported.

Table 2.2: The twenty most fragile coagulation mechanisms in the absence of inhibitors.[2]

$\mu \pm \sigma$	Reaction	Description
0.85±0.12	TF-FVIIa-Xa → TF-FVIIa+Xa	X activation by TF-FVIIa (catalytic)
0.85±0.21	X+P10s ⇌ X-P10s	X binding with platelet active sites (on)
0.85±0.21	X-P10s ⇌ X+P10s	X binding with platelet active sites (off)
0.83±0.22	Xa+P10s ⇌ Xa-P10s	Xa binding with platelet active sites (on)
0.77±0.17	PL-IIa → AP+IIa	Platelet activation by thrombin (catalytic)
0.62±0.18	X+TF-FVIIa ⇌ X-TF-FVIIa	X binding with TF-FVIIa (on)
0.57±0.28	II-P2s-Va-P5s-Xa-P10s → IIa-P2s+Va-P5s-Xa-P10s	IIa activation by prothrombinase (catalytic)
0.53±0.20	Xa+IX ⇌ Xa-IX	Binding of IX by Xa (on)
0.52±0.25	II-P2s+Va-P5s-Xa-P10s ⇌ II-P2s-Va-P5s-Xa-P10s	IIa interaction with prothrombinase (on)
0.50±0.18	Xa-IX ⇌ Xa+IX	Binding of IX by Xa (off)
0.48±0.19	X+TF-FVIIa ⇌ X-TF-FVIIa	X binding with TF-FVIIa (off)
0.38±0.17	IX+TF-FVIIa ⇌ IX-TF-FVIIa	Binding of IX by TF-FVIIa (on)
0.38±0.17	Va-P5s + Xa-P10s ⇌ Va-P5s-Xa-P10s	Formation of prothrombinase (on)
0.35±0.17	Va-P5s+Xa-P10s ⇌ Va-P5s-Xa-P10s	Formation of prothrombinase (off)
0.31±0.18	IIa+P2s ⇌ IIa-P2s	IIa binding with platelet active sites (off)
0.31±0.17	IX+TF-FVIIa ⇌ IX-TF-FVIIa	Binding of IX by TF-FVIIa (off)
0.23±0.19	V-P5s + IIa-P2s ⇌ V-P5s-IIa-P2s	Activation of V by IIa (on)
0.23±0.10	PL + IIa ⇌ PL-IIa	Activation of platelets by IIa (on)
0.22±0.10	TF-FVIIa ⇌ TF + FVIIa	Interaction of FVIIa with TF (off)
0.20±0.08	IX+P9s ⇌ IX-P9s	IX binding with platelet active sites (on)
0.20±0.08	IX+P9s ⇌ IX-P9s	IX binding with platelet active sites (off)
0.19±0.08	X+II ⇌ X-II	X binding with II (on)
0.19±0.13	II+P2s ⇌ II-P2s	II binding with platelet active sites (on)
0.18±0.10	IIa → IIa	IIa inactivation (catalytic)
0.18±0.15	IX-P9s+Xa-P10s ⇌ IX-P9s-Xa-P10s	IX binding with Xa on platelet surface (on)

Table 2.3: Treatement cases considered in the sensitivity analysis.

Case	FVIIa-TF (pM)	TFPI (nM)	ATIII (μM)	PC (nM)	TM (nM)
A	1.25	–	–	–	–
B	1.25	2.5	–	–	–
C	1.25	–	3.4	–	–
D	1.25	2.5	3.4	–	–

the control (became more fragile), then that interaction assumed increased importance in the treatment case. Conversely, a decrease in sensitivity relative to the control (mechanism became more robust) indicated a decrease of the overall impact of the mechanism. The anticoagulants TFPI and ATIII modulate thrombin formation by different mechanisms and have distinct regions of molecular influence. Although ATIII and TFPI share a common target (FXa), only two of 15 significant OSSC shifts were shared between the treatment cases (cases B and C) relative to the control (case A). TFPI was found to influence thrombin formation primarily through the FXa-specific interaction with TF-FVIIa; there were 13 mechanisms whose OSSC values changed significantly in response to TFPI (case A versus case B), nine of which become more robust, while two become more fragile (Figure 2.3.2B). TFPI reduced the fragility of the affinity of fIX and fX for TF-FVIIa, the sensitivity of TF-FVIIamediated formation of FXa, the affinity of FXa for fluid phase fIX, the stability of the TF-FVIIa complex, and the binding of fX and FXa with free-platelet binding sites. Conversely, TFPI increased the fragility of the off rate governing the disassociation of FXa from platelet binding sites and the interaction of itself with FXa. While ATIII had a more pronounced effect on FIIa generation than TFPI alone (Figure 2.2B), only four mechanisms were significantly affected by ATIII (case A versus case C). ATIII influenced

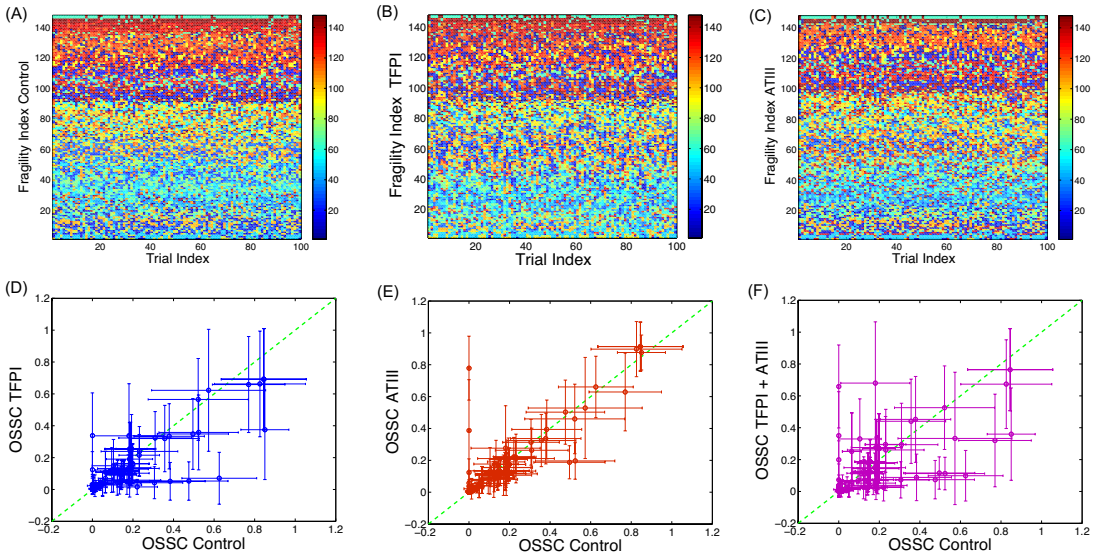

Figure 2.3: Sensitivity analysis of the coagulation cascade. OSSCs were calculated using randomly generated parameter sets constructed by perturbing the nominal parameter set by up to ± 50% for each parameter (N=100). (A-C): The x-axis denotes the trial index (index of the random parameter set), while the y-axis denotes the fragility index. The fragility index is calculated by determining the parameter index of the rank-ordered the OSSC values (The parameter index corresponding to the most fragile parameter has fragility index of 1; the next fragile is 2, while the most robust parameter has a fragility index of 148). The fragility index shows the robustness of a parameter; the smaller the fragility index, the more fragile the parameter. The parameter types are color-coded (shown in the color bar) and organized by biological function: 1-16, subendothelium interactions; 17-40, plasma interactions; 41-62, platelet surface binding; 63-77, platelet activation; 78-107, reactions on platelet surface; and 108-148, inhibitory reactions. (D-F) The OSSC values from TFPI, ATIII, and TFPI+ATIII cases versus the control.

thrombin formation through direct interaction with FXa and FIIa; ATIII reduced the sensitivity of the affinity of FXa for fIX in the fluid phase, while the on rate governing the binding of FXa and FIIa with ATIII was found to be of increased importance.

The predicted mechanism of action of anticoagulant combinations is not equivalent to the union of the individual treatment cases. The combination of TFPI + ATIII (case D) resulted in 14 statistically significant shifts relative to the control. Initiation mechanisms, e.g., the affinity of TF-FVIIa for fX and the affinity of FXa for fIX in the bulk fluid, were predicted to be less important. Conversely, the sensitivity of the off rate governing FXa interaction with the platelet surface was found to increase. Some amplification mechanisms became more robust, while others became fragile. The activation of platelets by FIIa via the protease-activated receptor family of surface receptors became less important, but the retention of FXa and the affinity of the surface FVaFXa complex increased in importance. Last, trivial interactions resulting from the addition of TFPI and ATIII (the direct interactions of TFPI and TF-FVIIa in an FXa-dependent manner and ATIII with FXa) were predicted to become fragile relative to the control. Shifts in sensitivity coefficients were not additive across treatment cases; e.g., the compilation of significant shifts resulting from TFPI and ATIII addition was found not to be equivalent to the combination treatment. Of the 14 significant shifts observed in the TFPI + ATIII case (relative to the control), four mechanisms found to be sensitive in the individual cases were missing in the combination, while three novel shifts were observed. Interaction of fX/FXa with surface binding sites and the disassociation of the TFFVIIa complex were found not to be significantly different than the control. The novel shifts in the TFPI + ATIII combination were all amplification mechanisms; the catalytic rate of IIa formation by FVa-FXa and the rate of platelet activation by IIa were found to be less important in the ATIII + TFPI combination, while interaction of surface-bound fV and FXa was found to increase in importance.

2.4 Discussion

The predicted fragile mechanisms in the control are molecular targets in current anticoagulation preclinical development, clinical therapies, and clinical trials. Four of the top five fragile mechanisms involved fX/FXa or the activation of platelets by FIIa. Anti-fX/FXa and direct thrombin inhibitors (DTIs) are two important classes of anticoagulants (see Table 2.4 for a sampling of current clinical trials involving anti-fX/FXa strategies and DTIs). Fondaparinux, a 1.7 kDa pentasaccharide which selectively binds ATIII, is approved for the prevention of venous thromboembolism following hip fracture surgery, total hip replacement, total knee replacement, and major abdominal surgery in addition to the initial treatment of patients with deep venous thrombosis and pulmonary embolism [118, 119, 120, 121, 122]. Fondaparinux increases the natural inhibitory effect of ATIII against FXa approximately 300-fold [123, 124]; selective inhibition of FXa by fondaparinux interrupts thrombin generation and clot formation without inactivating thrombin itself [125, 126]. Elalamy and coworkers showed in a whole-blood in vitro assay that fondaparinux prolonged the lag time of prothrombin activation for all concentrations explored, and for physiologically relevant concentrations (0.110.28 anti-FXa IU/ml), reduced the maximal rate of thrombin formation to approximately 47%55% of its nominal value [127]. Herbert and colleagues explored fondaparinux and the sulfated analog SANORG 32701 in in vivo mouse, rat, and rabbit coagulation models [128, 129]; SANORG 32701 has a high affinity for ATIII (Kd = 3.7 0.7 nM) and shows more potent anti-FXa activity (1,100 31 versus 850 21 U/mg for fondaparinux). DTIs have also been explored as anticoagulants [130]. Thrombin activity is mediated by three protein domains; an active site catalyzing protease activity and two exosites controlling

Table 2.4: Ten example clinical trial for FXa and DTIs.[3]

Trial Identifier	Treatment	Purpose	Target Mechanisms
NCT00412464	Fondaparinux	Dose/PK study in thrombotic children	ATIII-dependent FXa inhibitor
NCT00413374	Enoxaparin	Outpatient treatment for DVT and/or PE	ATIII-dependent FXa inhibitor
NCT00423683	Arixtra	Clot prevention in cancer patients	ATIII-dependent FXa inhibitor
NCT00245856	Fragmin	Treatment of upper extremity DVT	ATIII-dependent FXa/FIIa inhibitor
NCT00353678	YM150	Prevention of clot formation following HRS	Direct FXa inhibitor
NCT00371683	Apixaban	Prevention thrombosis following KRS	Direct FXa inhibitor
NCT00180674	Ximelagatran	Anticoagulation in liver fibrosis	Direct II/IIa inhibitor
NCT00334464	Warfarin	Establish pharmacogenetic warfarin dosing	FVII, IX, X, and II inhibitor
NCT00206089	Melagatran	Safety and efficacy of combination treatment	Direct II/IIa inhibitor
NCT00206063	Ximelagatran	Long-term tolerability of ximelagatran	Direct II/IIa inhibitor

substrate binding [131]. Our sensitivity analysis predicts thrombin activation of platelets is a key mechanism; Sarich *et al.* have explored the DTI ximelagatran in healthy male volunteers [132]. Thrombin generation, platelet activation, and the thrombinantithrombin complex were monitored in shed blood collected from skin incisions in 120 healthy male volunteers following oral administration of ximelagatran. Oral ximelagatran showed a rapid and statistically significant decrease in all endpoints relative to control. When taken together, the fondaparinux, SANORG 32701, and ximelagatran results present a clinical basis in both in vitro and in vivo coagulation studies for the prediction that fX/FXa and IIa are fragile components of the coagulation architecture.

Mechanisms involving fIX/FIXa, consistent with multiple lines of experimental evidence, were predicted to be moderately robust. Feuerstein *et al.* ex-

[3]Clinical trial information was assembled on May 15, 2007, from http://ClinicalTrials.gov using the search terms *thrombosis* and *thromboembolism*, where both open and closed trials were accepted; the search generated 215 clinical trials for *thrombosis* and 51 studies for *thromboembolism*. DVT, deep venous thrombosis; HRS, hip replacement surgery; KRS, knee replacement surgery; PE, pulmonary embolism.

plored inhibition of fIX/FIXa using a murine anti-fIX/FIXa antibody (BC2) in a male Sprague-Dawley rat model [133]. The fIX/FIXa activity and the activated partial thromboplastin time (aPTT) endpoints were monitored ex vivo following intravenous infusion of the BC2 antibody. Feuerstein *et al.* found that fIX/FIXa activity could be reduced by as much as 2.5-fold before any significant change in the aPTT was observed; only after > 90% of the fIX/FIXa activity was eliminated was there a 3.5- to 4-fold increase in aPTT. Benedict *et al.* explored the contribution of fIX/FIXa to intravascular thrombosis in a canine coronary thrombosis model [134]. Animals received an intravenous bolus of saline (vehicle), bovine glutamyl-glycyl-arginyl-FIXa (FIXai; a competitive inhibitor which prevents the assembly of the FVIIIa-FIXa complex [135, 136, 137]), bovine fIX, or heparin. Animals that received saline or bovine fIX developed a coronary occlusion due to a fibrin/platelet thrombus in approximately 1 h; conversely, FIXai decreased coronary thrombus occlusion in a dose-dependent manner. However, FIXai administration was not accompanied by increased bleeding at abdominal and chest-wall incision sites, leading Benedict *et al.* to conclude, consistent with the earlier work of Weiss and Lages [138], that direct TF-FVIIamediated activation of fX may be the primary mechanism of fX activation in blood obtained from bleeding wounds. While our prediction that FVIIIa-FIXamediated fX activation is robust is consistent with Benedict et al., the robustness of fIX mechanisms should be further explored using in vivo animal models or cell-based assays to control for artifacts introduced by the synthetic plasma model.

Overall state sensitivity coefficients and shifts in sensitivity provide insight into the potential method of action of coagulation inhibitors, including synergistic effects, but are not predictors of clinical performance. The naive perspective that a specific inhibitor influences *only* its target and nothing else is not con-

sistent with our sensitivity analysis. Consider the sensitivity results for TFPI; 13 different mechanisms were predicted to change significantly relative to the control. These shifts included not only the direct interactions of TFPI with FXa and TF-FVIIa, but also secondary effects like FXa interaction with fluid phase fIX. Moreover, the direction of shift, i.e., toward sensitivity or robustness, gives insight into the mechanism of action and the response of the network to the anticoagulant. In the case of TFPI, parameters associated with fluid phase FXa activity became more robust relative to the control, indicating these mechanisms were of decreased importance. Conversely, the off rate governing the disassociation of surface-bound FXa became more fragile relative to the control; keeping FXa bound became important as only fluid phase FXa binds TFPI in our model. However, while shifts in sensitivity coefficients might be a useful predictor of the network response, they are not predictors of clinical performance. No information about practical issues in patients, e.g., bioavailability, therapeutic window, unexpected toxicities, etc., was gained from sensitivity analysis of the network in isolation. Perhaps embedding the network into a pharmacokinetic or physiologically based pharmacokinetic (PBPK) model and then exploring the sensitivity profile of the augmented system could give insight into factors such as bioavailability and therapeutic window.

Despite parametric and structural uncertainty, the model captured the bulk of the thrombin generation dynamics resulting from TF-FVIIainitiated coagulation in the presence and absence of natural anticoagulants. However, several challenges remain before the model is relevant to *in vivo* phenomena. First, pro- and antiplatelet activation mechanisms operating on the endothelium should be refined and/or included in the model. Predicted thrombin and APC concentrations in the presence of TM were not consistent with *in vitro* synthetic plasma

measurements for TM concentrations > 10 nM. The discrepancy between IIa and APC values remained despite changes in parameters indicating a potential structural issue with the model. Also not considered was the active role played by the endothelium; endothelial cells secrete anticoagulants (e.g., nitric oxide [NO] and prostacyclin) and express surface proteins (e.g., CD39). CD39 inhibits platelet activation by converting adenosine diphosphate, a potent inducer of platelet activation, into adenosine monophosphate [139]; however, CD39 may play a dual role, as Eniyoji *et al.* showed ΔCD39 mice had prolonged bleeding times and decreased platelet activation [140]. Second, the predicted fraction of activated platelets and the concentration of key complexes on the platelet surface need to be quantified under a variety of conditions. Initial simulations of simultaneous thrombin formation and platelet activation were consistent with the cell-based assay of Roberts and coworkers [115] (after changing three parameter values). However, these simulations and the cell-based assay were conducted assuming no flow and no regulatory input from the endothelium. Moreover, given the role that activated platelets play in the amplification of the thrombin signal, the predicted concentration of key complexes on the platelet surface, e.g., the FVIIIaFIXa and FVaFXa complexes, need to be validated. Third, the cell biology of coagulation and clot formation must be embedded in a description of physics occurring in clot formation. Several researchers have explored the role that blood flow plays upon the formation of clots. Antaki and coworkers developed a 2-D model of platelet deposition and activation in flowing blood [69]. The Antaki model was able to describe the axial platelet deposition on collagen under parallel-plate Poiseuille flow for a range of wall shear rates [70]. Diamond and coworkers have produced a rich body of work exploring the reaction complexity of human blood, cell aggregation and adhesion under flow,

the formation of key complexes on the surface of activated platelets under flow conditions, establishing high-throughput techniques for real-time monitoring of coagulation dynamics and have done stochastic modeling of the initiation of coagulation [141, 142, 143, 144, 145]. These literature sources (and others) will form the basis of our future development.

2.5 Methods

2.5.1 Formulation of the Model Equations.

The reactions considered in the coagulation model have been compiled from literature and are given in Appendix A Table A.3. Mass balance equations are written around each protein or protein complex yielding the set of differential equations (vector-form):

$$\frac{d\mathbf{x}}{dt} = \mathbf{S}\mathbf{r}(\mathbf{x}, \mathbf{k}) \qquad \mathbf{x}(t_o) = \mathbf{x}_o \tag{2.1}$$

The symbol $\mathbf{S}$ denotes the stoichiometric matrix (92×148), while $\mathbf{x}$ denotes the 92-dimensional concentration vector of proteins or protein complexes and $\mathbf{r}(\mathbf{x}, \mathbf{k})$ denotes the 148-dimensional vector of reaction rates. Each row in $\mathbf{S}$ describes a particular protein or protein complex, while each column describes the stoichiometry associated with a specific interaction in the network. Thus, the (i, j) element of $\mathbf{S}$ denoted by σ_{ij}, describes how protein i is connected to rate process j. If $\sigma_{ij} < 0$, then protein i is consumed in r_j; conversely, if $\sigma_{ij} > 0$, protein i is produced by r_j, and if $\sigma_{ij} = 0$, there is no connection between protein i and rate j. We have assumed mass action kinetics for each interaction in Appendix A Table A.3; under the mass action assumption the rate expression

for the general reaction q:

$$\sum_{j \in \{\mathbf{R}_q\}} \sigma_{jq} x_j \rightarrow \sum_{k \in \{\mathbf{P}_q\}} \sigma_{kq} x_k \tag{2.2}$$

is given by:

$$r_q\left(\mathbf{x}, k_q\right) = k_q \prod_{j \in \{\mathbf{R_q}\}} x_j^{-\alpha_{jq}} \tag{2.3}$$

where $\{\mathbf{R_q}\}$ denotes the set of reaction q, $\{\mathbf{P_q}\}$ denotes the product set for reaction q, k_q denotes the rate constant governing the qth reaction, and σ_{jq}, σ_{kq} denote stoichiometric coefficients (elements of the matrix $\mathbf{S}$). We have treated every rate as nonnegative; all reversible reactions in Appendix A Table A.3 were split into two irreversible reaction steps. Thus, every element of the reaction rate vector $\mathbf{r}(\mathbf{x}, \mathbf{k})$ takes the form shown in Equation 2.3.

The model equations were solved using the LSODE routine of the OCTAVE programming environment (v2.1.71) on an Apple Computer MacOSX (Cupertino, CA; v10.4.8) workstation. Model parameters and structure were compiled from literature; see Appendix A Table A.3 and [52, 54, 60, 52, 146, 9, 8, 53]. Initial conditions were taken from each experiment and roughly correspond to *in vivo* physiological conditions (see Appendix A Table A.2). While the model presented here was developed from literature (including other models), it is, to the best of our knowledge, the only coagulation model to simultaneous describe all 21 datasets, including coupled platelet and thrombin activation and the activity of three different anticoagulants, using only minimal parameter variation (three-parameter change for a single case).

2.5.2 Error Analysis of the Coagulation Simulations.

The correlation between model simulations and experimental data and the scaled standard error were used to quantify the simulation uncertainty. The correlation between simulation and experimental observation was calculated using the relationship:

$$r^2 = \frac{\sum_{k=1}^{N_T} \left(Y_m(t_k) - \bar{Y} \right)^2}{\sum_{k=1}^{N_T} \left(\bar{Y}(t_k) - Y_m(t_k) \right)^2 + \sum_{k=1}^{N_T} \left(Y_m(t_k) - \bar{Y} \right)^2} \tag{2.4}$$

where $Y_m(t_k)$ denotes the model value at time point k, $\bar{Y}$ denotes the global average experimental value (average of experimental measurements over time), $\bar{Y}(t_k)$ denotes the average experimental value at time point k (average of experimental trials at single time point), and N_T denotes the number of time points. The numerator of Equation 5.4 is the variation in the experimental data explained by the model, while the denominator is the total variation; thus, Equation 5.4 describes the fraction of the dynamics explained by the model across all time points. In addition to correlation, the scaled standard error was used to measure the agreement between the model and the experiment:

$$s_E = \frac{1}{\max_k \left(\bar{Y}(t_k) \right)} \left(\frac{\sum_{k=1}^{N_T} \left(\bar{Y}(t_k) - Y_m(t_k) \right)^2}{N_T} \right)^{1/2} \tag{2.5}$$

Both error metrics were taken from Spiegel [147].

2.5.3 Computation of the OSSCs.

The sensitive or *fragile* elements of the coagulation architecture were determined by computing OSSCs [89]. Because each parameter corresponds directly to a particular molecular interaction in the cascade, OSSC values were used to

gauge which elements of the architecture influence thrombin formation; large OSSC values for parameters relative to their peers indicates *fragility* or sensitivity, while small OSSC values indicates robustness. OSSC values were calculated by first calculating the first-order sensitivity coefficients:

$$\sigma_{ij}(t_k) = \left.\frac{\partial x_i}{\partial p_j}\right|_{t_k} \tag{2.6}$$

which are solutions of the matrix differential equation:

$$\frac{d\mathbf{s}_j}{dt} = \mathbf{A}(t)\,\mathbf{s}_j + \mathbf{b}_j(t) \qquad j = 1, 2, , P \tag{2.7}$$

subject to the initial condition $\mathbf{s}_j(t_0) = \mathbf{0}$. In Equation 5.8, the quantity j denotes the parameter index, P denotes the number of parameters, $\mathbf{A}$ denotes the Jacobian matrix, and $\mathbf{b_j}$ denotes the jth column of the matrix of first-derivatives of the mass balances with respect to the parameter values ($\mathbf{B}$) are given by:

$$\mathbf{A} = \left.\frac{\partial \mathbf{f}}{\partial \mathbf{x}}\right|_{(\mathbf{x}^*,\mathbf{p}^*)} \qquad \mathbf{B} = \left.\frac{\partial \mathbf{f}}{\partial \mathbf{p}}\right|_{(\mathbf{x}^*,\mathbf{p}^*)} \tag{2.8}$$

where $(\mathbf{x}^*, \mathbf{p}^*)$ denotes a point along the *nominal* or *unperturbed* system solution. We solved Equation 5.8 for each parameter using the ODE15s routine of MATLAB 2006b (The Mathworks, http://www.mathworks.com). The matrices $\mathbf{A}$ and $\mathbf{B}$ were estimated at each time step using a generalized gradient algorithm [148]. The OSSC value for parameter j defined as:

$$S_{o_j}(t) = \frac{p_j^*}{N_s}\left(\sum_{k=1}^{N_T}\sum_{i=1}^{N_s}\left[\frac{1}{x_i^*}\left.\frac{\partial x_i}{\partial p_j}\right|_{t_k}\right]^2\right)^{1/2} \tag{2.9}$$

were computed using the scaled first-order sensitivities. The quantity N_T denotes the number of time points used in the simulation, while N_s denotes the number of proteins/protein complexes in the model. To account for parametric uncertainty, the OSSC values (S_{o_j}) were calculated over a *family* of random parameter sets; we randomly perturbed each nominal parameter by up to ±50%, then solved the sensitivity balances for *each* family member.

2.5.4 Statistical analysis of the shifts in OSSCs.

Two different statistical tests were performed to identify large statistically significant shifts in the OSSC values between treatment cases. A Welch t-test [149] was used to find all statistically significant shifts resulting from the different treatments, and then a secondary test on the z-score of each shift was preformed to find only the most prominent significant shifts. The OSSC values calculated over the family of random parameter sets were assumed to follow normal distributions in each treatment case. The standard test to determine if the means of normal distributions are equal is the student t-test; however, the student t-test assumes the two distributions in question have equal variances. We cannot a priori guarantee this is true for the OSSC distributions in different treatment cases; thus, we have chosen the Welch t-test. The Welch t-test is very similar to the student t-test, with the exception that the two distributions being compared are not required to have equal variances. The statistical significance of shifts in OSSC values for each treatment case relative to the control were determined by performing a Welch t-test with the null hypothesis that the means of the OSSC values were equal at a 1% significance level. The list of significant OSSC values was further restricted to only those shifts with a magnitude larger than a specified z-score (0.1) away from the squared mean displacement over the significant OSSC values. We defined the displacement of an OSSC value relative to the control as:

$$d_{j,q} = \left(\bar{S}^{q}_{o_j} - \bar{S}^{c}_{o_j}\right)^2, \qquad j = 1, 2, , 148 \tag{2.10}$$

where $\bar{S}^{c}_{o_j}$ denotes the mean OSSC value over the family of random parameter sets for parameter j in the control, while $\bar{S}^{q}_{o_j}$ denotes the same quantity for

treatment case q. A significant shift in OSSC value is *accepted* if:

$$d_{j,q} > z\sigma_{d_q} + \mu_{d_q} \tag{2.11}$$

where z denotes a desired z-score, σ_{d_j} denotes the standard deviation of the total displacement over all significant OSSC values for the qth treatment case, and μ_{d_q} denotes the mean of the significant displacements for treatment case q.

CHAPTER 3

FALSE NEGATIVE STRUCTURAL UNCERTAINTY DESTROYS THE ABILITY TO ASSESS THE ROBUSTNESS AND FRAGILITY OF MOLECULAR INTERACTIONS IN A HUMAN CASCADE

3.1 Abstract

Mechanistic mathematical modeling has not played a significant role in the development of new therapies for cancer, cardiovascular diseases or the treatment of acute events such as thrombosis during or after surgery. A critical issue often cited for the lack of modeling has been uncertainty. The conventional wisdom is that the data requirement to fully identify and validate mechanistic models is too large. One tool that could potentially extract qualitative properties about interactions in molecular networks, despite model uncertainty, is monte-carlo sensitivity analysis. In this study, we explored two critical open questions surrounding sensitivity-based knowledge discovery, namely, the impact of parametric sampling strategies and network structural uncertainty upon the assessment of the qualitative importance of molecular interactions in an archetype human network. We tested the working hypothesis that the determination of fragile and robust mechanisms using sensitivity analysis and uncertain mechanistic models was independent of parameter sampling strategy but strongly dependent upon network structural uncertainty. We tested our working hypothesis by analyzing a mechanistic model of the well-studied human extrinsic coagulation cascade. Overall state sensitivity coefficients generated using random and Latin Hypercube Sampling (LHS) were compared for two different perturbation sizes. Random and LHS sampling produced a qualitatively simi-

lar ranking of coagulation mechanisms as measured by the Spearman rank correlation for both small and large parameter perturbations. Sensitivity analysis of structurally defective coagulation networks was strongly influenced by false negative structural defects but tolerant to false positive errors. Surprisingly, no relationship was observed between network connectivity and the impact of structural errors. However, there was a linkage between the biological function of proteins and the impact of missing network structural information. When taken together, these results indicate that while parametric uncertainty can be partially overcome by sampling feasible parameter regions using one of several strategies, structural uncertainty remains a critical determinant of our ability to classify mechanisms as fragile or robust in networks relevant to human health.

3.2 Introduction

The role that mechanistic mathematical modeling and systems biology will play in molecular medicine and clinical development remains uncertain. Kitano suggested that understanding of critical questions in biology requires the integration of experimental and computational research [73]. Assmus *et al.,* and others maintain that analysis of the dynamics of human relevant networks using predictive computer models and high-throughput data generation will play an increasingly important role in medical research and the elucidation of disease mechanisms [76, 77]. However, mechanistic mathematical modeling at the cellular or network level has not been widely adopted as a data integration or knowledge generation platform in cell-biology, despite thoughtful discussion to the contrary [150]. The primary issue limiting the use of mathematical modeling in molecular medicine is uncertainty. The conventional wisdom is that

the data requirement to fully identify and validate mechanistic models is too large. Two schools of thought have emerged on the manner in which uncertain mechanistic models can be used to gain qualitative insight into the function of protein-protein and protein-DNA networks. Bailey hypothesized that critical qualitative properties of metabolic or signaling networks and perhaps even entire cells could be determined largely on the basis of network structure [151]. Certainly, there is literature evidence to support the Bailey hypothesis in metabolic networks [152, 153, 154, 155] and studies focused upon identifying the modularity of networks [85, 156, 157] have identified recurrent motifs that perhaps betray natural design principles. More recently, a second line of inquiry in the computational and systems biology community has focused upon extracting qualitative information about networks, for example the robustness of network interactions, using uncertain models and sensitivity analysis.

Sensitivity analysis is an enabling tool for the investigation of robustness and fragility in networks relevant to human health and more generally for model-based knowledge discovery. Robustness, a long-recognized property of living systems and networks, allows function in the face of uncertainty while fragility, i.e., extreme sensitivity, can potentially lead to catastrophic failure following seemingly innocuous perturbations [85, 158, 159, 160, 84]. Several researchers have used sensitivity analysis to better understand the robustness and fragility of metabolic and signalling networks [86, 87, 80, 89, 88, 161]. In the context of molecular medicine, sensitivity analysis has been used to predict fragile interactions involved in coagulation [162] and mammalian cell-cycle [163] where these fragile interactions were shown to be consistent with anti-coagulation and anti-cancer therapeutic strategies. The link between fragility and possible novel therapeutics has also been suggested by Kitano [164]. Sensitivity analysis has

also been used to integrate model identification and discrimination with optimal experimental design. Several optimal experimental design and model identification studies are resident in the literature [100, 101, 103, 104, 105, 165, 166] along with many techniques to estimate sensitivity coefficients for models composed of ordinary differential equations, differential algebraic and stochastic equations [167, 168, 169, 170, 171, 172, 173, 174, 175, 176].

In this study, we explore two open questions surrounding sensitivity-based knowledge discovery using uncertain network models, namely, the impact of parametric sampling strategies and the influence of network structural uncertainty on the determination of the qualitative importance of mechanisms involved in networks relevant to human health. We explore the working hypothesis that the determination of fragile and robust mechanisms using sensitivity analysis and uncertain mechanistic models is independent of the parameter sampling strategy but strongly dependent upon the fidelity of the network structure. We test our working hypothesis by analyzing a mechanistic model of the well-studied human extrinsic coagulation cascade developed and validated from literature [162] using two-different parameter sampling strategies in combination with sensitivity studies of structurally defective coagulation networks in which we systematically remove structural knowledge from the cascade. While the current development is restricted to coagulation, the broader strategy and conclusion drawn from this study may be applicable to other molecular networks with a similar cascade architecture, e.g., the MAPK cascade, Caspase activation cascade or the human complement system.

3.3 Results

The mechanistic extrinsic coagulation cascade model of Luan *et al.,* [162], used in this study, consisted of 92 proteins and 148 protein-protein interactions (Fig. 2.2.1 and Supplemental Materials). The Luan *et al.,* coagulation model was formulated using literature parameter values and was validated using 21 different *in-vitro* data sets taken from two different *in-vitro* coagulation models [116, 108, 115]. The robustness and fragility of mechanisms involved in TF-FVIIa initiated coagulation was determined by computing Overall State Sensitivity Coefficients (OSSCs) over a family of parameter sets constructed by randomly perturbing the published parameter set by up to ±50% (N=100, unless otherwise noted). To control for possible artifacts introduced because of random sampling and the choice of the perturbation size, we performed two sets of computational experiments in which the size of the parameter perturbation was varied along with the method used to generate the family of parameter sets explored. The role of structural uncertainty was explored by introducing structural *defects* into the coagulation network and then quantifying the shifts in the sensitivity ranking of interactions relative to the unperturbed control. The network structure was perturbed by the addition of single and multiple false positive and false negative defects. In the nominal network, sensitivity analysis of TF-FVIIa initiated coagulation predicted two key coagulation factors, FXa and FIIa, mediated the majority of fragile mechanisms while other coagulation factors, such as FIXa activity, were found to be moderately robust. These results were found to be independent of both the size of perturbation and the strategy used to generate the family of parameter sets sampled. Conversely, the ability to estimate the relative importance of interactions in the coagulation network was found to be strongly

dependent upon structural knowledge. While false positive defects had little effect, the introduction of false negative interactions, i.e., connections present in the control but missing in the defective networks, significantly impacted our ability to forecast the qualitative significance of mechanisms.

3.3.1 FXa and FIIa mediate fragile mechanisms in TF-FVIIa initiated coagulation.

Fragile mechanisms for TF-FVIIa initiated coagulation were previously reported by Luan *et al.,* [162] and are shown in Fig. 3.3.2A; four of the top five fragile mechanisms involved the binding or activation of fX/FXa with the fifth being platelet activation by FIIa. Other sensitive mechanisms included the formation of the FVa-FXa surface complex, the activation of thrombin by the FVa-FXa complex and the activation of surface or fluid phase fIX and fV. Fragility was spread across initiation and amplification mechanisms; 14/25 fragile mechanisms were upstream of the FVa-FXa or FVIIIa-FIXa surface complexes while the remaining 11/25 involved platelet activation, FVa-FXa activity and IIa inactivation. Binding interactions were found to be the majority of fragile mechanisms; 21/25 of the top fragile mechanisms were binding interactions. Six paired binding interactions were found to be sensitive indicating affinity was controlling in these cases; the exception was the TF-FVIIa-X and Va-P5s-Xa-P10s complexes where on-rate, catalytic turnover and off-rate were all found to be sensitive. Of the predicted robust mechanisms, the most non-intuitive were the formation and activity of the FVIIIa-FIXa surface complex responsible for FXa amplification.

3.3.2 The qualitative assessment of fragile and robust coagulation mechanisms was invariant to parameter sampling methodology.

The coagulation model parameters, although derived experimentally, do not equally well describe each of the 21 *in-vitro* data sets used to validate the model. Thus, a *family* of parameter sets, generated from the nominal set by random perturbation, was used to estimate the OSSC distributions shown in Fig. 3.3.2A. There were at least two potential drawbacks to random parameter sampling; first, there was no guarantee that all of the interesting behavior was sampled and similar behavior was likely oversampled and; second, perhaps a qualitatively different picture of how the TF-FVIIa initiated coagulation response varies with model parameters would have emerged if we employed a larger perturbation size, more parameter sets, etc.

We tested the working hypothesis that the determination of important interactions in coagulation using sensitivity analysis and uncertain mechanistic models was **independent** of the parameter sampling strategy. We compared the results of random sampling with Latin Hypercube Sampling (LHS) [177], which generates a distribution of plausible collections of parameter values from a multidimensional distribution, for two different perturbation sizes. OSSC values calculated using random parameter families constructed by perturbing the nominal parameter set by < ±50% (N=100; control-small) and < ±2-orders of magnitude (N=100; control-large) were compared with OSSCs generated using LHS over the same parameter ranges (maximum/minimum perturbation ±50% and ±2-orders of magnitude, Fig. 3.3.2B and 3.3.2C). Random and LHS

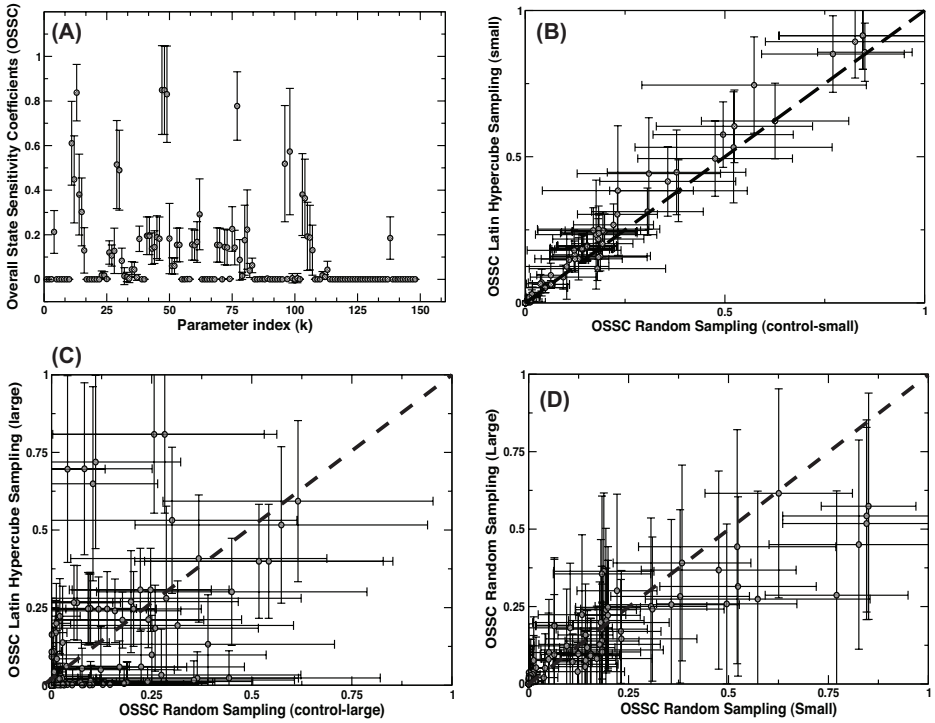

Figure 3.1: Parametric uncertainty studies using random and latin hypercube sampling strategies. (A) OSSC values for TF-FVIIa initiated coagulation generated using the random sampling over the small perturbation family (N=100;±50%). (B) Comparison of OSSC results for TF-FVIIa initiated coagulation for random versus latin hypercube sampling strategies for the small perturbation family (N=100;±50%). (C) Comparison of OSSC results for TF-FVIIa initiated coagulation for random versus latin hypercube sampling strategies for the large perturbation family (N=100;±2-orders of magnitude). (D) Comparison of OSSC results for TF-FVIIa initiated coagulation for small versus a large random sampling strategy (N=100)

sampling generated a qualitatively similar ranking of fragile and robust mechanisms with a Spearman rank of 0.98 (Fig. 3.3.2B) for the small-perturbation and 0.89 for the large-perturbation (Fig. 3.3.2C) when compared to the control, respectively. The small-versus large random-random perturbation had a Spearman rank of 0.96 (Fig. 3.3.2D) indicating that perturbation size was not a factor for the coagulation network. When taken together, the sampling results indicate, at least for the extrinsic coagulation network explored here, that the qualitative ranking of the importance of coagulation interactions was independent of the size and method of the perturbation used to generate the family of parameter sets sampled. These results were consistent with previous work by Stelling *et al.*, which showed similar ranking of parameters in models of circadian rhythm between exhaustive and random sampling [89].

3.3.3 The qualitative assessment of fragile and robust coagulation mechanisms was sensitive to false negative but robust to false positive interactions.

We tested the working hypothesis that the prediction of fragile and robust interactions in molecular networks was **dependent** upon structural fidelity by performing monte-carlo sensitivity analysis on four classes of structurally perturbed coagulation networks containing both false positive and negative interactions. In each of the structurally perturbed networks, unless otherwise noted, the nominal parameter set reported by Luan *et al.*, was used to generate a family of parameter sets ($N = 50$) by randomly perturbing each nominal parameter by $< \pm 50\%$. OSSCs were calculated for each of the structurally perturbed networks

and compared with the unperturbed parent network (control) by calculating the Spearman rank correlation.

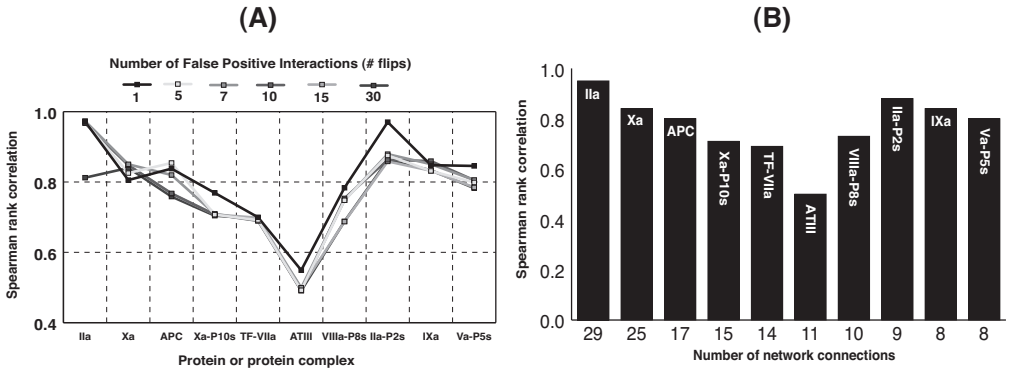

Figure 3.2: Impact upon the qualitative classification of interactions because of single and multiple false-positive structural defects. (A) Protein connectivity versus the Spearman rank correlation between structurally perturbed and control networks as a function of the number of false positive interactions. (B) Protein connectivity versus the Spearman rank correlation between structurally perturbed and control networks as a function of protein species for 30 false positive interactions.

Single and multiple false positive interactions in the coagulation network had a limited impact upon the classification of mechanisms as fragile or robust. The addition of single pairwise false positive binding interactions for 100 randomly generated defective networks (see methods) resulted in Spearman rank coefficients ranging from 0.96 to 1 (data not shown) when compared to the nominal network (control). Moreover, for multiple false positive interactions, the Spearman rank correlation was invariant to the number of structural defects introduced into the cascade. Over the top ten connected species, the Spearman rank between the perturbed and unperturbed networks showed small variation (< 0.02) within individual species as the number of defects increased from 1 to 30, with the exception of IIa and IIa-P2s (Fig 3.3.3A). Conversely, large variation in the spearman rank was observed between different species; the average

spearman rank over all defects for free and bound thrombin was 0.94 and 0.88, while the inhibitors, ATIII and APC, showed 0.50 and 0.80 correlation, respectively. While no obvious relationship was observed between the spearman rank and the connectivity of the species in false-positive networks (Fig. 3.3.3B), a correlation between the biological function and shift in spearman rank was observed. Structural uncertainty in initiation factors such as TF-FVIIa, resulted in average spearman rank over all trials of 0.69 ± 0.004, and the spearman rank coefficients for control elements such as ATIII and APC were 0.50 ± 0.023 and 0.80 ± 0.042, respectively. On the other hand, components involved in the amplification of the thrombin signal, e.g., IIa, IIa-P2s, Va-P5s, or VIIIa-P8s were less effected with an average spearman rank of 0.82. Thus, structural uncertainty in mechanisms mediating the initiation of coagulation and control elements restraining the cascade was more influential than uncertainty in amplification interactions.

Single and multiple simultaneous false-negative structural defects hindered or destroyed the ability to correctly classify coagulation interactions as fragile or robust. OSSC values calculated for 15 different coagulation networks corrupted with single pairwise false-negative defects (see methods) were compared to the unperturbed network using the Spearman rank correlation over a family of random parameters sets (N=50, ±50%). While the influence of single false-negative interactions was dependent upon which proteins or protein complexes were affected, no obvious connection with reaction connectivity was observed (Fig. 3.3). The largest shift in Spearman rank occurred when platelet activation was disrupted (correlation of 0.68) while the other 14 mechanisms selected had an average Spearman rank of 0.89 ± 0.04, indicating that on average 90% of the mechanisms would have been classified correctly in the structurally defective

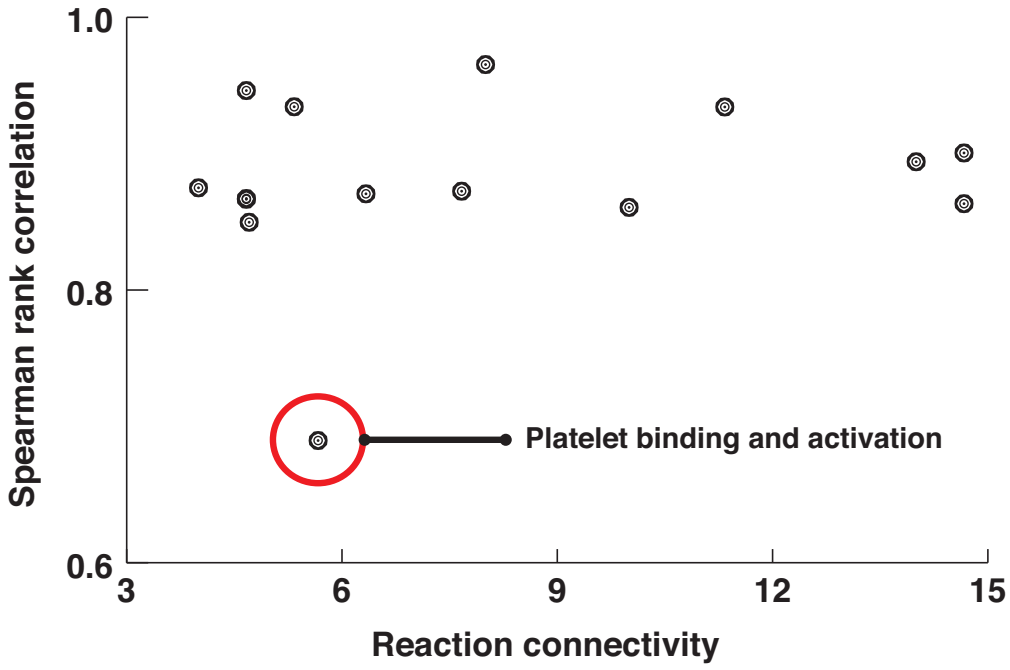

Figure 3.3: Impact upon the classification of coagulation interactions following the introduction of single pairwise false-negative structural defects.

networks. Although single pairwise false-negative defects had a limited impact upon the classification of coagulation mechanisms, multiple simultaneous false-negative interactions destroyed the ability to classify mechanisms as fragile or robust. OSSC values generated for 2- (Fig. 3.3.3A), 4- (Fig. 3.3.3B) and 8- (Fig. 3.3.3C) partitions showed statistically significant deviation from the unpartitioned control, where the Spearman rank correlation for the partitioned networks was found to be inversely proportional to the number of partitions (Fig. 3.3.3D). Partitioned subnetworks, independent of parameter values, displayed a similar *fracture pattern* versus the control where mechanisms important in the control were no longer sensitive in the subnetwork and vice-versa. Consider the 4-partitioned case (Fig. 3.3.3B). The 4-partitioned subnetworks (37 ± 5 interactions in each partition) had a global cut of 8 proteins, including TF-FVIIa, FXa and FIIa. Interestingly, only 30% of the statistically significant

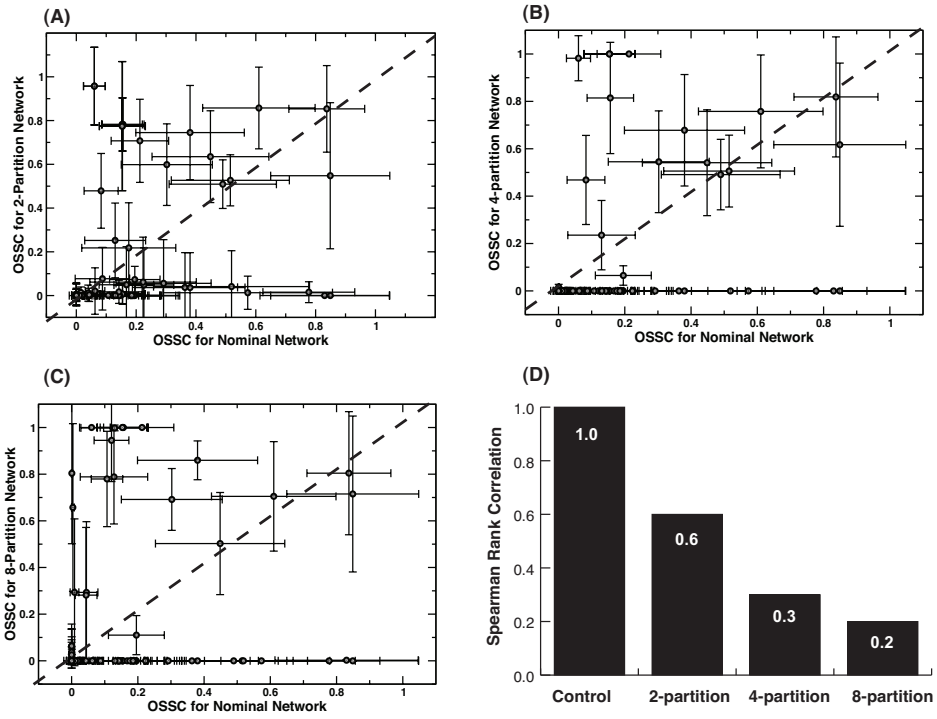

Figure 3.4: Impact of multiple false-negative structural defects upon the qualitative classification of interactions in the network. The coagulation cascade was partitioned into 2, 4 or 8 connected subnetworks using hMetis and screened for fragile and robust mechanisms using a random parameter family (N=100; ±50% perturbation). The partitioned subnetworks were compared to the unpartitioned control over the same family of random parameter sets; the 45^o dashed-line indicates perfect correlation. (A) OSSC values for the unpartitioned control versus the 2-partitioned subnetwork. (B) OSSC values for the unpartitioned control versus the 4-partitioned subnetwork. (C) OSSC values for the unpartitioned control versus the 8-partitioned subnetwork. (D) Spearman rank correlation as a function of the number of partitions.

fractured interactions involved cut proteins as reactants, thus, more complex interactions were responsible for up- or downplaying the importance of significant mechanisms. Conversely, a core subset of interactions were predicted to be important in both partitioned and unpartitioned networks, e.g., interactions

involving TF-FVIIa activity. However, the persistence of these key interactions as fragile mechanisms across 2-, 4- and 8-partitions could have been an artifact of the partitioning as hMetis solutions are not deterministic.

To test for partitioning artifacts, ten different 4-partitioned subnetworks were constructed and OSSC values were calculated over the same random parameter family as the original partitioning studies (Fig. 3.5). The average Spearman rank for the family of 4-partitioned subnetworks when compared to the original was 0.87 ± 0.07 indicating that on average 80 - 94% of the mechanism ranking was conserved across different partitioning trials. The persistent interactions associated with TF-FVIIa activity appeared on average 70% ± 19%, indicating these interactions were independent of partitioning.

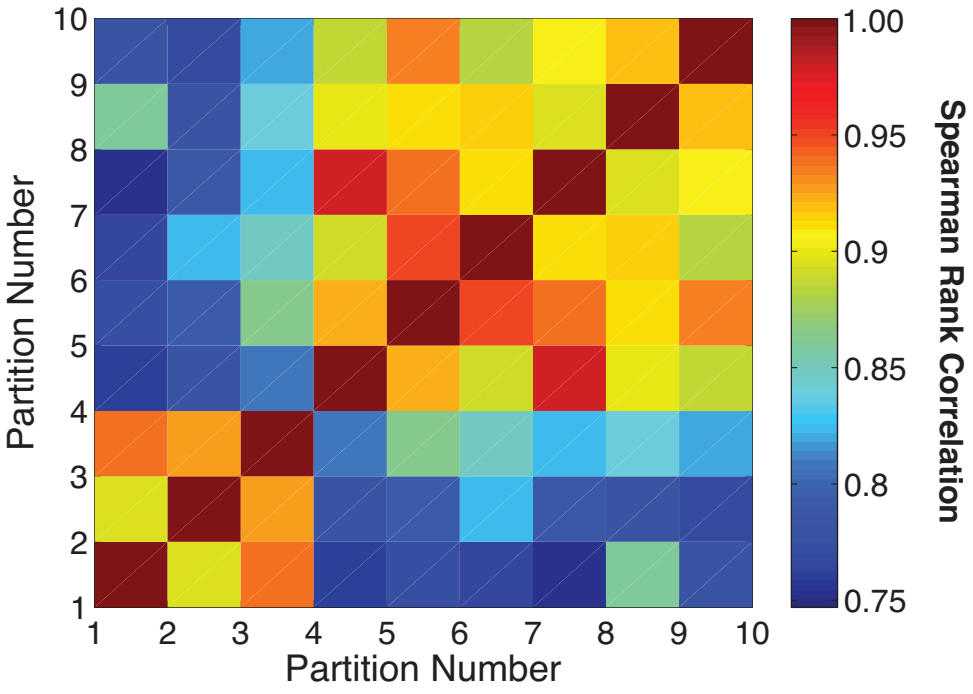

Figure 3.5: Pairwise Spearman Rank Correlation for the estimated OSSC distributions calculated for ten different 4-partitioned coagulation networks over the same family of random parameter sets.

3.4 Discussion

Consistent with the conclusions drawn by Nayak *et al.,* [163] and the hypothesis of Kitano [164], the predicted fragile mechanisms in TF-FVIIa initiated coagulation are molecular targets in current anticoagulation preclinical development, clinical therapies and clinical trials. Four of the top five fragile mechanisms involved fX/FXa or the activation of platelets by FIIa. Anti-fX/FXa and Direct Thrombin Inhibitors (DTIs) are two important classes of anticoagulants. Fondaparinux, a 1.7 kDa pentasaccharide which selectively binds ATIII, is approved for the prevention of venous thromboembolism following hip fracture surgery, total hip replacement, total knee replacement and major abdominal surgery in addition to the initial treatment of patients with Deep Venous Thrombosis (DVT) and Pulmonary Embolism (PE) [118, 119, 120, 178, 121, 122]. Fondaparinux increases the natural inhibitory effect of ATIII against FXa approximately 300-fold [123, 124]; selective inhibition of FXa by fondaparinux interrupts thrombin generation and clot formation without inactivating thrombin itself [125, 126]. Elalamy and coworkers showed in a whole blood *in-vitro* assay that fondaparinux prolonged the lag time of prothrombin activation for all concentrations explored, and for physiologically relevant concentrations (0.11 - 0.28 anti-FXa IU/ml), reduced the maximal rate of thrombin formation to approximately 47 - 55% of its nominal value [127]. Herbert and colleagues explored fondaparinux and the sulfated analog SANORG 32701 in *in-vivo* mouse, rat and rabbit coagulation models [128, 129]; SANORG 32701 has a high-affinity for ATIII ($K_d = 3.7 \pm 0.7$ nmol/L) and shows more potent anti-FXa activity (1100 ±31 versus 850 ± 21 U/mg for fondaparinux). Direct Thrombin Inhibitors (DTIs) have also been explored as anticoagulants [130]. Thrombin activity is

mediated by three protein domains; an active site catalyzing protease activity and two exosites controlling substrate binding [131]. Our sensitivity analysis predicts thrombin activation of platelets is a key mechanism; Sarich *et al.,* have explored the DTI ximelagatran in healthy male subjects [132]. Thrombin generation, platelet activation and the thrombin-antithrombin complex were monitored in shed blood collected from skin incisions in 120 healthy male volunteers following oral administration of ximelagatran. Oral ximelagatran showed a rapid and statistically significant decrease in all endpoints relative to control. When taken together, the fondaparinux, SANORG 32701 and ximelagatran results present a clinical basis in both *in-vitro* and *in-vivo* coagulation studies for the prediction that fX/FXa and IIa are fragile components of the coagulation architecture.

Mechanisms involving fIX/FIXa, consistent with multiple lines of experimental evidence, were predicted to be moderately robust. Feuerstein *et al.,* explored inhibition of fIX/FIXa using a murine anti-fIX/FIXa antibody (BC2) in a male sprague-dawley rat model [133]. The fIX/FIXa activity and the Activated Partial Thromboplastin Time (aPTT) endpoints were monitored *ex-vivo* following IV-infusion of the BC2 antibody. Feuerstein *et al.,* found that fIX/FIXa activity could be reduced by as much as 2.5-fold before any significant change in the aPTT was observed; only after > 90% of the fIX/FIXa activity was eliminated was there a 3.5 - 4 fold increase in aPTT. Benedict *et al.,* explored the contribution of fIX/FIXa to intravascular thrombosis in a canine coronary thrombosis model [134]. Animals received an IV-bolus of saline (vehicle), bovine glutamyl-glycyl-arginyl-FIXa (FIXai; a competitive inhibitor which prevents the assembly of the FVIIIa-FIXa complex [136, 135, 137]), bovine fIX or heparin. Animals that received saline or bovine fIX developed a coronary occlusion due to a fib-

rin/platelet thrombus in approximately 1 hr, conversely, FIXai decreased coronary thrombus occlusion in a dose dependent manner. However, FIXai administration was not accompanied by increased bleeding at abdominal and chest-wall incision sites leading Benedict *et al.*, to conclude, consistent with the earlier work of Weiss and Lages [138], that direct TF-FVIIa mediated activation of fX may be the primary mechanism of fX activation in blood obtained from bleeding wounds. While our prediction that FVIIIa-FIXa mediated fX activation is robust is consistent with Benedict *et al.*, the robustness of fIX mechanisms should be further explored using *in-vivo* animal models or cell-based assays to control for artifacts introduced by the synthetic plasma model.

The capability to gather cellular protein-protein and protein-DNA interaction data has far outstripped our ability to understand it. Transforming large-scale interaction data sets e.g., the B-cell interactome compiled by Califano and coworkers [179], into a better cell or a new therapy requires tools to extract the qualitatively significance of protein-protein and protein-DNA interactions. The sampling and structural fidelity studies reported here support the Bailey hypothesis that network structure is a critical factor in our ability to extract qualitative information about a network or system. The sampling results suggest that given even an approximate parameter set it is possible to overcome parametric uncertainty by sampling regions of parameter space with one of many possible strategies. Clearly, the more critical issue is structural uncertainty. Single false positive and false negative structural defects were shown to have little impact. Moreover, multiple false positive interactions appeared to have limited influence with exception of particular inhibitors. However, multiple false negative structural defects made it impossible to infer the qualitative significance of interactions. Unfortunately, protein-protein and protein-DNA interactions de-

rived both computationally and experimentally are prone to both false positive and false negative errors. The Yeast Two-Hybrid (Y2H) system [180, 181, 91, 92], Fluorescence Resonance Energy Transfer (FRET) [182], quantitative Mass Spectrometry (MS) proteomic or Chromatin Immunoprecipitation (ChIP)-DNA microarray techniques [183, 93, 94, 95] have all been used to identify *in-vivo* binding interactions. Computational techniques have also contributed significantly to network identification [184, 185]. However, Y2H assays are prone to false-positive predictions e.g., in some cases >50% of the reported interactions are false positives [185]. Moreover, Bork reported that none of the genomics methods for detecting connections cover more than 60% of the proteins in the yeast genome and most are biased toward evolutionarily old, highly abundant proteins that are localized in specific subcellular locations [186]. Bader and coworkers have estimated that in yeast 25 - 45% of the reported interactions are likely false positives and the false negative rates for worm and fly are possibly as high as 75% and 90%, respectively [187]. When taken together, our results suggest that using monte-carlo sensitivity analysis to explore large structurally uncertain networks, especially networks corrupted with false negative interactions, is likely to produce a small number of correct classifications dispersed among many false results. Until interaction identification tools produce interaction maps with a higher degree of fidelity, sensitivity analysis will likely have to be limited to hand annotated networks.

3.5 Conclusions

In this study, we explored two open questions surrounding sensitivity-based knowledge discovery using uncertain network models, namely the impact of

parametric sampling strategies and the influence of network structural uncertainty. We showed that conclusions drawn from monte-carlo sensitivity analysis of the human coagulation cascade were largely invariant to the method used to generate the family of parameter sets sampled and the size of the parameter perturbation used. However, structural defects strongly influenced the qualitative conclusions drawn from sensitivity analysis. The introduction of single and multiple false positive defects showed limited impact on the classification of mechanisms as fragile or robust. Moreover, the introduction of single false negative structural defects did not have a great influence upon the classification of interactions in the control. However, multiple simultaneous false negative interactions introduced by partitioning the coagulation network into 2-, 4- and 8-partitions greatly altered conclusions drawn from our analysis. Thus, these results indicated that while parametric model uncertainty can be partially overcome by sampling feasible parameter regions using one of several strategies, structural uncertainty remains a critical determinant of our ability to classify mechanisms as fragile or robust.

3.6 Methods

3.6.1 Formulation of the model equations.

The human extrinsic coagulation model of Luan *et al.*, composed of 92 proteins and 148 protein-protein interactions, was used in this study [162]. Mass balance equations were written around each protein or protein complex yielding the set

of differential equations (vector-form):

$$\frac{d\mathbf{x}}{dt} = \mathbf{S}\mathbf{r}\left(\mathbf{x}, \mathbf{k}\right) = \mathbf{g}\left(\mathbf{x}, \mathbf{k}\right) \qquad \mathbf{x}\left(t_o\right) = \mathbf{x}_o \tag{3.1}$$

The symbol $\mathbf{S}$ denotes the stoichiometric matrix, $\mathbf{x}$ denotes the concentration vector of proteins or protein complexes, $\mathbf{r}\left(\mathbf{x}, \mathbf{k}\right)$ denotes the vector of interaction rates and $\mathbf{k}$ denotes the parameter vector. Each row in $\mathbf{S}$ describes a particular protein or protein complex while each column describes the stoichiometry associated with a specific interaction in the network. Thus, the (i, j) element of $\mathbf{S}$, denoted by σ_{ij}, describes how protein i is connected to rate process j. If $\sigma_{ij} < 0$, then protein i is consumed in r_j, conversely, if $\sigma_{ij} > 0$ protein i is produced by r_j and if $\sigma_{ij} = 0$ there is no connection between protein i and rate process j. We have assumed mass action kinetics for each interaction in the network; under the mass action assumption the rate expression for protein-protein interaction q:

$$\sum_{j \in \left\{\mathbf{R}_q\right\}} \sigma_{jq} x_j \rightarrow \sum_{p \in \left\{\mathbf{P}_q\right\}} \sigma_{pq} x_p \tag{3.2}$$

is given by:

$$r_q\left(\mathbf{x}, k_q\right) = k_q \prod_{j \in \left\{\mathbf{R}_q\right\}} x_j^{-\sigma_{jq}} \tag{3.3}$$

where $\left\{\mathbf{R}_q\right\}$ denotes the set of reactants for reaction q, $\left\{\mathbf{P}_q\right\}$ denotes the product set for reaction q, k_q denotes the rate constant governing the qth interaction and σ_{jq}, σ_{pq} denote stoichiometric coefficients (elements of the matrix $\mathbf{S}$). We have treated every protein-protein interaction and catalytic mechanism as non-negative. All reversible interactions were split into two irreversible steps, thus, every element of the reaction rate vector $\mathbf{r}\left(\mathbf{x}, \mathbf{k}\right)$ took the form shown in Eqn. 5.3. The model equations were solved using the LSODE routine of the OCTAVE programming environment (v2.9.9; www.octave.org) on an Apple Computer MacOSX (Cupertino, CA; v10.4.8) workstation.

3.6.2 Computation of overall state sensitivity coefficients.

The sensitive or fragile interactions of the coagulation architecture were determined by computing Overall State Sensitivity Coefficients (OSSC) [89]. Because each parameter corresponds directly to a particular molecular interaction in the cascade, OSSC values were used to gauge which interactions were qualitatively important. Large OSSC values for interactions relative to their peers indicated fragility or sensitivity while small OSSC values indicated robustness. The OSSC value for interaction j was defined as:

$$O_j(t) = \frac{k_j^*}{N_S}\left(\sum_{h=1}^{N_T}\sum_{i=1}^{N_S}\left[\frac{1}{x_i^*}\frac{\partial x_i}{\partial k_j}\bigg|_{t_h}\right]^2\right)^{1/2} \tag{3.4}$$

where N_T denotes the number of time points used in the simulation while N_S denotes the number of proteins/protein complexes in the model. The first-order sensitivity coefficients:

$$s_{ij}(t_h) = \frac{\partial x_i}{\partial k_j}\bigg|_{t_h} \tag{3.5}$$

were computed by solving the differential equation:

$$\frac{d\mathbf{s}_j}{dt} = \mathbf{A}(t)\,\mathbf{s}_j + \mathbf{b}_j(t) \qquad j = 1, 2, , N_P \tag{3.6}$$

subject to the initial condition $\mathbf{s}_j(t_0) = \mathbf{0}$. In Eqn. 5.8, the quantity j denotes the parameter index, N_P denotes the number of parameters, $\mathbf{A}$ denotes the Jacobian matrix of the model equations and $\mathbf{b}_j$ denotes the jth column of the matrix $\mathbf{B}$, which contains first-derivatives of the mass balances w.r.t. the parameter values. The quantity $\mathbf{s}_j$ denotes the vector of first-order sensitivity coefficients w.r.t parameter j. The Jacobian matrix ($\mathbf{A}$) and the matrix of first-derivatives of the mass balances w.r.t the parameter values ($\mathbf{B}$) are given by:

$$\mathbf{A} = \frac{\partial \mathbf{g}}{\partial \mathbf{x}}\bigg|_{(\mathbf{x}^*,\mathbf{k}^*)} \qquad \mathbf{B} = \frac{\partial \mathbf{g}}{\partial \mathbf{k}}\bigg|_{(\mathbf{x}^*,\mathbf{k}^*)} \tag{3.7}$$

where $(\mathbf{x}^*, \mathbf{k}^*)$ denotes a point along the *nominal* or *unperturbed* system solution. The matrices **A** and **B** were numerically estimated at each time step using a generalized gradient algorithm [148] while the sensitivity balances were solved using the LSODE routine of the OCTAVE programming environment (v2.9.9; www.octave.org) on an Apple Computer MacOSX (Cupertino, CA; v10.4.8) workstation.

3.6.3 Statistical analysis of the shifts in overall state sensitivity coefficients.

Three different tests were performed to identify large statistically significant shifts in OSSC values between defective networks and the control. A Welch t-test [149] was used to find all statistically significant shifts resulting from the different structural perturbations and then a secondary test on the $z-$score of each shift was preformed to find only the most prominent. The OSSC values calculated over the family of parameter sets were assumed to follow normal distributions for all cases. The statistical significance of shifts in OSSC values relative to the control were determined by performing a Welch t-test with the null hypothesis that the means of the sensitivity coefficients were equal at a 1% significance level. The Welch t-test is similar to the student t-test with the exception that the two distributions being compared are not required to have equal variances. The list of significant OSSC values was further restricted to only those shifts with a magnitude larger than a specified z-score (0.1) away from the squared mean displacement relative to the control:

$$d_{j,q} = \left(\bar{O}_j^q - \bar{O}_j^c\right)^2, \qquad j = 1, 2, , N_P \tag{3.8}$$

where $\bar{O}_j^c$ denotes the mean OSSC value over the family of parameter sets for parameter j in the control while $\bar{O}_j^q$ denotes the same quantity for defective case q. A significant shift in OSSC value was *accepted* if:

$$d_{j,q} > z\sigma_{d_q} + \mu_{d_q} \tag{3.9}$$

where z denotes a desired z-score, σ_{d_j} denotes the standard deviation of the total displacement over all significant OSSC values for the *qth* defective case and μ_{d_q} denotes the mean of the significant displacements for the structurally defective case q.

A large statistically significant shift in OSSC value, while indicative of the shifting importance of an interaction, does not guarantee that an interaction is ranked differently between cases. To this end, we used the Spearman rank correlation denoted by ρ and defined as:

$$\rho = 1 - \frac{6\sum_{i=1}^{N_P} d_i^2}{N\left(N^2 - 1\right)} \tag{3.10}$$

to measure the difference in qualitative ranking between cases. The quantity d_i denotes the difference in the ordinal rank of interaction i between a structurally defective network and the control, N denotes the number of pairs of values and N_P denotes the number of parameters considered. The Spearman rank is bounded by $-1 \leq \rho \leq 1$; a Spearman rank of one indicates that two ranked lists are identical, a Spearman rank equal to negative one indicates that two ranked lists are perfectly negatively correlated, while a Spearman rank of zero indicates that two ranked lists are uncorrelated.

3.6.4 Generation of structurally perturbed coagulation networks.

Single pairwise false positive binding interactions were added to the coagulation model by generating a single binding connection between two randomly selected proteins. A family of structurally defective models was constructed (N=100), where each model contained a single false-positive interaction. Sensitivity analysis was conducted on each of the models using only the nominal parameter set. The Spearman rank correlation between each of the structurally perturbed networks and the control was calculated to estimate the effect of adding the false-positive interaction. The 10 models with the lowest Spearman rank, i.e., the largest degree of disruption were then selected for further study. To control for possible artifacts stemming from the use of only the nominal parameter set, a parameter set family (N=50) was constructed by randomly perturbing each of the nominal parameters by $< \pm 50\%$. Sensitivity analysis was conducted using the worst 10 models where sensitivity coefficients were computed for each model and parameter set.

Multiple false positive binding and catalytic errors were introduced into the coagulation network by randomly modifying the mass balance equations of the ten most connected proteins. The connectivity of the top ten connected proteins, free and bound thrombin, two inhibitors (ATIII and APC), five upstream coagulation factors (free FIXa and FXa and bound FVa, FVIIIa, and FXa), and one initiating complex (FVIIa-TF), was manipulated by adding either 1, 5, 7, 10, 15 or 30 false positive interactions to the stoichiometric matrix. The same monte-carlo procedure was used for each of the connected species. First, a species was selected from the list of connected proteins (row i) along with a random interac-

tion in the network (column j). Second, a discrete number of randomly selected zero stoichiometric coefficients (σ_{ij}) in column j were flipped from 0 to 1 where different columns were selected for each number of false positives. For example, if column j_1 was selected and stoichiometric coefficients were flipped, then column $j_2 \neq j_1$ would be selected for the next iteration of the algorithm. Because our sampling protocol connected multiple previously unconnected proteins together via random interactions, we did not consider cases where the mass balance of more than one of the connected proteins was explicitly manipulated simultaneously. Sensitivity analysis was conducted on each of the structurally perturbed models using the nominal parameter set only.

Networks with single false negative structural errors were constructed by removing a single protein-protein interaction from the network. Each of the 148 interactions were removed, in turn, and sensitivity analysis was conducted, using the nominal parameter set, on each of the structurally defective networks. The difference in the ranking of interactions between the structurally perturbed networks and the control was quantified using the Spearman rank correlation. The 15 networks with the lowest Spearman rank, i.e., the largest degree of disruption were then selected for further study. To control for possible artifacts stemming from the use of only the nominal parameter set, a parameter set family (N=50) was constructed by randomly perturbing each of the nominal parameters by $< \pm 50\%$. Sensitivity analysis was conducted using the worst 15 models where sensitivity coefficients were computed for each model and parameter set.

Simultaneous false negative errors were investigated by partitioning the extrinsic coagulation network into 2-, 4- and 8-partitions using hMetis [188]. hMetis partitioned the coagulation network by minimizing the number of

shared proteins or protein complexes employed across partitions where any given protein-protein interaction was resident in a single partition. Thus, the partitioned subnetworks represent cases where defects, i.e., missing structural information, has been introduced into the network; the larger the number of partitions the more defects in the network. Sensitivity analysis was conducted on each partitioned subnetwork in isolation using a random parameter set family (N=50) where each of the nominal parameters was perturbed by < ±50%.

3.6.5 Calculation of protein and interaction connectivity.

The connectivity of the *i*th protein or protein complex, denoted by C_{x_i}, was calculated by summing the absolute values of the stoichiometric coefficients (σ_{ij}) from the corresponding row of the stoichiometric matrix:

$$C_{x_i} = \sum_{j=1}^{N_S} \left|\sigma_{ij}\right| \qquad i = 1, 2, , N_S \tag{3.11}$$

The connectivity of reaction j, denoted by C_{r_j}, was taken to be the average connectivity of the proteins or protein-complexes involved in the reaction:

$$C_{r_j} = \frac{1}{N_{r_j}} \sum_{i \in \{\mathbf{R}_j \cup \mathbf{P}_j\}} C_{x_i} \qquad j = 1, 2, , N_R \tag{3.12}$$

where N_{r_j} denotes the total number of reactants and products associated with reaction j and N_R denotes the number of interactions in the network.

CHAPTER 4

A MATHEMATICAL MODEL SUCCESSFULLY PREDICTS THROMBIN GENERATION IN PATIENT-DERIVED PLASMA

4.1 Abstract

The complex system regulating hemostasis, as well as an increasing number of inherited and acquired conditions associated with their dysregulation, need to be understood fully before meaningful clinical development can take place. Mechanistic mathematical modeling plays a significant role in the development of new therapies for a number of diseases. In this study, a mechanistic model, composed of 193 proteins and 301 protein-protein interactions, was built to describe the complex hemostatic system. A family or *ensemble* of probable parameter sets were estimated using nine experimental data sets from a cell-based model. The model and the parameter ensemble was used to predict the thrombin generation in experiments using patient-derived plasma from coronary artery and hemophilia A patients. In experiments, thrombin generation in platelet-rich plasma from 4 coronary artery patients who are on aspirin treatment and in platelet-poor plasma from healthy and hemophilia A patients was initiated by the addition of tissue factor. The mean model predictions over the parameter ensemble were generally consistent with the experimental observations with a normalized standard error less than 30% and a correlation greater than 0.66. Furthermore, in order to study the initiating effects of TF-FVIIa and FVIIa only, the model was used to predict thrombin concentrations following the addition of 25 pM TF-FVIIa or 120 nM FVIIa to the synthetic plasma with platelets. The mean model predicted values agreed well with the experiments

as proved by a normalized error of less than 22 % and a correlation greater than 0.85. Sensitivity analysis revealed that the propagation of thrombin could be highly influenced by the perturbation in the parameter values in the TF-FVIIa initiating case, while the initiation of thrombin generation were profoundly affected by the perturbation in the parameter values in the FVIIa initiating case.

4.2 Introduction

Factor VIII (fVIII) and factor IX (fIX) are the X-chromosomally encoded coagulation factors which are deficient in hemophilia A and B, respectively [24]. The frequency of hemophilia A is often stated to be 1 in 5,000-10,000 male births; while hemophilia B occurs at about 1 in about 35,000-50,000 male births [25]. The existence of hemophilia was noted very early in the medical literature, and has been a prime stimulus for attempts to understand the mechanism of blood coagulation. Bleeding in hemophilia A and B correlates well with the residual level of the coagulation activity in the patient's plasma [25]. A hemophilia patient do not bleed more intensely than a normal person, but for a much longer amount of time. In severe hemophiliacs even a minor injury could result in blood loss lasting days, weeks, or not ever healing completely. The critical risk here is with normally small injuries which, due to missing coagulation factors, take long times to heal. In areas such as the brain or inside joints this can be fatal or permanently debilitating. The bleeding with external injury is normal, but incidence of late re-bleeding and internal bleeding is increased, especially into muscles, joints, or bleeding into closed spaces. Major complications include hemarthrosis, hemorrhage, gastrointestinal bleeding, and menorrhagia.

Though there is no cure for hemophilia, it can be controlled with regular infusions of the deficient clotting factor, i.e. fVIII in hemophilia A or fIX in hemophilia B. Replacement therapy markedly improves the management of bleeding of most patients with hemophilia. However, fVIII and fIX inhibitors have developed in 18-32% and 2-3% of hemophiliacs A and B in response to fVIII and fIX, respectively [28] and those inhibitors make the subsequent management of patient, using coagulation factor concentrates, difficult. In the 1980s, activated prothrombin complex concentrates (aPCC) from pooled plasma were developed for hemophiliacs with inhibitors, assuring 'fVIII bypassing activity' [29, 30]. However, aPCCs induce disseminated intravascular coagulation syndromes or acute myocardial infarction [31]. Recently, recombinant factor VIIa (rFVIIa) was developed as a new bypassing agent, and its clinical efficacy and safety have been established [32, 33]. Hemophilia patients with inhibitors most frequently bleed in the joints. Clinical data have demonstrated that rFVIIa has a response rate of 91% in joint bleeds and 86% in muscle bleeds in as few as 5 hours [189]. rFVIIa has also been shown to effectively control bleeding during surgical procedures in people with inhibitors. Four separate studies involving more than 200 procedures showed that rFVIIa was effective and safe [189]. However, because of its short half-life, therapy with rFVIIa requires frequent administration (at intervals of 2-3 h) to achieve hemostasis and therapeutic dose of rFVIIa is not always predictable [28].

Both bypassing products (aPCC and rFVIIa) have been shown to be effective, to some extend, in treating hemophilia with inhibitors [190]. Yet their hemostatic efficacy can be difficult to predict [28] and does not reach the overall success rates obtained with replacement therapy in patients without inhibitors [191]. Furthermore, responsiveness to bypassing therapy may change from one

bleed to the next in the same patient and even from hour to hour during the course of a single bleeding event. Thus, sequential use of bypassing agents was proposed to treat bleeding disorder, especially refractory bleeds [192, 193, 194]. However, increased risk for thrombosis is often a concern of using such therapy; this aggressive therapy was recommended to use only in the inpatient setting with careful monitoring of the physical examination and frequent laboratory screening to assess for thrombosis [195, 30].

Given all the difficulties faced in treating hemophiliacs, the lack of understanding the principal mechanism of action of all these agents could be one of the obstacles in developing effective treatment regimes. For example, it is generally believed that the mechanism of action of rFVIIa is either TF-dependent or TF-independent. Both mechanisms have their experimental evidence; thrombin generation could be activated by small amount of TF-FVIIa or large amount of FVIIa only [196, 197, 198, 199, 200, 32, 115, 201]. Thus the understanding of mechanism of action of rFVIIa could provide some insights into determining the therapeutic dosages in different pathological conditions. Furthermore, the potential synergy of rFVIIa and APCCs is proposed to treat hemophilia in more complex conditions [194].

In order to study the complex system regulating hemostasis, our group previously built a mechanistic model with 92 proteins and 148 protein-protein interactions [162]. The model was validated using published datasets generated from synthetic plasma and a cell-based model. However, in order to fit datasets from both experiments, 3 kinetic parameters were modified. Here in the study, we modified our previous model using more realistic interactions for platelet activation and more involving proteins. The new model, with 193 protein and

301 protein-protein interactions, was trained using nine cell-based experiment measurements that were more representative to the *in vivo* conditions.

4.3 Results

The mechanistic model was formulated based on our previous coagulation model [162] with additional interactions describing platelets activation via PARs, the intrinsic pathway, etc (see supplementary table). A family or *ensemble* of probable parameter sets (N = 437) were estimated using nine experimental data sets from a cell-based model [29]. The model predictions and the training data sets were shown in Figure 4.1. As the results of training with the experiment data, a normalized standard error less than 30% and a correlation greater than 0.66 (Table 4.1) were observed for the mean model predictions over the parameter ensemble. The model and the parameter ensemble was used to predict the thrombin generation in experiments using patient-derived plasma for coronary artery and hemophilia A patients. In experiment, thrombin generation in platelet-rich plasma from 4 coronary artery patients who are on aspirin treatment and in platelet-poor plasma from healthy and hemophilia A patients was initiated by the addition of tissue factor. As shown in Figure 4.2, the model successfully predicted thrombin generation in patient-derived plasma with the error quantifications shown in Table 4.1. Furthermore, in order to study the initiating effects of TF-FVIIa and FVIIa only, the model was used to predict thrombin concentrations following the addition of 25 pM TF-FVIIa or 120 nM FVIIa to the synthetic plasma with platelets. The mean model predicted values agreed well with the experiments as proved by a normalized error of less than 22 % and a correlation greater than 0.85. Sensitivity analysis revealed that the propagation

of thrombin could be highly influenced by the perturbation in the parameter values in the TF-FVIIa initiating case, while the initiation of thrombin generation were profoundly affected by the perturbation in the parameter values in the FVIIa initiating case.

4.3.1 The model predicted thrombin generations in patient-derived plasma.

Computational simulations and experimental observations from a cell-based model [29] and from an analysis of patient plasma were shown in Figure 4.1 and Figure 4.2, respectively. To address uncertainty in the model parameters, we estimated a family or *ensemble* of parameter sets that minimized errors between model simulations and the training data sets. Nine data sets with different concentrations of rFVIIa and prothrombin in the presence and absence of fVIII and fIX from a cell-based model were selected to train the model (Figure 4.1). Parameter values were adjusted to minimize the squared error between model simulations and experimental measurements. We obtained an ensemble of parameter sets (N = 437).

In each figure, the dashed lines in each case denote the mean simulated values over the ensemble of model parameters while the shaded regions denote one ensemble standard deviation (N = 437). A typical thrombin generation consists of three phases: the initiation, the propagation and the termination [202, 203]. It is generally believed the initially formed thrombin is produced upon the cleavage of prothrombin by fluid phase activated factor X (FXa) [200]. The picomolar amount of initially formed thrombin activates cofactors factors

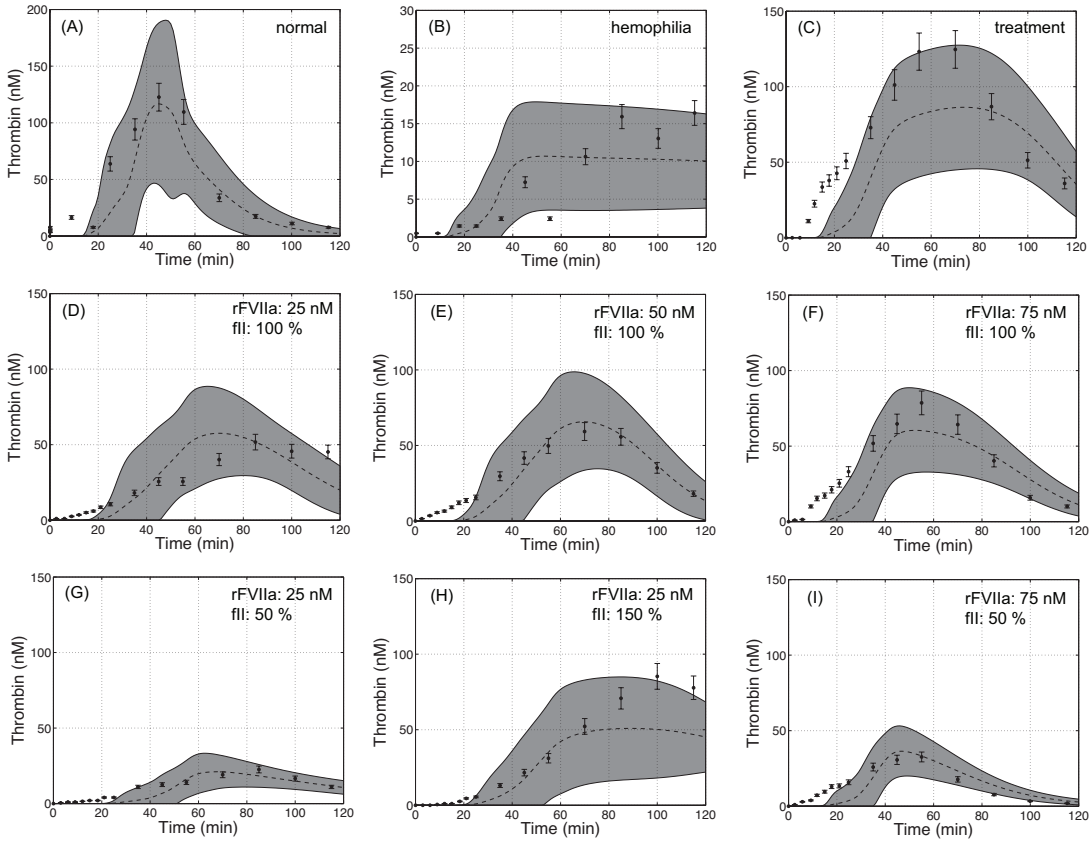

Figure 4.1: Comparison of model simulations versus training data from a cell-based model. The dashed lines in each case denote the mean simulated value over the ensemble of model parameters while the shaded regions denote one ensemble standard deviation (N = 437). Experimental data are shown with error bars (10% of the experimental values). The quantified errors are shown in Table 4.1.

V and VIII (fV and fVIII) and platelets, resulting in the formation of surface complexes *tenase* and *prothrombinase*. Massive prothrombin activation occurs as the results of interactions on activated platelet surface during the propagation phase. This is followed by the termination phase in which the reactions of the coagulation cascade subside and thrombin is consumed by the dynamic inhibitor APC and the potent thrombin inhibitor ATIII.

Table 4.1: Quantification of model errors. The nomarlized standard errors (SE) and the correlation (defined in the text) were calculated for the mean simulated values of the ensemble versus the experimental measurements.

Simulation	Normalized SE	Correlation r^2	Simulation	Normalized SE	Correlation r^2
Figure 4.1			**Figure 4.2**		
Panel A	0.13	0.84	Panel A	0.12	0.88
Panel B	0.22	0.66	Panel B	0.05	0.96
Panel C	0.22	0.68	Panel C	0.17	0.77
Panel D	0.19	0.82	Panel D	0.30	0.66
Panel E	0.13	0.90	Panel E	0.17	0.74
Panel F	0.18	0.75	Panel F	0.19	0.76
Panel G	0.15	0.84	**Figure 4.4**		
Panel H	0.15	0.74	Panel A	0.22	0.85
Panel I	0.21	0.77	Panel B	0.08	0.94

Thrombin generations in normal and hemophilia cases with various concentrations of FVIIa and *prothrombin* and the training data sets generated using a cell-based model [29] are shown in Figure 4.1. The standard errors and the correlations between the mean simulated values and the experimental measurements are shown in Table 4.1. On average, the model has a standard error of 18% and explained about 78% of the thrombin generation dynamics. In the normal case where physiological amounts of the plasma clotting factors, inhibitors and platelets were present in the system (Figure 4.1A), a characteristic patten of thrombin generation was observed. Little amount of thrombin was generated in the initiation phase and subsequently quantitative thrombin was formed during propagation, followed by the termination of thrombin. Thrombin generation reached its maximum of about 120 nM at 45 min and our model predicted a faster rate of thrombin formation. The normalized standard error in this case

is 13% and the correlation between the model prediction and the training data was 0.84. While in the hemophilia case (Figure 4.1B) when no fVIII and fIX were present, the maximum thrombin generated was less than 20 nM at 120 min. The normalized standard error in this case was 22% and a correlation of 0.66 was observed. When a combination of 75 nM FVIIa and 150% level of prothrombin were added, the normal thrombin generation was almost restored and we termed this case as treatment case. In the treatment case, the concentration of thrombin generated reached the normal maximum level at about 40 min and further increase to about 140 nM at about a hour. Our model resulted a slower thrombin generation rate and a lower maximum thrombin concentration with a correlation of 0.68 as compared to the training data.

The thrombin concentrations following the addition of FVIIa (25, 50 or 75 nM) to synthetic plasma at 100% prothrombin level were constrained by the *in vitro* training data sets (Figure 4.1D, E and F) and resulted in an average correlation of 0.82. Both the rate and the peak of thrombin generation were increased with the increase in the concentration of FVIIa. Thrombin generation has been shown to be influenced by concentrations of various clotting factors, especially prothrombin and ATIII [146, 111]. The increase of prothrombin concentration form 100% to 150% would result in 72% to 121% increase in the amount of thrombin generated [146, 111]. The model showed that when the level of prothrombin varied over 50-150% of the physiological ranges at fixed FVIIa concentrations of 25 nM (Figure 4.1G, D and H) or 75 nM (Figure 4.1I, F and C), the maximal concentration of thrombin generated increased with the increase in the level of prothrombin concentrations. However, discrepancies between the model prediction and the experimental training data were observed in the first 20 min of all simulations.

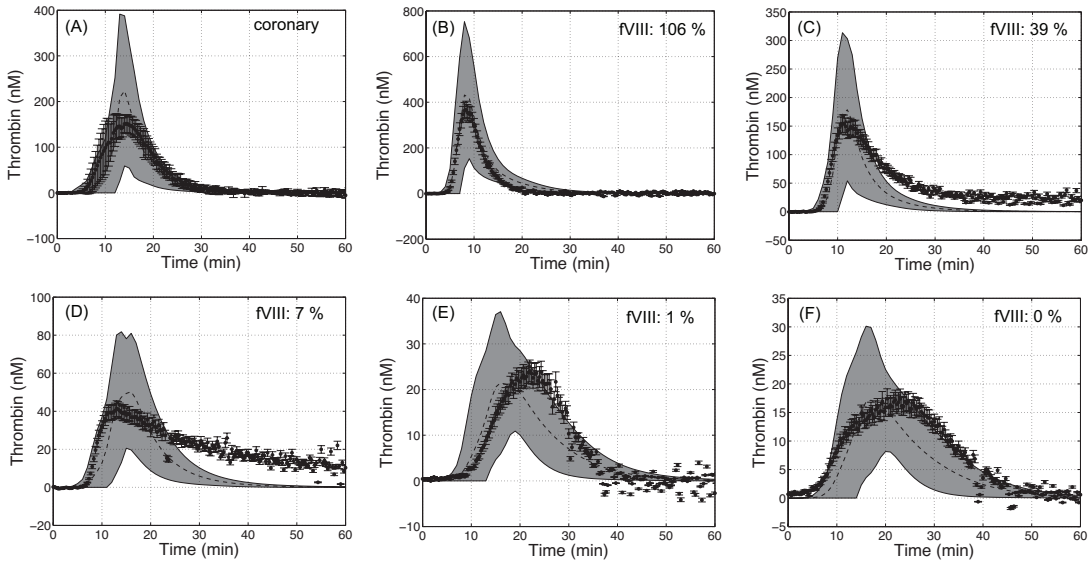

Figure 4.2: Predicted time course of thrombin generation versus experimental measurements using patient-derived plasma. The dashed lines in each case denote the mean simulated values over the ensemble of model parameters while the shaded regions denote one ensemble standard deviation. (A) The experiments were conducted using plasma from 4 patients with coronary artery disease (on aspirin); the generation of thrombin was initiated using 1 pM TF. Experimental data are shown with error bars, which were calculated as one standard deviation of the 4 different patient data sets. (B-F) The experiments were conducted using plasma from healthy or hemophilia A patients; the levels of fVIII concentration with respect to the normal concentration (0.3 nM) were shown in the corner. The generation of thrombin was initiated using 5 pM TF. Experimental data are shown with error bars, which were 10% of the experimental values.

The model and the parameter ensemble was then used to predict the thrombin generation in experiments using patient plasma for coronary artery diseases and hemophilia A. Platelet-rich and platelet-poor plasma were prepared using the coronary artery and hemophilia A patients plasma, respectively. TF was added to initiate the generation of thrombin. In the simulations, we assumed TF binds with FVIIa immediately to form TF-FVIIa complex, which therefore initiate the cascade. Platelet-rich plasma prepared using the blood drawn from 4 coronary artery patients who were on aspirin treatment was used in the experiments. The profile of thrombin concentrations in time has shown the typical characteristics of thrombin generation with a normalized standard error of 0.12 and a correlation of 0.88 (Figure 4.2 A and Table 4.1). The maximum thrombin concentration was about 150 nM at 15 min, while our model predicted a higher maximum of 220 nM at almost the same time point. Both the peak and rate of thrombin generation in this case were much lower than those in the case with 106% fVIII (plasma from healthy volunteer, Figure 4.2 B), which was mostly likely to be the results of the smaller amount of initiating TF used (1 pM in Figure 4.2 A and 5 pM Figure 4.2 B-F). The model gave the best prediction in the case with 106% fVIII (Figure 4.2 B), as shown by the small standard error of 0.05 and a high correlation of 0.96. While decreasing in fVIII concentrations resulted in decreases in both the peak and the rate of thrombin generation, the model explained more than 67% of the thrombin generation dynamics (Figure 4.2 C-F and Table 4.1). As we know, the level of coagulation factors is often related to the severity of hemophilia [25]. When fVIII decreased, the bleeding time was prolonged as a result of less and slower thrombin generation. The above results proved that the mechanistic model, trained using nine experimental data sets from an *in vitro* cell-based experiment, was able to predict thrombin generations

in patient-derived plasma.

4.3.2 Sensitivity analysis revealed the bypassing activity of rFVIIa.

The scaled OSSC values were clustered into three groups with high, medium and low sensitivities using a k-mean algorithm (see Methods). The parameters with high and medium sensitivities in the normal, hemophilia and treatment cases (Figure 4.1 A, B and C) were shown in Table 4.2. In the normal, hemophilia and treatment cases, the activation of platelets by ADP and TXA2 were clustered as the top 2 most sensitive parameters. Although the inhibition of FXa by ATIII (on rate), the formation and activity of *prothrombinase*, and the binding of FXa on platelet active sites (off rate) were clustered in the medium sensitive group in the treatment case, they showed similar ranks as those in the normal and hemophilia cases. While the on rate of FXa binding and the on/off rates of fX bindings showed similar ranks in the treatment and hemophilia cases, they were much higher than those in the normal case. This indicated that the sensitivity of fX/FXa bindings were generally higher in the case of hemophilia and treatment. In addition, 11 fVIII/fIX mechanisms that were clustered in the medium sensitive group in the normal case were shown to be robust in the hemophilia and treatment cases; 6 fV/FVa mechanisms, 2 activated platelets mechanisms, 3 inhibitory mechanisms (by TFPI or ATIII) and the on rate of TF-FVIIa activating fX were shown to have moderate sensitivity in the hemophilia and treatment cases, but robust in the normal case. In general, comparing to the normal case, the mechanisms related to fX/FXa and fV/FVa became more sensitive, while

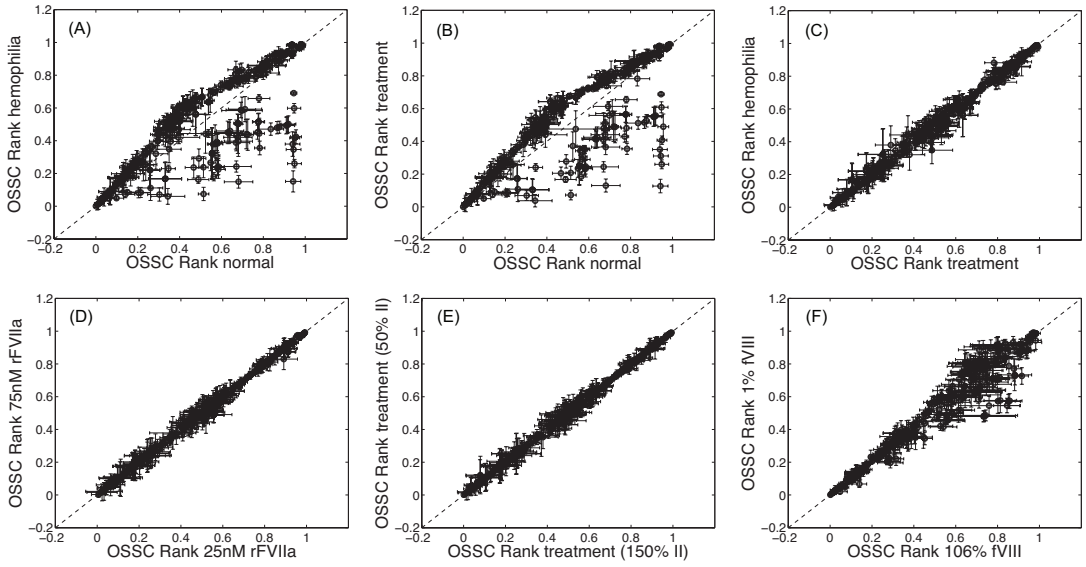

Figure 4.3: The normalized ranks of the OSSC values calculated over the selected parameter ensemble (N = 100) were compared in pairs among different cases.

the mechanisms related to fVIII/FVIIIa and fIX/FIX became more robust in the treatment and hemophilia cases.

The statistically significant shifts were calculated using the Welch T-Test among normalized ranks of the OSSC values in the normal, hemophilia, treatment cases (Figure 4.3 A, B and C). Compare with the normal case, 24 and 23 statistically significant shifts were found in hemophilia and treatment cases, respectively (data not shown). Except for the off-rate of fIX binding with platelet active site, the remaining 23 shifts were identical in these two cases. And all these shifts, related to fVIII and fIX activities, were shown to have increases sensitivity in the normal case. This result proved that the treatment of hemophilia using rFVIIa bypassed the activity of fVIII and/or fIX. It is reasonable as rFVIIa is often used to treat hemophiliacs with inhibitors of fVIII and fIX. Compare to the hemophilia case, 7 shifts were shown to have slightly increased sensitivities

and 7 shifts were shown to have slightly reduced sensitivities in the treatment case. Among the 7 decreased shifts, 4 of them were related to the activity of *tenase*, which was probably due to the addition of the 'by-passing' agent rFVIIa in the treatment case. The addition of rFVIIa is believed to activate fX when fVIII and fIX were not available.

Table 4.2: Distribution of OSSCs for normal, hemophilia and treatment cases [4].

p-index	normal		hemophilia		treatment		Description
Cluster I							
p-index	Rank	$\mu \pm \sigma$	Rank	$\mu \pm \sigma$	Rank	$\mu \pm \sigma$	Description
172	4±4	0.91±0.13	7±7	0.78±0.22	2±2	0.98±0.04	TXA2 activates platelets (off)
175	6±7	0.78±0.14	4±5	0.90±0.14	3±3	0.76±0.15	ADP activates platelets (off)
126	5±3	0.71±0.23	3±1	0.70±0.20	–	–	ATIII inhibits FXa (on)
97	8±5	0.61±0.22	9 ±1	0.55±0.18	–	–	FXa binds FVa on platelet surface (on)
98	9±5	0.61±0.22	9±1	0.55±0.18	–	–	FXa binds FVa on platelet surface (off)
90	9±4	0.61±0.22	11±1	0.54±0.18	–	–	Prothrombinase activates fII (on)
50	5±4	0.69±0.24	6±2	0.67±0.22	–	–	FXa binds platelet active sites (off)
49	–	–	5±2	0.67±0.22	–	–	FXa binds platelet active sites (on)
48	–	–	4±2	0.68±0.22	–	–	fX binds platelet active sites (off)
47	–	–	4±1	0.68±0.22	–	–	fX binds platelet active sites (on)
Cluster II							
p-index	Rank	$\mu \pm \sigma$	Rank	$\mu \pm \sigma$	Rank	$\mu \pm \sigma$	Description
126	–	–	–	–	4±2	0.58±0.25	ATIII inhibits FXa (on)
97	–	–	–	–	9±2	0.49±0.25	FXa binds FVa on platelets (on)
98	–	–	–	–	10±1	0.49±0.25	FXa binds FVa on platelets (off)
90	–	–	–	–	11±2	0.49±0.25	Prothrombinase activates fII (on)
50	–	–	–	–	8±2	0.53±0.25	FXa binds platelet sites (off)
49	21±6	0.35±0.10	–	–	6±2	0.53±0.25	FXa binds platelet sites (on)

Continued on next page

Table 4.2 (Continued)

p-index		normal		hemophilia		treatment	Description
48	19±7	0.35±0.10	–	–	6±1	0.53±0.25	fX binds platelet active sites (off)
47	19±6	0.35±0.10	–	–	5±2	0.53±0.25	fX binds platelet active sites (on)
58	13±8	0.54±0.28	–	–	–	–	FVIIIa binds platelet sites (off)
57	15±7	0.54±0.28	–	–	–	–	FVIIIa binds platelet sites (on)
45	15±10	0.52±0.28	–	–	–	–	FIXa binds specific platelet sites (on)
46	16±10	0.52±0.28	–	–	–	–	FIXa binds specific platelet sites (off)
81	17±11	0.52±0.29	–	–	–	–	Tenase activates fX (on)
95	17±11	0.52±0.29	–	–	–	–	FIXa (specific) binds FVIIIa (on)
96	18±11	0.52±0.29	–	–	–	–	FIXa (specific) binds FVIIIa (off)
123	16±4	0.49±0.20	–	–	–	–	ATIII inhibits FIXa (on)
29	24±11	0.40±0.22	–	–	–	–	FXa activates fIX (on)
30	26±11	0.38±0.21	–	–	–	–	FXa activates fIX (off)
31	27±12	0.38±0.22	–	–	–	–	FXa activates fIX (catalytic)
284	35±16	0.23±0.14	22±10	0.31±0.21	23±12	0.23±0.12	FVIIa activates fX (catalytic)
282	34±12	0.22±0.13	21±7	0.30±0.18	22±9	0.23±0.11	FVIIa activates fX (on)
283	35±12	0.22±0.12	22±7	0.30±0.18	23±9	0.23±0.11	FVIIa activates fX (off)
165	16±11	0.47±0.18	14±9	0.43±0.18	10±7	0.46±0.15	Activate platelets secret TXA2
13	20±12	0.38±0.22	14±6	0.40±0.16	15±5	0.36±0.21	TF-FVIIa activates fX (catalytic)
121	25±12	0.30±0.12	17±5	0.38±0.15	18±4	0.22±0.15	TFPI inhibits X-VIIa-TF (on)
59	19±5	0.44±0.23	22±7	0.30±0.14	23±10	0.30±0.24	fII binds platelets sites (on)
60	19±5	0.44±0.23	23±7	0.30±0.14	23±10	0.30±0.24	fII binds platelets sites (off)
54	24 ±8	0.28±0.14	17±4	0.35±0.11	19±3	0.24±0.13	FVa binds platelet sites (off)
53	–	–	21±3	0.31±0.12	21±3	0.23±0.13	FVa binds platelet sites (on)
52	–	–	23±5	0.31±0.13	23±3	0.22±0.13	fV binds platelet sites (off)
51	–	–	22±5	0.31±0.13	22±3	0.22±0.13	fV binds platelet sites (on)
23	–	–	21±6	0.34±0.19	25±6	0.19±0.15	Thrombin activates fV (on)
24	–	–	25±7	0.32±0.19	31±9	0.17±0.14	Thrombin activates fV (off)
25	–	–	22±7	0.33±0.20	28±9	0.19±0.15	Thrombin activates fV (catalytic)
164	–	–	23±9	0.27±0.11	20±7	0.23±0.07	Activate platelets secret ADP

Continued on next page

Table 4.2 (Continued)

p-index		normal		hemophilia		treatment	Description
147	–	–	34±26	0.21±0.14	26±14	0.21±0.11	FIIa activates PL (catalytic)
129	–	–	22±5	0.32±0.16	27±5	0.19±0.11	ATIII inhibits thrombin (on)
133	–	–	35±13	0.19±0.16	36±14	0.17±0.20	ATIII inhibits TF-FVIIa (on)
122	–	–	29±6	0.20±0.09	25±5	0.21±0.14	TFPI inhibits X-VIIa-TF (off)
11	–	–	32±8	0.17±0.13	29±8	0.17±0.16	TF-FVIIa activates fX (on)

In order to explore the dosage effect of rFVIIa, the ranks of OSSCs with normal prothrombin and 25 nM or 75 nM rFVIIa were compared against each other (Figure 4.3D). The sensitivities of almost all parameters were comparable in these two cases, indicating that the parameter sensitivities were not dependent on the dosage of rFVIIa. Similar analysis was conducted on the effect of prothrombin level (50% fII vs 150% fII, 75 nM rFVIIa); the result was shown in Figure 4.3E. The sensitivities of parameters were not related to the prothrombin level (at least the levels we considerer here).

Figure 4.4F shows the comparison of the ranks of the OSSC values in the cases with different amount of fVIII (106% vs 1% fVIII). There are 16 mechanisms statistically significant changed when the level of fVIII changed (data not shown). Among the 16 shifts, 11 fVIII/FVIIIa mechanisms became more robust and the other 5 shifts, related to the activation of fVII and fV by thrombin, became more fragile when fVIII was only 1% of the normal concentration (0.3 nM) as compared to 106% fVIII. When fVIII is not enough to generate FXa, the alternated pathway of thrombin generation, related to fVII and the formation of *prothrombinase*, could become more important. This could be the reason why fVII and fV mechanisms became more important in the 1% fVIII (hemophilia A)

[4]The OSSC values were clustered using a k-means algorithm into three parts. The most fragile parameters were shown in Cluster I; the most robust ones were shown in Cluster III. The mean OSSC value (μ) ± one standard deviation (σ) in Cluster I and II are reported. p-index denotes the parameter index in the reaction file.

case.

The ranks and the clustered OSSC values of the cases with 106% and 1% fVIII (hemophilia A) are shown in Table 4.3. 5 fX/FXa mechanisms were shown to have increased sensitivity, while 2 mechanisms related with activated platelets became more robust when the level of fVIII was reduced to 1% from 106%. In addition, 2 FXIa mechanisms, 6 fV/FVa mechanisms, 3 inhibitory mechanisms by TFPI or ATIII, 3 fI mechanisms and 2 TF mechanisms were more sensitive when only 1% fVIII was present. As the concentration of fVIII reduced, the pathway of FXa activation by *tenase* was shut down, the activation of FXa by other mechanisms, e.g. by TF-FVIIa, became more important. This could possibly explain why the TF mechanisms and fX/FXa activities became important when the fVIII was only 1% of the normal level.

Table 4.3: The distribution of the OSSCs for 106% and 1% fVIII cases.

p-index		106% fVIII ($\mu \pm \sigma$)		1% fVIII ($\mu \pm \sigma$)	Description
Cluster I					
p-index	Rank	$\mu \pm \sigma$	Rank	$\mu \pm \sigma$	Description
178	5±8	0.81±0.28	–	–	TXA2 activates platelets (catalytic)
165	14±17	0.52±0.25	–	–	Activate platelets secret TXA2
50	5±6	0.62±0.26	4±1	0.87±0.10	FXa binds platelet active sites (off)
49	5±4	0.56±0.25	4±2	0.86±0.10	FXa binds platelet active sites (on)
48	7±4	0.56±0.24	5±2	0.86±0.10	fX binds platelet active sites (off)
47	6±4	0.56±0.24	5±1	0.86±0.10	fX binds platelet active sites (on)
126	–	–	3±2	0.93±0.12	ATIII inhibits FXa (on)
13	–	–	3±2	0.88±0.11	TF-FVIIa activates fX (catalytic)
97	–	–	9±2	0.63±0.10	FXa binds FVa (on)
98	–	–	10±2	0.63±0.11	FXa binds FVa (off)

Continued on next page

Table 4.3 (Continued)

p-index	106% fVIII ($\mu \pm \sigma$)		1% fVIII ($\mu \pm \sigma$)		Description
90	–	–	11±2	0.62±0.11	Prothrombinase activates fII (on)

Cluster II

p-index	Rank	$\mu \pm \sigma$	Rank	$\mu \pm \sigma$	Description
178	–	–	17±17	0.55±0.27	TXA2 activates platelets (catalytic)
165	–	–	21±12	0.41±0.17	Activate platelets secret TXA2
126	8±6	0.44±0.11	–	–	ATIII inhibits FXa (on)
13	10±5	0.41±0.10	–	–	TF-FVIIa activates fX (catalytic)
97	12±6	0.38±0.13	–	–	FXa binds FVa (on)
98	14±6	0.35±0.11	–	–	FXa binds FVa (off)
90	12±4	0.37±0.10	–	–	Prothrombinase activates fII (on)
92	36±25	0.24±0.27	–	–	Prothrombinase activates fII (catalytic)
58	25±10	0.19±0.13	–	–	FVIIIa binds platelet active sites (off)
176	17±12	0.32±0.12	35±15	0.24±0.12	TXA2 activates platelets (on)
177	19±11	0.30±0.11	36±15	0.22±0.11	TXA2 activates platelets (off)
175	16±10	0.35±0.18	14±8	0.54±0.22	ADP activates platelets (off)
164	27±15	0.21±0.10	38±14	0.20±0.11	Activate platelets secret ADP
11	15±6	0.32±0.09	15±6	0.48±0.12	TF-FVIIa activates fX (on)
12	20±6	0.25±0.07	20±6	0.37±0.08	TF-FVIIa activates fX (off)
14	25±7	0.19±0.09	37±12	0.19±0.09	TF-FVIIa activates fIX (on)
15	28±8	0.17±0.08	41±12	0.17±0.08	TF-FVIIa activates fIX (off)
72	19±7	0.28±0.14	31±14	0.25±0.11	FXa activates fV (on)
54	14±5	0.34±0.12	13±2	0.52±0.07	FVa binds platelet active sites (off)
62	19±6	0.25±0.12	37±12	0.19±0.08	FIIa binds platelets active sites (off)
59	27±10	0.20±0.14	24±9	0.32±0.10	fII binds platelets active sites (on)
60	27±10	0.20±0.14	24±9	0.32±0.10	fII binds platelets active sites (off)
204	31±13	0.16±0.08	40±13	0.18±0.07	Thrombin activates fXI (on)
197	–	–	21±11	0.42±0.23	FXIa self-activation (on)
199	–	–	26±11	0.34±0.16	FXIa self-activation (catalytic)

Continued on next page

Table 4.3 (Continued)

p-index		106% fVIII ($\mu \pm \sigma$)		1% fVIII ($\mu \pm \sigma$)	Description
121	–	–	22±7	0.35±0.15	TFPI inhibits X-VIIa-TF (on)
53	–	–	25±15	0.34±0.16	FVa binds platelet active sites (on)
52	–	–	27±15	0.34±0.16	fV binds platelet active sites (off)
51	–	–	25±14	0.34±0.16	fV binds platelet active sites (on)
23	–	–	29±12	0.28±0.14	Thrombin activates fV (on)
24	–	–	34±16	0.26±0.14	Thrombin activates fV (off)
25	–	–	31±15	0.28±0.19	Thrombin activates fV (catalytic)
129	–	–	29±13	0.28±0.16	ATIII inhibits thrombin (on)
123	–	–	32±14	0.25±0.16	ATIII inhibits FIXa (on)
166	–	–	34±13	0.22±0.09	Activate platelets secret fibrinogen
179	–	–	35±12	0.21±0.09	Thrombin activates fibrinogen (on)
180	–	–	36±12	0.21±0.08	Thrombin activates fibrinogen (off)
2	–	–	32±7	0.22±0.08	TF binds fVII (off)
4	–	–	41±18	0.20±0.14	TF binds FVIIa (off)

4.3.3 TF-FVIIa is a more potent activator of thrombin generation than FVIIa only.

In order to study the initiating effects of TF-FVIIa and FVIIa in the generation of thrombin, our model was used to predict thrombin concentrations following the addition of 25 pM TF-FVIIa or 120 nM FVIIa to the synthetic plasma with platelets (Figure 4.4A and B). The model predictions were generally consistent with *in vitro* observations as proved by correlations of 0.85 and 0.94, resepectively (Table 4.1). The initiation (lag) phase was about 5 minutes in the TF-FVIIa initiating case, which is much shorter than that in the FVIIa case. In addition, both the rate and the peak of thrombin generation in the TF-FVIIa case were larger than those in the FVIIa case, which was consistent with the theory that

the initiating potential of FVIIa was much smaller than TF-FVIIa [200]. It is clear that TF-FVIIa has a much greater effect in initiating the coagulation cascade than FVIIa only. In addition, TF also helps in the localization of the blood clot to the wound site in physiological conditions.

Sensitivity analysis using ensembles of mechanistic models could be used to robustly rank-order the fragility of proteins in the network. In order to explore the differences in the mechanism of action by TF-FVIIa and FVIIa, the normalized ranks of the OSSC values and the species sensitivity results for the TF-FVIIa versus FVIIa cases were shown in Figure 4.4C and D. Statistically significant shifts between these two cases were calculated using Welch T-test (data not shown). In Figure 4.4C, among the 24 statistically significant shifts, 3 shifts that have increased sensitivity in the FVIIa case than the TF-FVIIa case are related to the activation of fX and fIX by FVIIa; the other shifts were shown to be less sensitive in the FVIIa case and amongst them, 16 shifts related to TF/TF-FVIIa activities, and the other 5 were inhibitory mechanisms related to TFPI, APC and ATIII. In Figure 4.4D, among the 10 significantly shifted species, fX-FVIIa complex has shown to be more sensitive in the FVIIa case; the other 9 species, including 7 TF related complexes and 2 *tenase* complexes, were more sensitive in the TF-FVIIa case. These results show that fluid phase activation of fIX and fX by FVIIa was the more important in the FVIIa case while the surface interactions of *tenase* were more important in the TF-FVIIa case.

Because the above results do not clearly state the differences in the mechanism of action for TF-FVIIa and FVIIa, we further analyzed the sensitivities in different phases of thrombin generation. The different phases were noted in Figure 4.4 A and B, and the OSSC values were calculated as summing over the

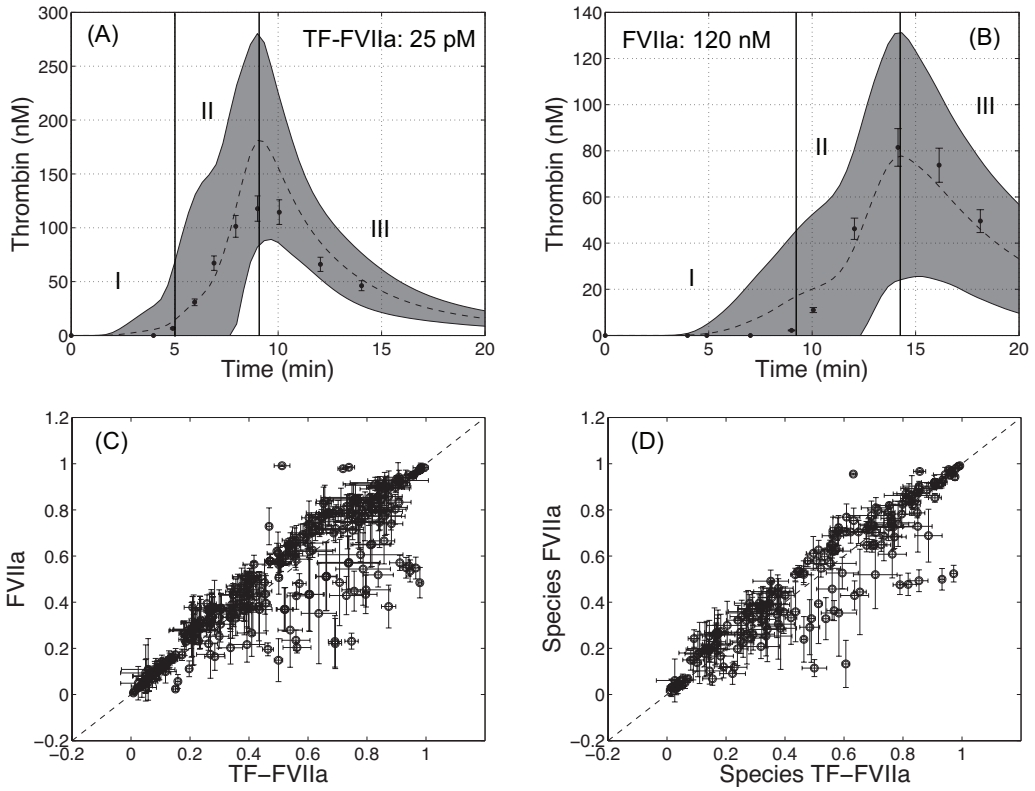

Figure 4.4: Model prediction and sensitivity analysis of TF-FVIIa and FVIIa initiated thrombin generation. (A) and (B): Predicted time course of thrombin generation versus *in vitro* experimental measurements [200]. Thrombin generation was initiated either by 25 pM TF-FVIIa (we assumed TF binds with FVIIa to form TF-FVIIa complex immediately) or by 120 nM FVIIa in the presence of physiological concentrations of pro- and anti-coagulants. Different phases of thrombin generation were noted: Phase I: initiation; Phase II: propagation; Phase III: degradation. The dashed lines in each case denote the mean simulated values over the ensemble of model parameters while the shaded regions denote one ensemble standard deviation (N = 437). Experimental data are shown with error bars (10% of the experimental values). (C) The normalized ranks of the OSSC values calculated over the selected parameter ensemble (N = 100) were compared between TF-FVIIa and FVIIa cases. (D) The normalized ranks of the species sensitivity values calculated over the selected parameters ensemble (N = 100) between TF-FVIIa and FVIIa cases.

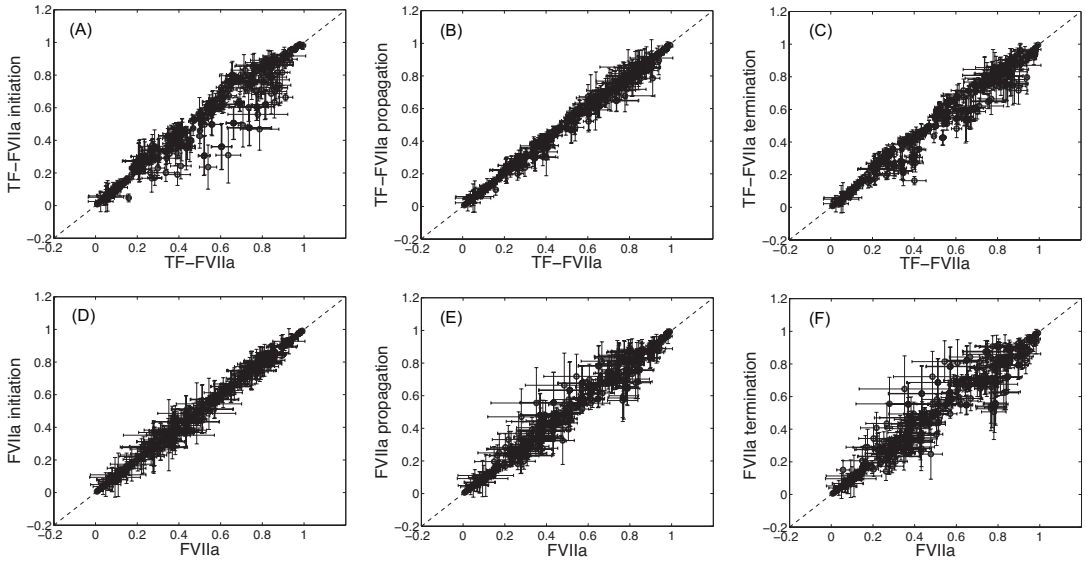

Figure 4.5: Comparisons of the parameter sensitivities (the normalized ranks of the OSSC values) in different phases with respect to that of the whole time span. (A-C) Normalized ranks of the OSSC values in different phases in thrombin generation versus that of the whole time span for TF-FVIIa case. (D-F) Normalized ranks of the OSSC values in different phases in thrombin generation versus that of the whole time span for FVIIa case.

first order sensitivity coefficients within the time span for separated phases. The comparison of rank-ordered OSSC values in individual phases versus the whole were shown in Figure 4.5. It is interesting to note that in the TF-FVIIa case, the OSSC ranks of the parameters in the propagation phase were the most representative across the whole time; while in FVIIa case, the OSSCs in the initiation phase were more representative to those of the whole time span.

Compare to the TF-FVIIa whole time case, 21, 12 and 23 statistically significant shifts were observed in the initiation, propagation and termination, respectively (data not shown). In the initiation phase, all shifts showed reduced sensitivity; 14 of them were related to the activity of PC/APC, 1 TF-fVII dissociation,

1 fVIII binding on platelet surface (on-rate), 2 related to the formation of *tenase*, 1 activation of PL by thrombin, 1 fibrin formation and 1 thrombin inhibition. In the propagation phase, 2 shifts, 1 fV activation by thrombin and 1 thrombin activation by *prothrombinase*, showed slightly increased sensitivity; while the other 10 shifts, including 1 TF-fVII dissociation,1 fVIII activation by FXa, 3 APC activity, 1 ATIII inhibition of thrombin, 2 activation of PL/PL-sub by thrombin, 2 fibrin activities, were less sensitive. In the termination phase, all shifts showed reduced sensitivity; 9 fluid phase activation of fV/fVIII by FXa/thrombin, 3 surface phase activation of fV/fVIII by FXa (surface), 7 platelets activation by thrombin/subendothelium, 3 fXI activities and 1 binding interaction of FVa.

Table 4.4: The distribution of the OSSCs for TF-FVIIa and FVIIa cases.

p-index	TF-FVIIa ($\mu \pm \sigma$)		FVIIa ($\mu \pm \sigma$)		
Cluster I					
p-index	Rank	$\mu \pm \sigma$	Rank	$\mu \pm \sigma$	Description
178	28±31	0.39±0.26	–	–	TXA2 activates platelets (catalytic)
172	2±1	0.86±0.13	5±4	0.87±0.16	TXA2 activates platelets (off)
165	5±8	0.75±0.28	5±6	0.72±0.25	Activate platelets secret TXA2
284	–	–	3±1	0.81±0.17	FVIIa activates fX (catalytic)
282	–	–	5±1	0.76±0.16	FVIIa activates fX (on)
283	–	–	7±1	0.74±0.15	FVIIa activates fX (off)
126	–	–	6±2	0.74±0.16	ATIII inhibits FXa (on)
50	–	–	8±4	0.76±0.19	FXa binds platelet active sites (off)
49	–	–	9±2	0.67±0.14	FXa binds platelet active sites (on)
48	–	–	8±2	0.67±0.14	fX binds platelet active sites (off)
47	–	–	8±2	0.67±0.14	fX binds platelet active sites (on)
97	–	–	14±4	0.53±0.16	FXa binds FVa (on)
98	–	–	15±3	0.52±0.16	FXa binds FVa (off)

Continued on next page

Table 4.4 (Continued)

p-index	TF-FVIIa ($\mu \pm \sigma$)		FVIIa ($\mu \pm \sigma$)		
90	–	–	15±3	0.52±0.16	Prothrombinase activates fII (on)

Cluster II

p-index	Rank	$\mu \pm \sigma$	Rank	$\mu \pm \sigma$	Description
178	–	–	22±23	0.33±0.21	TXA2 activates platelets (catalytic)
126	5±2	0.58±0.15	–	–	ATIII inhibits FXa (on)
50	5±3	0.57±0.16	–	–	FXa binds platelet active sites (off)
49	8±2	0.53±0.12	–	–	FXa binds platelet active sites (on)
48	6±3	0.54±0.12	–	–	fX binds platelet active sites (off)
47	6±2	0.54±0.12	–	–	fX binds platelet active sites (on)
97	12±2	0.40±0.11	–	–	FXa binds FVa (on)
98	13±2	0.40±0.11	–	–	FXa binds FVa (off)
90	13±2	0.40±0.11	–	–	Prothrombinase activates fII (on)
13	6±2	0.55±0.12	–	–	TF-FVIIa activates fX (catalytic)
12	16±4	0.35±0.09	–	–	TF-FVIIa activates fX (off)
11	10±4	0.45±0.13	–	–	TF-FVIIa activates fX (on)
14	17±5	0.31±0.10	–	–	TF-FVIIa activates fIX (on)
15	20±7	0.28±0.10	–	–	TF-FVIIa activates fIX (off)
175	21±11	0.32±0.17	19±10	0.36±0.20	ADP activates platelets (off)
164	28±11	0.24±0.12	18±9	0.24±0.11	Activate platelets secret ADP
25	36±17	0.20±0.18	57±29	0.24±0.18	Thrombin activates fV (catalytic)
129	28±12	0.23±0.13	50±6	0.16±0.13	ATIII inhibits thrombin (on)
59	26±8	0.22±0.10	23±8	0.27±0.10	fII binds platelets active sites (on)
60	27±8	0.22±0.10	23±8	0.27±0.10	fII binds platelets active sites (off)
54	18±2	0.31±0.07	15±1	0.43±0.12	FVa binds platelet active sites (off)
53	–	–	28±11	0.29±0.14	FVa binds platelet active sites (on)
52	–	–	26±9	0.29±0.13	fV binds platelet active sites (off)
51	–	–	25±8	0.29±0.13	fV binds platelet active sites (on)
58	–	–	62±30	0.18±0.09	FVIIIa binds platelet sites (off)

Continued on next page

Table 4.4 (Continued)

p-index	TF-FVIIa ($\mu \pm \sigma$)		FVIIa ($\mu \pm \sigma$)		
57	–	–	68±26	0.17±0.08	FVIIIa binds platelet sites (on)
45	–	–	59±27	0.17±0.07	FIXa binds specific platelet sites (on)
46	–	–	60±27	0.17±0.07	FIXa binds specific platelet sites (off)
95	–	–	76±36	0.15±0.08	FIXa (specific) binds FVIIIa (on)
96	–	–	76±34	0.15±0.08	FIXa (specific) binds FVIIIa (off)
81	–	–	76±35	0.15±0.08	Tenase activates fX (on)
72	–	–	20±5	0.25±0.07	FXa activates fV (on)
166	–	–	31±6	0.22±0.10	Activate platelets secret fibrinogen
29	–	–	29±5	0.17±0.06	FXa activates fIX (on)
30	–	–	30±5	0.16±0.06	FXa activates fIX (off)
31	–	–	44±17	0.15±0.06	FXa activates fIX (catalytic)
23	–	–	43±20	0.24±0.16	Thrombin activates fV (on)
24	–	–	48±20	0.22±0.15	Thrombin activates fV (off)
20	–	–	61±18	0.13±0.13	Thrombin activates fVII (on)
21	–	–	63±17	0.12±0.13	Thrombin activates fVII (off)
22	–	–	77±33	0.13±0.15	Thrombin activates fVII (catalytic)
179	–	–	42±8	0.18±0.08	Thrombin activates fibrinogen (on)
180	–	–	44± 8	0.17±0.08	Thrombin activates fibrinogen (off)
135	–	–	59±19	0.14±0.07	Thrombin activated PC (on)
137	–	–	78±27	0.12±0.07	Thrombin activated PC (catalytic)
170	–	–	30±14	0.14±0.06	TXA2 activates platelets (on)
171	–	–	31±14	0.13±0.05	TXA2 activates platelets (off)
176	–	–	31±21	0.17±0.09	TXA2 activates platelets (on)
177	–	–	33±22	0.16±0.08	TXA2 activates platelets (off)

Compare to the TF-FVIIa whole time case, no shifts found in the initiation phase; while 21 and 29 shifts found in the propagation and termination phases, respectively (data not shown). In the propagation phase, 11 shifts, related to APC activities, showed increased sensitivity; while the other 10 shifts, including 3 fluid phase activation of fVIII by FXa and 7 platelet activations by AP,

subendothelium, thrombin and ADP, became more robust. In the termination phase, 18 shifts, including 15 APC mechanisms, 1 activation of PL by thrombin, 1 fibrin formation and 1 thrombin inhibition, were more sensitive; while the other 11 shifts, including 3 fluid phase activation of fVIII by FXa and 8 platelet activations by AP, subendothelium, thrombin and ADP, became more robust.

In general, APC activities were more important in the propagation and termination phases than in the initiation phase, which were reasonable as APC was formed only after certain amount of thrombin was generated.

4.4 Discussion

In this study, we modeled thrombin generation in different conditions using the mechanistic model with 193 proteins or protein complexes connected by 301 interactions. A family or *ensemble* of model parameters (N = 437) was estimated using nine experimental training sets compiled from a cell-based experimental model. Sensitivity analysis was then used, over the selected parameter sets from the ensemble (N = 100), to estimate which parameters were critical globally and key to specific model outputs (thrombin concentration).

Numerous wet experimental studies on the complex system regulating hemostasis have been done using synthetic plasma or cell-based models [196, 111, 108, 115]. One of the most important aspects of our research is the choice of a model, which determines to a large extent the view of physiological reality that we develop. Our previous model [162] was mainly based on the experiments using synthetic plasma. However, *in vivo* conditions most likely require the presence of platelets. Thus in this study, we enriched our model with more

details to simulate physiological reality; for example, the activation of platelets through different G protein-coupled protease-activated receptors (PARs), the intrinsic pathway, etc, were added. We then trained the model using nine cell-based model data sets (Figure 4.1) and obtained an *ensemble* of parameters. Furthermore, plasma from coronary artery and hemophilia A patients was used in the measurements of thrombin generation; our model predictions using the parameter *ensemble* correlated well with the experimental measurements (Figure 4.2). These results suggested our model could capture the generation of thrombin in the environment as close to the physiological conditions as possible.

Factor VIII (fVIII) and factor IX (fIX) are the X-chromosomally encoded coagulation factors which are deficient in hemophilia A and B, respectively [24]. A hemophilia patient do not bleed more intensely than a normal person, but for a much longer amount of time. The critical risk here is with normally small injuries which, due to missing coagulation factors, take long times to heal. Although replacement therapy markedly improves the management of bleeding of most patients with hemophilia, the development of inhibitors during treatment is always a challenge. rFVIIa, as a newly developed bypassing agent, is often considered a universal hemostatic agent that used in treating hemophilas with inhibitors. Our study confirmed that in the treatment of hemophilia with rFVIIa and 150% level of prothrombin would restore normal thrombin generation. Further sensitivity analysis revealed the robust behavior of fVIII and fIX in the treatment case, while fX/FXa mechanisms became more important. This is consistent with the theory that rFVIIa or TF-FVIIa bypasses fVIII and fIX to produce FXa, which then restores thrombin production.

Given all the difficulties faced in treating hemophiliacs, the lack of understanding the principal mechanism of action of all these agents could be one of the obstacles in developing effective treatment regimes. For example, it is generally believed that the mechanism of action of rFVIIa is either TF-dependent or TF-independent. Both mechanisms have their experimental evidence [196, 197, 198, 199, 200, 32, 115, 201]. It is generally believed that TF-FVIIa is a more potent activator than FVIIa only. TF-FVIIa activates fX at a 4-fold higher rate than that of FVIIa only [196, 200]. The sensitivity analysis was also used to study differences in the initiating mechanisms of TF-FVIIa and FVIIa. As mentioned above, thrombin generation can be divided into 3 phases [202, 203]. Our sensitivity analysis on the initiation, propagation and termination phases revealed that TF-FVIIa initiating mechanism would highly influence thrombin generation in the propagation stage, while FVIIa initiating mechanisms were more important in the initiation region.

4.5 Materials and Methods

4.5.1 Formulation and solution of the model equations.

The reactions considered in the coagulation model have been compiled from literature [162, 204, 113, 69, 17, 205, 206, 16, 15, 60, 52, 146, 9, 8, 53]. Mass balance equations are written around each protein or protein complex yielding the set of ordinary differential equations (ODEs):

$$\frac{d\mathbf{x}}{dt} = \mathbf{S} \cdot \mathbf{r}(\mathbf{x}, \mathbf{p}) \qquad \mathbf{x}(t_o) = \mathbf{x}_o \tag{4.1}$$

The symbol $\mathbf{S}$ denotes the stoichiometric matrix (193×301). The quantity $\mathbf{x}$ denotes the species concentration (193×1). The term $\mathbf{r}(\mathbf{x}, \mathbf{p})$ denotes the vector of reaction rates (301×1). Each row in $\mathbf{S}$ described a species while each column described the stoichiometry of network interactions. Thus, the (i, j) element of $\mathbf{S}$, denoted by σ_{ij}, described how protein i was involved in rate j. If $\sigma_{ij} < 0$, then protein i was consumed in r_j. Conversely, if $\sigma_{ij} > 0$, protein i was produced by r_j. Lastly, if $\sigma_{ij} = 0$, protein i was not involved in rate j.

We assumed mass-action kinetics for each interaction in the network. The rate expression for protein-protein interaction or catalytic reaction q:

$$\sum_{j \in \{\mathbf{R}_q\}} \sigma_{jq} x_j \rightarrow \sum_{p \in \{\mathbf{P}_q\}} \sigma_{pq} x_p \tag{4.2}$$

was given by:

$$r_q\left(\mathbf{x}, k_q\right) = k_q \prod_{j \in \{\mathbf{R}_q\}} x_j^{-\sigma_{jq}} \tag{4.3}$$

The set $\left\{\mathbf{R}_q\right\}$ denotes reactants for reaction q. The quantity $\left\{\mathbf{P}_q\right\}$ denotes the set of products for reaction q. The k_q term denotes the rate constant governing the qth interaction. Lastly, σ_{jq}, σ_{pq} denote stoichiometric coefficients (elements of the matrix $\mathbf{S}$). We treated every interaction in the model as non-negative. All reversible interactions were split into two irreversible steps. The mass-action formulation, while expanding the dimension of the model, regularized the mathematical structure. The regular structure allowed automatic generation of the model equations. Model parameters and structure, shown in Supplement Table 1, were taken from the literature [60, 52, 146, 9, 8, 53]. Initial conditions were taken from each experiment and roughly correspond to *in-vivo* physiological conditions. An *ensemble* of parameters (N = 437) were estimated to minimize the objective functions that describe the errors between model simulations and experimental data sets. Among the parameter ensemble, 100 parameter sets that

resulted in a CV of 2 were selected for the sensitivity analysis.

4.5.2 Error Analysis of the Coagulation Simulations.

The correlation between model simulations and experimental data was calculated using the relationship:

$$r^2 = \frac{\sum_{h=1}^{N} \left(Y_m(t_h) - \bar{Y} \right)^2}{\sum_{h=1}^{N} \left(\bar{Y}(t_h) - Y_m(t_h) \right)^2 + \sum_{h=1}^{N} \left(Y_m(t_h) - \bar{Y} \right)^2} \tag{4.4}$$

where $Y_m(t_h)$ denotes the model value at time point h, $\bar{Y}$ denotes the global average experimental value (average of experimental measurements over time) and $\bar{Y}(t_h)$ denotes the average experimental value at time point h (average of experimental trials). Eqn. 5.4 measures the fraction of variation captured by the model. In addition to correlation, the scaled standard error was used to measure the agreement between the model:

$$s_E = \frac{1}{\max_h \left(\bar{Y}(t_h) \right)} \left(\frac{\sum_{h=1}^{N} \left(\bar{Y}(t_h) - Y_m(t_h) \right)^2}{N} \right)^{1/2} \tag{4.5}$$

Both Eqn. 5.4 and 5.5 were taken from [147].

4.5.3 The Measurement of Thrombin Generation

Platelet-poor plasma (PPP) samples with varied levels of factor VIII were obtained from George King Biomedical (Overland Park, KS). Platelet-rich plasma (PRP) samples were obtained from four patients scheduled to undergo coronary vascular procedures. They gave an informed written consent for blood sampling according to the IRB-approved protocol. Whole blood samples were collected into 3.2% (0.105 M) buffered sodium citrate tubes containing 100 μg/ml

corn trypsin inhibitor (CTI) to prevent platelet activation during the blood draw, and isolation of platelet rich plasma. These patients were not being treated with antithrombotic agents except for aspirin (81 mg per day). PRP and PPP were isolated by centrifugation (10 min at 150 x g and 20 min at 2000 x g, respectively). Platelet count (PLT) of PRP was adjusted to $200x10^3$ per μl with autologous PPP (AcT10 Coulter counter, Beckman Coulter, Miami FL).

Thrombin generation was measured by the calibrated automated thrombography method using a fluorogenic thrombin substrate (Z-Gly-Gly-Arg-AMC, Diagnostica Stago, Parsipanny, NJ) [207, 208]. Briefly, 80 μl of PRP or PPP sample was added, and then 20 μl of tissue factor (TF)-based activator (Biodis, Signes, France) was added to wells of the 96-well plate. The plate was incubated for 2 to 3 min at 37^oC and then 20 μl of the substrate buffer was added. A thrombin calibrator with known thrombin-like activity was monitored in parallel sample wells to allow for calculation of generated thrombin in nM. The progress of the reaction was continuously monitored for 70 min at 37^oC with a fluorescence reader (Fluoroscan Ascent, Thermo Labsystems, Franklin, MA) equipped with a 390 nm excitation filter and a 460 nm emission filter. A dedicated software program (Thrombinoscope, Synapse BV, Maastricht, The Netherlands) was used to record the peak thrombin level.

4.5.4 Computation of overall state sensitivity coefficients.

The sensitive or fragile interactions of the coagulation architecture were determined by computing Overall State Sensitivity Coefficients (OSSC) [89]. Because each parameter corresponds directly to a particular molecular interaction in the

cascade, OSSC values were used to gauge which interactions were qualitatively important. Large OSSC values for interactions relative to their peers indicated fragility or sensitivity while small OSSC values indicated robustness. The OSSC value for interaction j was defined as:

$$O_j(t) = \frac{k_j^*}{N_S}\left(\sum_{h=1}^{N_T}\sum_{i=1}^{N_S}\left[\frac{1}{x_i^*}\frac{\partial x_i}{\partial k_j}\bigg|_{t_h}\right]^2\right)^{1/2} \tag{4.6}$$

where N_T denotes the number of time points used in the simulation while N_S denotes the number of proteins/protein complexes in the model. The first-order sensitivity coefficients:

$$s_{ij}(t_h) = \frac{\partial x_i}{\partial k_j}\bigg|_{t_h} \tag{4.7}$$

were computed by solving the differential equation:

$$\frac{d\mathbf{s}_j}{dt} = \mathbf{A}(t)\,\mathbf{s}_j + \mathbf{b}_j(t) \qquad j = 1, 2, , N_P \tag{4.8}$$

subject to the initial condition $\mathbf{s}_j(t_0) = \mathbf{0}$. In Eqn. 5.8, the quantity j denotes the parameter index, N_P denotes the number of parameters, $\mathbf{A}$ denotes the Jacobian matrix of the model equations and $\mathbf{b}_j$ denotes the jth column of the matrix $\mathbf{B}$, which contains first-derivatives of the mass balances w.r.t. the parameter values. The quantity $\mathbf{s}_j$ denotes the vector of first-order sensitivity coefficients w.r.t parameter j. The Jacobian matrix ($\mathbf{A}$) and the matrix of first-derivatives of the mass balances w.r.t the parameter values ($\mathbf{B}$) are given by:

$$\mathbf{A} = \frac{\partial \mathbf{g}}{\partial \mathbf{x}}\bigg|_{(\mathbf{x}^*,\mathbf{k}^*)} \qquad \mathbf{B} = \frac{\partial \mathbf{g}}{\partial \mathbf{k}}\bigg|_{(\mathbf{x}^*,\mathbf{k}^*)} \tag{4.9}$$

where $(\mathbf{x}^*, \mathbf{k}^*)$ denotes a point along the *nominal* or *unperturbed* system solution. The matrices $\mathbf{A}$ and $\mathbf{B}$ were numerically estimated at each time step using a generalized gradient algorithm [148] while the sensitivity balances were solved using the LSODE routine of the OCTAVE programming environment (v2.9.9; www.octave.org) on an Apple Computer MacOSX (Cupertino, CA; v10.4.8) workstation.

The connectivity matrix **S** (193 × 301) was used to rearrange the parameter OSSC values to the species OSSCs through the equation:

$$\mathbf{Q} = |\mathbf{S}|\mathbf{O} \tag{4.10}$$

The rank orders of the species OSSCs were used to access the fragility of different species in the model.

4.5.5 Statistical and clustering analysis of the shifts in overall state sensitivity coefficients.

Three different tests were performed to identify large statistically significant shifts in OSSC values between defective networks and the control. A Welch t-test [149] was used to find all statistically significant shifts resulting from the different structural perturbations and then a secondary test on the $z-$score of each shift was preformed to find only the most prominent. The OSSC values calculated over the family of parameter sets were assumed to follow normal distributions for all cases. The statistical significance of shifts in OSSC values relative to the control were determined by performing a Welch t-test with the null hypothesis that the means of the sensitivity coefficients were equal at a 1% significance level. The Welch t-test is similar to the student t-test with the exception that the two distributions being compared are not required to have equal variances. The list of significant OSSC values was further restricted to only those shifts with a magnitude larger than a specified z-score (0.1) away from the squared mean displacement relative to the control:

$$d_{j,q} = \left(\bar{O}_j^q - \bar{O}_j^c\right)^2, \qquad j = 1, 2, , N_P \tag{4.11}$$

where $\bar{O}_j^c$ denotes the mean OSSC value over the family of parameter sets for parameter j in the control while $\bar{O}_j^q$ denotes the same quantity for defective case q. A significant shift in OSSC value was *accepted* if:

$$d_{j,q} > z\sigma_{d_q} + \mu_{d_q} \tag{4.12}$$

where z denotes a desired z-score, σ_{d_j} denotes the standard deviation of the total displacement over all significant OSSC values for the *qth* defective case and μ_{d_q} denotes the mean of the significant displacements for the structurally defective case q.

A large statistically significant shift in OSSC value, while indicative of the shifting importance of an interaction, does not guarantee that an interaction is ranked differently between cases. To this end, we used the Spearman rank correlation denoted by ρ and defined as:

$$\rho = 1 - \frac{6\sum_{i=1}^{N_P} d_i^2}{N\left(N^2 - 1\right)} \tag{4.13}$$

to measure the difference in qualitative ranking between cases. The quantity d_i denotes the difference in the ordinal rank of interaction i between a structurally defective network and the control, N denotes the number of pairs of values and N_P denotes the number of parameters considered. The Spearman rank is bounded by $-1 \leq \rho \leq 1$; a Spearman rank of one indicates that two ranked lists are identical, a Spearman rank equal to negative one indicates that two ranked lists are perfectly negatively correlated, while a Spearman rank of zero indicates that two ranked lists are uncorrelated.

The distributions of OSSC values obtained from monte-carlo sampling were clustered using a k-means algorithm [209]. The mean and standard deviation obtained from the monte-carlo sensitivity analysis was used to estimate the un-

derlying OSSC distribution (N = 100 points) where the OSSC values were assumed to be normally distributed. Two hundred different clustering attempts were run for each model to control for clustering artifacts. The most probable configuration was reported.

4.5.6 Coupling analysis

Coupling coefficients of the form:

$$\alpha\left(i, j, t_o, t_f\right) = \left(\int_{t_o}^{t_f} x_i\left(t\right) dt\right)^{-1} \left(\int_{t_o}^{t_f} x_i^{(j)}\left(t\right) dt\right) \tag{4.14}$$

were calculated to understand the sensitivity of the parameters in the model. The coupling coefficient $\alpha\left(i, j, t_o, t_f\right)$ is the ratio of the integrated concentration of a network output in the presence (numerator) and absence (denominator) of structural or operational perturbation. If $\alpha\left(i, j, t_o, t_f\right) > 1$, then the perturbation *increases* the output concentration. Conversely, if $\alpha\left(i, j, t_o, t_f\right) \ll 1$ the perturbation *decreases* the output concentration. Lastly, if $\alpha\left(i, j, t_o, t_f\right) \sim 1$ the perturbation does not influence the output concentration.

CHAPTER 5

FACTOR XI IS A POTENTIAL THERAPEUTIC TARGET FOR THROMBOSIS THAT MAINTAINS HAEMOSTASIS

5.1 Abstract

The systems biology approach, together with computational, experimental and observational inquiry, is highly relevant to drug discovery and the optimization of medical treatments. In this study, we test our working hypothesis that fXI related mechanisms are fragile in the process of blood coagulation and could be a potential therapeutic target for thrombosis treatment. A mathematical model of the blood coagulation cascade including fXI activities was built and validated against published datasets generated from a cell-based model. The model explained the time-resolved thrombin generation profile with normalized error ≤30% and correlation coefficients ≥72%. The simulation results show that the addition of intrinsic pathway protease fXI to the TF initiated coagulation resulted in the formation of extra amount of thrombin and thrombin was reciprocally generated in a fXI-dependent way. To gauge the robustness and fragility of each interaction in the cascade, overall state sensitivity coefficients (OSSC) were calculated for each of the 301 model parameters over a parameter ensemble that could predict reasonable thrombin generation profiles; the species sensitivity was also calculated using the connectivity matrix and parameter OSSCs. Analysis of the sensitivity results discloses that fX/FXa and thrombin were important species in the extrinsic case; while besides thrombin, fXI/FXIa was also sensitive in the combined and intrinsic cases. Theoretical considerations and experimental data suggest that fXI/FXIa could be excellent candidates as clinical targets

in treatment of thrombotic diseases. Inhibition of fXI/FXIa could potentially reduce the risk of occlusive thrombi formation without sacrificing hemostasis as deficiency of fXI results in bleeding manifestations only after trauma or surgery. When taken together, these preliminary results support our hypothesis that fXI related mechanisms are fragile in the process of blood coagulation and could be a potential therapeutic target for thrombosis treatment with the advantage of not affecting hemostasis.

5.2 Introduction

The systems biology approach, together with computational, experimental and observational inquiry, is highly relevant to drug discovery and the optimization of medical treatments. It has been frequently proposed that computer simulations and analysis significantly increase the efficiency of drug discovery [73]. Assmus *et al.* and others maintain that analysis of the dynamics of human relevant networks using predictive computer models and high-throughput data generation will play an increasingly important role in medical research and the elucidation of disease mechanisms [76, 77]. However, these techniques often suffer from parametric and structural uncertainties in diagnosing complex biological networks [73, 84]. The conventional wisdom is that the data requirement to fully identify and validate mechanistic models is too large. One tool that could partially eleviate model uncertainty and potentially elucidate qualitative properties of uncertain mechanistic models, such as robustness and fragility of particular mechanisms, is sensitivity analysis.

Sensitivity analysis is an enabling tool for the investigation of robustness and

fragility in networks relevant to human health and more generally for model-based knowledge discovery. Robustness, a long-recognized property of living systems and networks, allows function in the face of uncertainty while fragility, i.e., extreme sensitivity, can potentially lead to catastrophic failure following seemingly innocuous perturbations [85, 158, 159, 160, 84]. Cho *et al.* used sensitivity analysis to study TNF-α-mediated NK-κB signalling where parametric uncertainty was addressed using a monte-carlo parameter sampling protocol; a parameter ensemble, generated from the best parameter guess, was used to calculate the sensitivity profile in a region of parameter space [80]. Bullinger and coworkers explored the robustness of models of programmed cell death or apoptosis [88] while Stelling *et al.,* computationally identified points of robustness and fragility, using monte-carlo sensitivity analysis and Overall State Sensitivity Coefficients (OSSCs), in models of circadian rhythm [89]. Mahdavi *et al.,* employed sensitivity analysis to better understand stem cell differentiation [161], while our group used an uncertain mechanistic model of the coagulation cascade in combination with monte-carlo sensitivity analysis, to show that computationally derived sensitive mechanisms were consistent with anti-coagulation therapeutic strategies [162]. By screening a model of the extrinsic pathway of blood coagulation using sensitivity analysis, we have previously found that factor X/activated factor X (fX/FXa) and thrombin related mechanisms were fragile and factor IX/activated factor IX (fIX/FIXa) related mechanisms had moderately robust. Some anti-fX/FXa and direct thrombin inhibitors have been evaluated in phase III clinical trials or have been licensed in North America or Europe for the treatment of venous thromboembolism, deep venous thrombosis and pulmonary embolism [210]. And the treatment of thrombotic disease with anti-fIX/FIXa antibodies often require high dosages to have

an therapeutical effect [133]. However, the use of these anticoagulants is often associated with therapy-related bleeding problems and has no significant improvement in safety/efficacy ratio [210, 211, 212]. Hence the development of new therapies is necessary and requires the discovery of agents that are specific for thrombus-forming mechanisms without affecting hemostasis.

Factor XI (fXI), closely related to mild bleeding disorder[27, 213, 205], often receives less attention as a result of its *in vivo* insignificance. Deficiency in fXI only affects people who has trauma or under surgery. However, recent studies show that its feedback activation by thrombin consolidates blood coagulation and fibrin clot formation [15, 16]. Elevated fXI activity levels are not only a risk factor for deep venous thrombosis and possibly cardiovascular disease, but also associated with stroke or cerebrovascular events [214, 215]. All these studies motivate us to study of the role of fXI in coagulation and its possibility as potential therapeutic targets without a serious impact on hemostasis. In this study, we use mathematical modeling and sensitivity analysis to test our working hypothesis that fXI related mechanisms are fragile in the process of blood coagulation and could be a potential therapeutic target for thrombosis treatment. A mathematical model of the blood coagulation cascade including fXI activities (intrinsic pathway) was built and validated against published datasets generated from a cell-based model [15]. The model explained the time-resolved thrombin generation profile with normalized error $\leq$30% and correlation coefficients $\geq$72%. The simulation results show that the addition of intrinsic pathway protease fXI to the Tissue Factor (TF) initiated coagulation resulted in the formation of extra amount of thrombin and thrombin was reciprocally generated in a fXI-dependent way. We used monte-carlo sensitivity analysis to computationally screen the model for sensitive mechanisms in the presence of either intrinsic

pathway activators fXI and thrombin (intrinsic case), or extrinsic pathway activator TF (extrinsic case), or both pathways activators (combined case). Analysis of the sensitivity results discloses that fX/FXa and thrombin were important species in the extrinsic case; while besides thrombin, fXI/FIXa were also sensitive in the combined and intrinsic cases. We then validated the fragility of fXI related mechanisms in different cases and contrast with literature to determine if they could be a potential therapeutic target for thrombosis treatment, thereby proving or disproving our working hypothesis.

5.2.1 A review of the coagulation cascade.

Conventionally, the coagulation cascade has been known as two alternative or convergent pathways known as the intrinsic pathway and the extrinsic pathway [12, 52, 54, 60, 53, 8, 111, 109, 115, 110, 216, 217]. The extrinsic coagulation cascade is initiated by the formation of the TF and Factor VIIa molecular complex, following a series of enzymatic interactions leading to the formation of thrombin. The detailed interactions and the roles of pro- and anticoagulants in the coagulation cascade could be found in a number of articles [112, 10, 108, 20, 21, 22, 116, 117, 23]. The extrinsic pathway is believed to be the major activation mechanism *in vivo* [12, 52, 54, 60, 53, 8, 111, 109]. However, small quantities of active FXa generated by FVIIa-TF complex during the initiation of the extrinsic pathway could result in the inactivation of TF pathway by TFPI. When this inactivation occurs, an alternative system is needed to maintain coagulation. The classic intrinsic pathway of coagulation is triggered by contact activation of plasma protease factor XII, followed by sequential proteolytic activation of fXI and fIX [14]. However, patients with deficiency in fXII do not

experience abnormal hemostasis even after major trauma or surgery, whereas, patients with fXI deficiency frequently present with excessive or even life-threatening bleeding complication after trauma or surgical operations [14, 13]. Researches on this discrepancy indicate additional mechanisms for fXI activation *in vivo*, which is the activation of fXI by a catalytic amount of thrombin in the presence of dextran sulfate [14, 13]. Further studies show that the surface of activated platelets could substitute for dextran sulfate *in vivo* [18, 19]. Moreover, this feedback activation of fXI by thrombin is proven to be a preference over contact activation of FXIIa [17]. Hence, the activation of fXI by thrombin could serve as an alternative to maintain blood coagulation and has been well studied by several groups [13, 14, 15, 16, 17, 18, 19]. Therefore, besides activation by Factor XIIa, which is activated upon contact with negatively charged surface, factor XI (fXI) in the intrinsic pathway could also be activated by thrombin and its own active form, Factor XIa (FXIa) [13, 14, 18, 19, 17, 16, 15, 206, 205]. The intrinsic pathway of coagulation joins with the extrinsic at the point where fIX activated by FXIa to form FIXa (shown in Figure 5.1).

5.3 Results

Thrombin generation as a function of TF, FVIIa, fXI and thrombin were predicted, over an *ensemble* of parameter sets (N = 437, see Chapter 4), to be consistent with published datasets from a cell-based model [15]. To gauge the robustness and fragility of each interaction in the cascade, a hundred parameter sets were further selected from one parameter ensemble with a coefficient of variance (CV) equals 2 for sensitivity analysis. The overall state sensitivity coefficients (OSSCs) were calculated for each of the 301 model parameters over the

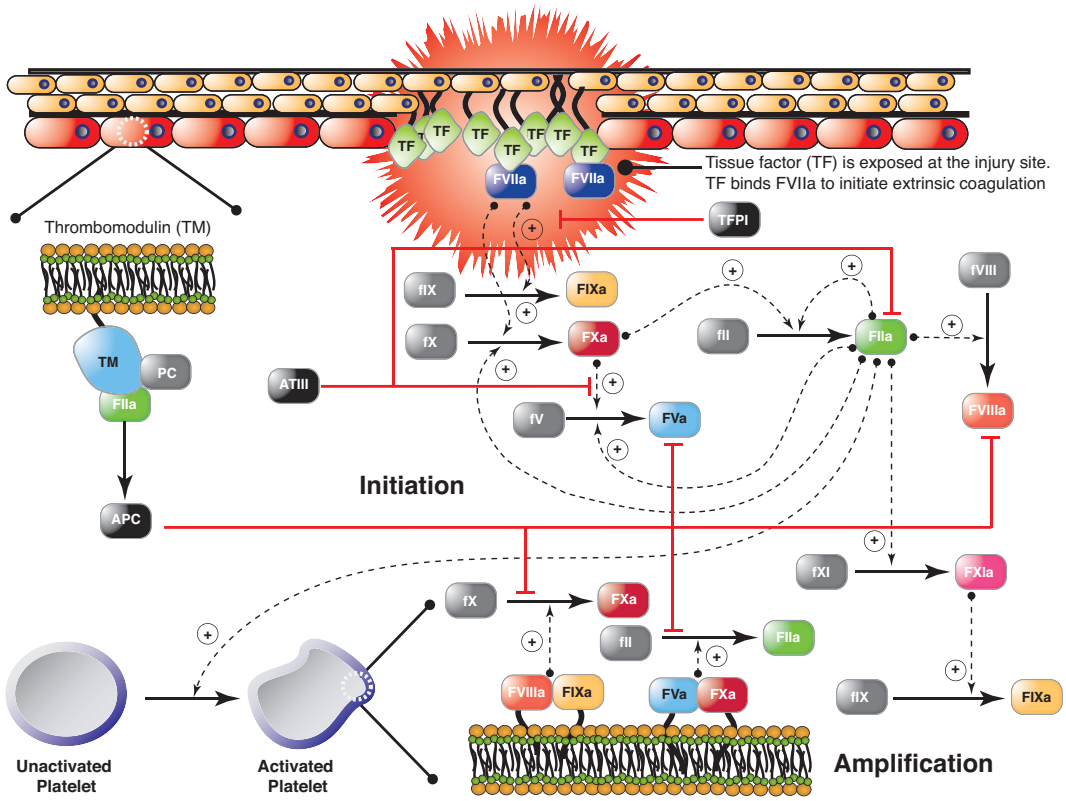

Figure 5.1: Schematic illustration of the coagulation cascade.

selected parameter sets (see Methods). Simulation results and error quantifications for different cases (Table 5.1) are shown in Figure 5.2. The model explained the time-resolved thrombin generation profile with normalized error ≤30% and correlation coefficients ≥72%. The simulation results show that the addition of intrinsic pathway protease fXI to the TF initiated coagulation resulted in the formation of extra amount of thrombin and thrombin was reciprocally generated in a fXI-dependent way. The OSSCs were clustered into groups with varied levels of sensitivity (high, medium and low); the high and medium sensitive groups for different cases are reported in Table 5.2. Pairwise comparison of the OSSCs are shown in Figure 5.3 and the parameter indices of statistically signif-

icant shifts for different pairs are reported in Table 5.3. The species sensitivity was calculated using the connectivity matrix and parameter OSSCs; and the average ranks of the top 10 most sensitive species and their connectivities for all cases are shown in Figure 5.4. Pairwise comparison of the rank-ordered species sensitivity are shown in Figure 5.5 and the statistically significant shifts for different pairs are reported in Table 5.4. Analysis of the sensitivity results discloses that fX/FXa and thrombin were important species in the extrinsic case; while besides thrombin, fXI/FXIa were also sensitive in the combined and intrinsic cases.

5.3.1 Thrombin generation in the presence and absence of fXI.

Figure 5.2 shows the time resolved generation of thrombin as a function of TF, FVIIa, fXI and thrombin. Figure 5.2 A is thrombin generation profile of the extrinsic case where only TF and FVIIa were present in the reaction system; Figure 5.2 B is thrombin generation in the combined case where fXI was also added in addition to TF and FVIIa; Figure 5.2 C and D show thrombin generation profiles in the intrinsic cases with different amounts of thrombin as the initiator of the intrinsic pathway, since fXII was not available. The dotted lines denoted the mean thrombin generation profile obtained from the parameter ensemble (437 sets). A hundred parameter sets were further selected with a CV of 2 for the sensitivity analysis. The model predictions of mean thrombin generation explained the generation of thrombin for all cases in Table 5.1 with the normalized standard errors $\leq 30\%$ and the correlation coefficients above 72%. Thrombin generation were simulated using the ensemble of parameter sets and the mean and standard deviation of thrombin concentrations at each time were

Table 5.1: Treatement cases considered in the sensitivity analysis. Case A denotes the 'Combined' case, where species for both extrinsic and intrinsic pathways are present, Case B denotes the 'Extrinsic' case while cases C and D denote the 'Intrinsic' case with two different initial thrombin concentrations.

Case	Name	TF (pM)	VIIa (nM)	XI (nM)	IIa (nM)
A	Extrinsic	1.0	20	–	–
B	Combined	1.0	20	60	–
C	Intrinsic	–	–	60	0.5
D	Intrinsic (5nM IIa)	–	–	60	5

calculated for all cases. The shadow areas denoted thrombin concentratrions within ±1-standard deviation of the ensemble.

Thrombin generation profile typically consists of three stages: the initiation, the propagation and the termination. The initiation stage is the part where no or little thrombin is generated, the propagation is the part where large amount thrombin formed in a short period of time due to increased thrombin generation rates, and the termination of thrombin is the result of fast consumption of thrombin. Figure 5.2A shows that in the extrinsic case, the initiation stage covered the first 15 min, followed by the propagation of thrombin. Thrombin reached its maximal of 30 nM at about 40 minutes, then it gradually degraded to 20 nM at one hour. The normalized standard error and the correlation coefficient in this case were 0.07 and 0.97, respectively, which was probably because of the discrepancy between the mean simulation results and the experiment data in the propagation stage. The thrombin generation profile in the extrinsic case (case A) was quite similar to that in the intrinsic case (case C). As shown in Figure 5.2C, after 0.5 nM thrombin was added to initialize the reaction, thrombin

propagation started at about 12 min, which was close to the lag time in extrinsic case; furthermore, the rate and maximal amount of thrombin generated in this case was about the same as those in the extrinsic case, especially when comparing the experimental data. The model predicted a faster thrombin generation in the propagation and a faster thrombin consumption in the termination stage. This discrepancy caused a larger standard error of 0.24 and a smaller correlation coefficient of 0.78. In the combined case (Figure 5.2B), both the rate and maximal thrombin generation were increased as compared to that in either the extrinsic or the intrinsic case . Thrombin concentration reached a maximum of 40 nM at about 30 min. Our model prediction was consistent with the experimental observation that feedback activation of fXI by thrombin resulted in additional production of thrombin [16, 15]. Our model predictions of the combined case (case B) correlated well with the experimental observation, which had a standard error of 0.10 and a correlation coefficient of 0.95.

The experimental observations of the thrombin generation in case C and case D show that thrombin was reciprocally generated in a fXI-dependent manner, i.e. increasing the initiating thrombin concentration resulted in increased FXIa formation, which then increased the amount of thrombin formation. In Figure 5.2D, after 5 nM thrombin was added, the experiment results illustrated gradually increased thrombin concentration to a maximum of 60 nM in a temporal range of 0 to 20 min, which indicated a much faster thrombin generation rate than that in case C. However, our simulation results in case D failed in predicting thrombin generation in the first 20 min; we predicted a lag time of 10 min and a faster thrombin generation rate where thrombin concentration reached its maximum within 15 min. As a result, a standard error of 0.30 and a correlation coefficient of 0.72 were observed in this case.

5.3.2 The fragility and robustness of the combined, intrinsic and extrinsic coagulation pathways.

The OSSCs were calculated for cases A-D in Table 5.1. The scaled OSSC values were clustered into three groups (high, medium and low sensitivity) using a k-mean algorithm. The mean and standard deviations of the OSSC values in the high (Cluster I) and medium (Cluster II) sensitive groups are reported in Table 5.2. 7 interactions in the extrinsic case (case A), 4 interactions in the combined case (case B), and 5 interactions in the intrinsic cases (case C and D) are shown in the most sensitive cluster (Cluser I). Among all these interactions, the off rates of platelet activations by TXA2 and ADP were clustered in the high sensitive group for all cases. In the extrinsic case, 3 out of 7 interactions were associated with fX/FXa activities, all other interactions were related to platelet activation by TXA2 or ADP. It is noted that, although all these 3 fX/FXa interactions were not in the high sensitive group for the combined case (case B), they were classified in the medium sensitive group (Cluster II). Furthermore, the secretion of TXA2 by activated platelets was also not shown in the high sensitive group for case B, in stead, it showed up in the medium sensitive group. In addition, the self-activation of intrinsic pathway protease fXI (on and catalytic rates) were shown in the high sensitive group for the case B, C and D.

The medium sensitive group (Cluster II) consisted 24 interactions in case A, 20 interactions in case B, 25 interactions in case C and 18 interactions in case D. For the extrinsic case (case A), one of the most important category of reactions in Cluster II was the surface binding interactions as 9 out of the total 24 interactions in Cluster II were binding interactions with active platelet sites; while among other interactions, 6 interactions related to the formation and ac-

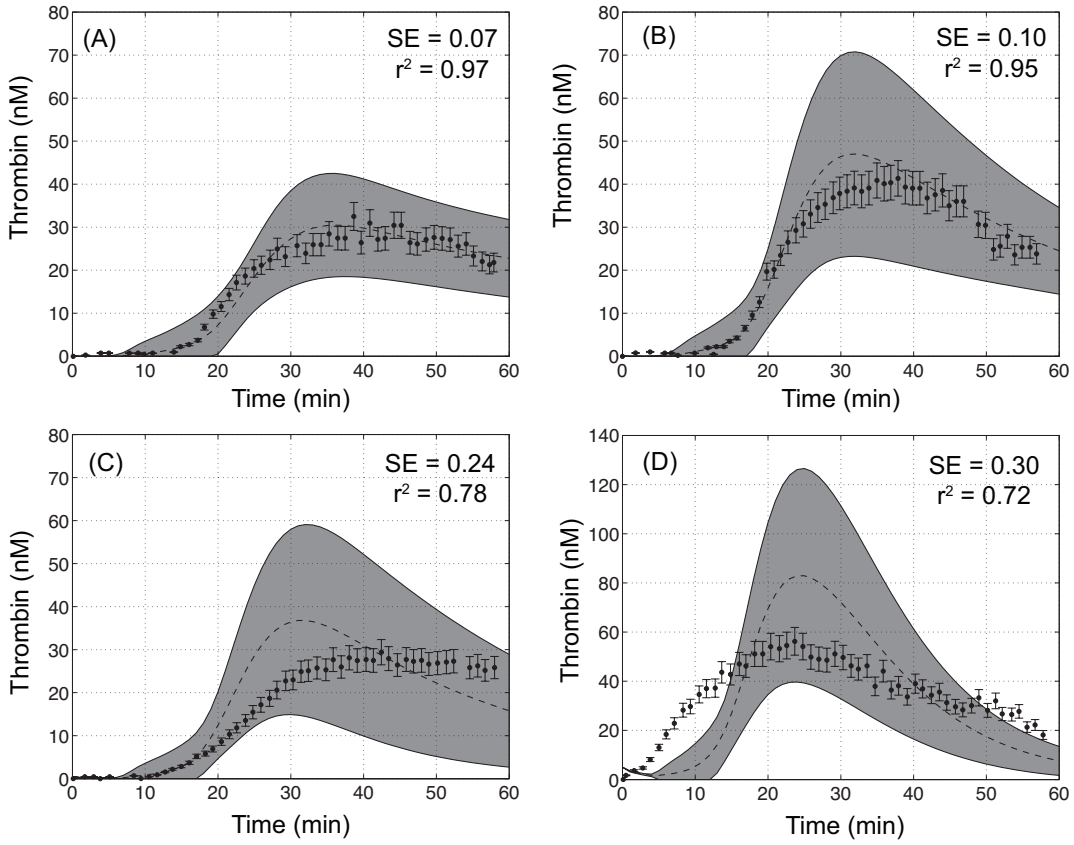

Figure 5.2: Model predictions of thrombin generation versus time as a function of TF, FVIIa, fXI and thrombin and experimental measurments from a cell-based model. (A-D) Thrombin generation in the case A, B, C and D in Table 5.1, respectively. The experimental thrombin generation assay was reproduced from Wielder et al [15]. An ensemble of parameter sets (N = 437) was generated using nine training data sets. The dotted lines denote the mean thrombin concentrations calculated from the parameter ensemble and the shadow areas denote one standard deviation of the ensemble. The normalized standard errors (SE) and the correlations between the mean simulation values of the ensemble are reported in the corner of each panel. In the experiments, recalcified PRP was incubated with different concentrations of FVIIa, fXI and thrombin (see Table 5.1) in the presence of collagen. Thrombin generation was initiated by TF or small amount of thrombin.

tivities of surface complex tenase or prothrombinase, 5 TF-VIIa activating interactions, 3 platelets activations by thrombin and 1 ATIII inhibitory interaction. Our findings in Cluster I and II for the extrinsic case were consistent to certain degree with our previous observations in the extrinsic pathway model [162] that fX/FXa and thrombin related mechanisms were fragile, while fIX/FIXa and fVIII/FVIIIa activation and activities were relatively robust.

Table 5.2: The distribution of the OSSCs for different cases [5].

p-index	case A	case B	case C	case D	Description
Cluster I					
172	0.83±0.23	0.76±0.20	0.84±0.19	0.76 ±0.18	TXA2 activates platelets (off)
175	0.74±0.27	0.48±0.17	0.57±0.24	0.63 ±0.25	ADP activates platelets (off)
126	0.62±0.18	–	–	–	ATIII inhibits FXa (on)
50	0.60±0.21	–	–	–	FXa binds platelet active sites (off)
13	0.54±0.19	–	–	–	TF-FVIIa activates fX (catalytic)
164	0.37±0.17	–	–	–	Activate platelets secret ADP
165	0.50±0.22	–	0.47±0.13	0.44±0.14	Activate platelets secret TXA2
197	–	0.68±0.40	0.80±0.23	0.62±0.33	FXIa self-activation (on)
199	–	0.50±0.27	0.65±0.13	0.49±0.16	FXIa self-activation (catalytic)
Cluster II					
90	0.56±0.23	0.41±0.24	0.29±0.14	0.34±0.18	Prothrombinase activates fII (on)
59	0.41±0.20	0.29±0.16	0.22±0.13	0.29±0.18	fII binds platelets activate sites (on)
60	0.40±0.20	0.28±0.15	0.22±0.13	0.28±0.17	fII binds platelets activate sites (off)
58	0.35±0.26	0.27±0.20	0.30±0.10	0.36±0.15	FVIIIa binds platelet active sites (off)
57	0.35±0.26	0.27±0.20	0.30±0.10	0.36±0.15	FVIIIa binds platelet active sites (on)
123	0.27±0.18	0.33±0.30	0.33±0.27	0.53±0.32	ATIII inhibits FIXa (on)
47	0.50±0.17	0.34±0.18	–	–	fX binds platelet active sites (on)
48	0.50±0.17	0.34±0.18	–	–	fX binds platelet active sites (off)
49	0.50±0.18	0.33±0.18	–	–	FXa binds platelet active sites (on)
11	0.44±0.13	0.28±0.13	–	–	TF-FVIIa activates fX (on)

Continued on next page

Table 5.2 (Continued)

p-index	case A	case B	case C	case D	Description
12	0.34±0.09	0.22±0.10	–	–	TF-FVIIa activates fX (off)
147	0.47±0.37	0.26±0.29	0.31±0.30	–	Thrombin activates platelets (catalytic)
97	0.45±0.18	0.29±0.16	0.20±0.08	–	FXa binds FVa on platelet surface (on)
98	0.45±0.18	0.29±0.16	0.20±0.08	–	FXa binds FVa on platelet surface (off)
95	0.32±0.28	–	0.17±0.11	0.25±0.18	FIXa (specific) binds FVIIIa (on)
96	0.32±0.28	–	0.17±0.11	0.25±0.18	FIXa (specific) binds FVIIIa (off)
81	0.32±0.28	–	0.17±0.11	0.24±0.18	Tenase activates fX on platelet surface (on)
45	0.32±0.25	–	0.15±0.09	0.22±0.14	FIXa binds specific platelet active sites (on)
46	0.31±0.25	–	0.14±0.09	0.21±0.13	FIXa binds specific platelet active sites (off)
156	0.27±0.21	–	0.19±0.19	–	Thrombin activates platelets via PAR4 (off)
155	0.27±0.21	–	0.19±0.19	–	Thrombin activates platelets via PAR4 (on)
14	0.31±0.11	–	–	–	TF-FVIIa activates fIX (on)
15	0.28±0.10	–	–	–	TF-FVIIa activates fIX (off)
16	0.23±0.15	–	–	–	TF-FVIIa activates fIX (catalytic)
13	–	0.37±0.19	–	–	TF-FVIIa activates fX (catalytic)
165	–	0.42±0.11	–	–	Activate platelets secret TXA2
164	–	0.24±0.10	0.24±0.14	0.29±0.11	Activate platelets secret ADP
198	–	0.21±0.14	0.25±0.10	0.19±0.11	FXIa self-activation (off)
50	–	0.41±0.21	0.24±0.09	0.17±0.04	FXa binds platelet active sites (off)
126	–	0.36±0.19	–	0.18±0.08	ATIII inhibits FXa (on)
129	–	–	0.19±0.12	0.19±0.06	ATIII inhibits thrombin (on)
93	–	–	0.14±0.11	–	FIXa binds FVIIIa on platelet surface (on)
94	–	–	0.14±0.11	–	FIXa binds FVIIIa on platelet surface (off)
78	–	–	0.13±0.11	–	Tenase activates fX on platelet surface (on)
144	–	–	0.11±0.10	–	Thrombin activates platelets via PAR1 (off)
143	–	–	0.11±0.10	–	FXa activates fV on platelet surface (on)
62	–	–	–	0.17±0.07	Thrombin binds platelet active sites (off)
210	–	–	–	0.16±0.08	FXIa activates fIX (on)

[5]The OSSC values were clustered using a k-means algorithm into three parts. The most fragile parameters were shown in Cluster I; the most robust ones were shown in Cluster III. The mean OSSC value (μ) ± one standard deviation (σ) in Cluster I and II are reported. p-index denotes the parameter index in the reaction file.

For the combined case (case B), 8 platelet binding interactions and 3 interactions related to the formation and activities of prothrombinase, 3 interactions of TF-VIIa activating fX, 2 ATIII inhibitions for FIXa and FXa and the others were related to platelet activation. In total, there were 11 interactions related to fX/FXa activities, 1 interaction related to fXI/FXIa, and 1 interaction related to fIX/FIXa, etc. For case C and D, most of the medium sensitive parameters were associated with the activities of platelets, thrombin, fIX/FIXa and fXI/FXIa. When taken together, thrombin and platelets interactions were the most sensitive interactions among all cases; fX/FXa activities were fragile in the extrinsic and combined case, while less fragile in other cases; binding interactions were moderately sensitive in the extrinsic and combined cases, but less important in all other cases. Furthermore, TF-FVIIa mechanisms were sensitive in the extrinsic case, while robust in all other cases; similarly, fXI/FXIa mechanisms were robust in the extrinsic case, while sensitive in the combined and intrinsic cases.

The statistically analysis of the pairwise comparisons of the OSSCs for different cases were used to gauge the importance of mechanisms in different cases (Figure 5.3 and Table 5.3). Increases or decreases in the OSSC value of a reaction in one case relative to the other indicated increased or decreased importance of the reaction in different pathways. And all the shifts found in these pairwise comparisons have shown to be in either high or medium sensitive group in one case or the other. Comparing the intrinsic cases with different amount of initiating thrombin (Figure 5.3D and Table 5.3), 6 statistically significant shifts were observed. Among all these 6 shifts, 3 of them involved thrombin activity, 2 related to fXI/FXIa activity and 1 related to ATIII inhibition of FIXa. The results indicated that the changes in the initiating thrombin concentration in the intrinsic cases not only affected the sensitivity of thrombin mechanisms, but also

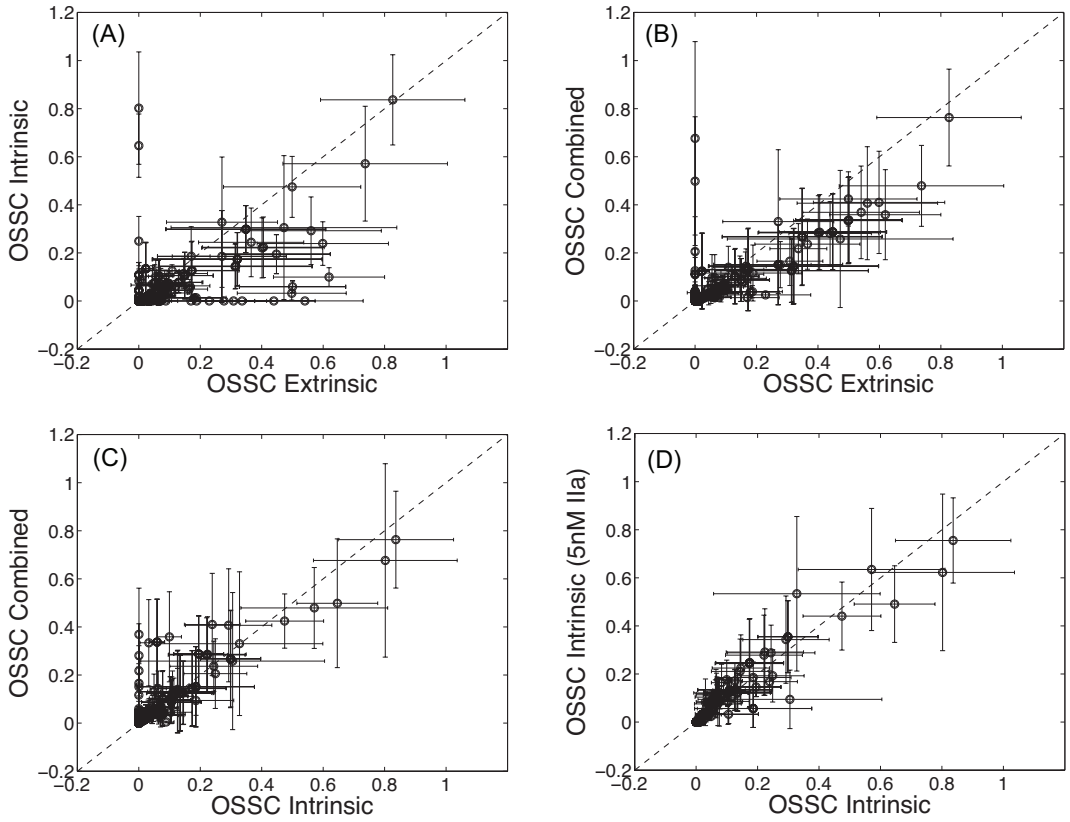

Figure 5.3: The pairwise parameter OSSC values calculated from sensitivity analyses for different cases in Table 5.1. Among the generated parameter ensemble, 100 parameter sets with a CV of 2 were selected for the sensitivity analyses. The mean and standard deviation of all parameter sets were shown in the figure.

had something to do with the fXI/FXIa mechanisms, and even fIX/FIX mechanism. After further investigating the OSSCs, although the relative importance of most parameters was statistically shifted between these two cases, 3 out of the 6 parameters were still clustered into the same sensitive group. For example, although the on and catalytic rates of FXIa self-activation (parameter index of 197 and 199) were statistically shifted when comparing case C with case D, they were clustered into the high sensitive group (Cluster I) for both cases. On the other hand, if a parameter was clustered into different groups, this param-

Table 5.3: Statistical results of the indices of shifted parameters in pairwise comparison of different cases (Table 5.1).

case C vs case A	case C vs case B	case A vs case B	case C vs case D
11	11	–	–
12	12	–	–
13	13	–	–
14	14	–	–
47	47	–	–
48	48	–	–
49	49	–	–
50	50	–	–
126	126	126	–
197	–	197	197
199	–	199	199
–	–	147	147
–	–	175	–
–	–	–	123
–	–	–	155
–	–	–	156

eter was highly possible to be one of the statistically significant shifts, e.g. the rates of thrombin activating platelets (parameter indices of 147, 155 and 156).

As compared to the combined case, 9 and 5 statistically significant shifts were observed in the intrinsic and extrinsic cases, respectively; while 11 significant shifts were observed when comparing the intrinsic case to the extrinsic case (Table 5.3). Comparing the intrinsic to the combined case, except for 1 fIX/FIXa mechanism (index 14), the remaining 8 mechanisms all related to fX/FXa activities; All these mechanisms were all shown to have reduced sensitivity in the intrinsic case. When comparing the extrinsic to the combined case, the on and

catalytic rates of fXI self-activation were shown to have increased sensitivity in the combined case; while the other 3 mechanisms that related to the activation of platelets and the inhibition of FXa became less significant in the combined case. Comparing the intrinsic to the extrinsic case, 8 out of 11 significant shifts related to fX/FXa activities and 1 related to FIXa were shown to have reduced sensitivities in the intrinsic case; while the remaining 2 shifts were related to fXI self-activation with apparently increased significance in the intrinsic case. Overall, the sensitivity of fX/FXa mechanisms was generally shifted to be more important in the extrinsic case; while the parameters related to fXI/FXIa interactions was more sensitive in the intrinsic cases. In the combined case, both fX/FXa and fXI/FXIa mechanisms were sensitive.

The sensitivity of species was accessed by multiplying the absolute connectivity matrix with the parameter OSSC values, therefore it evaluates the combination of the species connectivity and the parameter sensitivity. Figure 5.4 shows the average ranks of the top ten most sensitive species and their corresponding connectivity in different cases (Table 5.1). In all cases, at least 8 out of the top 10 most sensitive species show a connectivity greater than the mean connectivity (4.9) + 1 standard deviation (6.1) of all species, which indicated that the species sensitivity was highly influential by the species connectivity. Platelet activators ADP and TXA2 ranked within the top 3 most sensitive species for all cases; while thrombin ranked the 5th sensitive species except for the combined case. In the extrinsic case, free and surface bound fX/FXa and TF-FVIIa were ranked in the top 10 sensitive species (Figure 5.4A); while in the combined and intrinsic cases, FXIa became more sensitive as shown in the top 10 sensitive species (Figure 5.4B, C and D); FIXa was shown as the 8th sensitive species in case D. The relative importances of fX/FXa, TF-FVIIa, fXI/FXIa were consistent

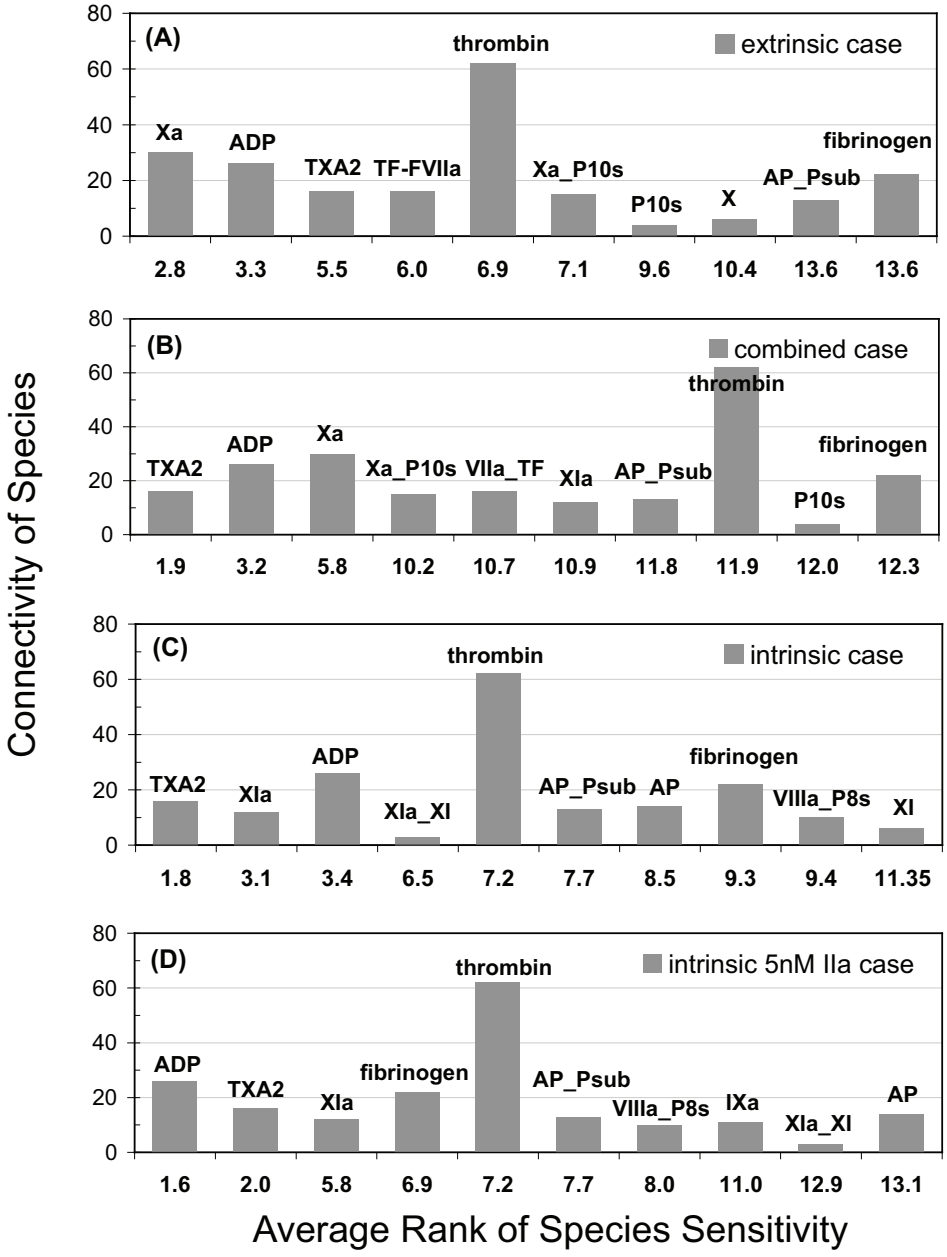

Figure 5.4: The connectivities of species ranked as the top ten most sensitive species for different cases in Table 5.1. The x-axis denotes the average ranks of the top ten most sensitive species in different cases, the y-axis denotes the corresponding connectivities of the species.

with our findings in the clustered parameter OSSCs (Table 5.2).

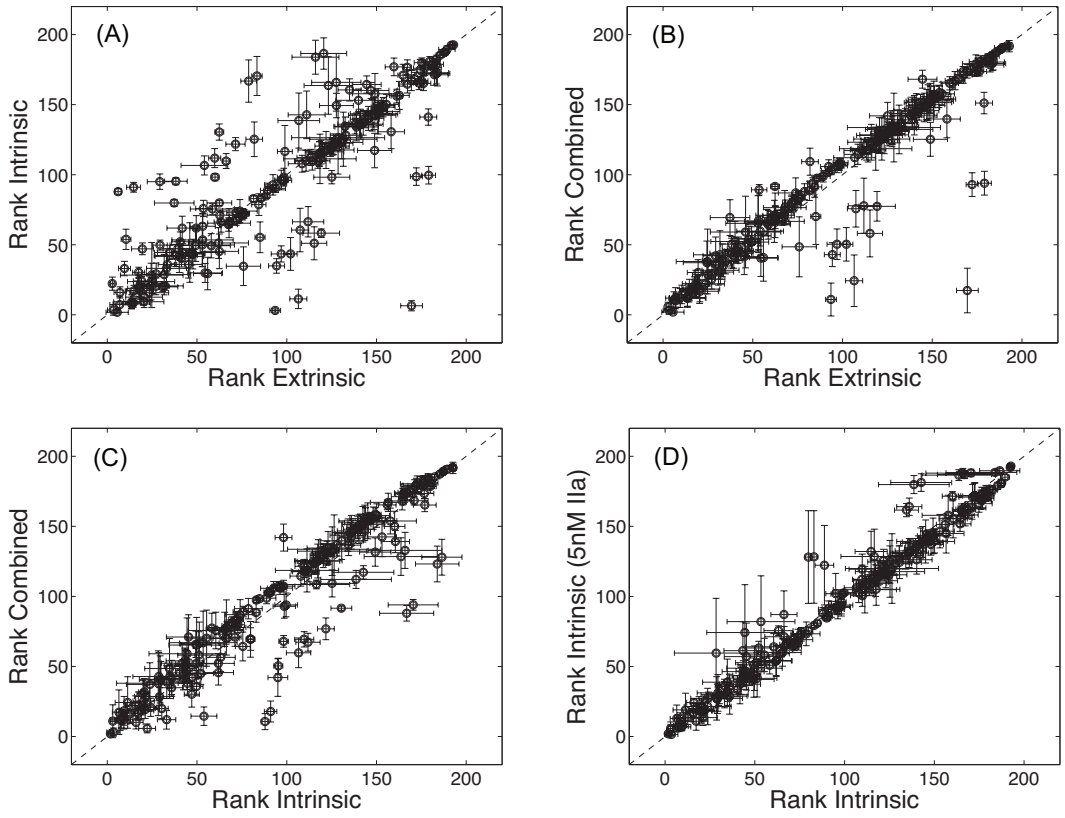

Figure 5.5: The pairwise species OSSC ranks calculated from sensitivity analyses for different cases in Table 5.1. The connectivity matrix $\mathbf{S}$ (193×301) was used to rearrange the parameter OSSC values to the species OSSCs. The rank orders of the species OSSCs were used to access the fragility of different species in the model. The mean and standard deviation of the ranks for species OSSC values (100 sets) were shown in the figure.

The pairwise comparisons of the rank-ordered species sensitivity of different cases are plotted in Figure 5.5 and the statistically significant shifts of the ranks are reported in Table 5.4. As compared to the combined case, 15 and 7 species were statistically significantly changed in the intrinsic and extrinsic cases, re-

[6]The mean ranks of the species OSSC values (μ) ± one standard deviation (σ) of the statistically shifted species are reported. s-index denotes species index in the pairwise comparison.

spectively; in the intrinsic case, all these 15 species, including 8 TF-FVIIa/FVIIa proteins or protein complexes and 4 PARs (protease-activated receptor) or PAR complexes, became less important approved by the increased species sensitivity ranks; in the extrinsic case, FXIIa and the other 6 fXI/FXIa or fXI/FXIa complexes became less fragile as compared to that in the combined case. Compare the intrinsic to the extrinsic cases, 6 fXI and fXII related species become more important, while the other 8 species including TF-FVIIa, FXa and PAR related species became less important in the intrinsic case. When considering the effect of initiating thrombin in the intrinsic cases, the different amount of initiating thrombin resulted in statistically significant changes in the sensitivity ranks of 7 PAR related species, 3 fVIII related species and 2 thrombin inhibitors. Those PARs were associated with the activation of platelets by thrombin; and the increased initial thrombin concentration (case D) resulted in decreased sensitivity of all species shifted.

5.4 Discussion

We have previously reported that fX/FXa activity and thrombin-mediated platelet activation were fragile mechanisms in the extrinsic pathway model, and these mechanisms were targets of current anticoagulation preclinical development, clinical therapies, and clinical trials in the treatment of thrombotic disorders [162]. In this study, we used parameter OSSCs and species sensitivity analysis to show that fX/FXa, thrombin and platelets were important species in the extrinsic case; while besides thrombin and platelets, fXI/FXIa became more important in the combined and intrinsic cases than that in the extrinsic case.

Table 5.4: Statistical results of the shifts in the rank of species OSSCs for pairwise comparison of different cases [6].

s-index	species	case C ($\mu \pm \sigma$)	case A ($\mu \pm \sigma$)	s-index	species	case C ($\mu \pm \sigma$)	case B ($\mu \pm \sigma$)
3	X-VIIa-TF	91.0±3.5	14.7±3.9	3	X-VIIa-TF	91.0±3.5	17.9±7.5
4	IX-VIIa-TF	95.0±5.5	29.3±7.0	4	IX-VIIa-TF	95.0±5.5	42.1±13.4
36	TF-FVIIa	87.9±2.2	6.0±1.9	6	VII-IIa	98.2±4.7	142.0±9.6
92	PAR3	170.4±13.9	83.4±2.9	35	VIIa	95.3±2.5	50.4±5.5
96	IIa-PAR3	186.5±11.2	120.6±12.8	36	TF-FVIIa	87.9±2.2	10.7±5.7
98	IIa-PAR4	166.8±15.1	78.8±4.4	39	X	53.8±7.2	14.5±6.6
102	PL-Psub-IIa-PAR4	183.9±12.1	116.0±13.1	78	VIIa-TF-ATIII	121.8±4.7	76.9±7.7
115	XIIa	98.6±6.3	172.2±3.3	81	TFPI-X-VIIa-TF	106.6±6.8	59.8±10.6
121	XI	11.4±6.9	106.5±4.7	82	TFPI-Xa-VIIa-TF	109.7±5.3	69.4±5.4
122	XIa	3.1±1.1	93.6±3.0	92	PAR3	170.4±13.9	94.0±3.8
127	XIIa-XI	99.6±6.3	179.1±3.8	96	IIa-PAR3	186.5±11.2	128.0±12.8
128	XIa-XI	6.5±3.6	169.6±6.1	98	IIa-PAR4	166.8±15.1	88.0±5.6
131	IIa-P2s-XI-P11s	51.0±11.8	115.3±7.0	102	PL-Psub-IIa-PAR4	183.9±12.1	123.2±12.8
185	IX-VIIa	130.4±5.8	62.4±2.5	184	X-VIIa	111.8±6.8	67.3±6.4
–	–	–	–	185	IX-VIIa	130.4±5.8	91.6±1.5
s-index	species	case A ($\mu \pm \sigma$)	case B ($\mu \pm \sigma$)	s-index	species	case C ($\mu \pm \sigma$)	case D ($\mu \pm \sigma$)
115	XIIa	172.2±3.3	92.9±8.5	11	Xa-VIII	79.8±1.9	128.1±33.1
121	XI	106.5±4.7	24.3±18.4	19	VIII-P8s-Xa-P10s	83.0±2.1	128.2±33.0
122	XIa	93.6±3.0	10.9±11.7	20	VIII-P8s-IIa-P2s	88.8±5.2	122.2±28.4
127	XIIa-XI	179.1±3.8	93.9±8.5	91	PAR1	53.4±18.9	82.0±32.7
128	XIa-XI	169.6±6.1	17.4±15.9	93	PAR4	44.5±21.3	74.2±34.1
129	XI-P11s	102.1±3.6	50.3±12.0	94	IIa-PAR1	142.7±17.0	181.3±6.3
131	IIa-P2s-XI-P11s	115.3±7.0	58.1±16.7	95	PL-IIa-PAR1	165.9±20.6	188.0±3.4
–	–	–	–	97	PL-IIa-PAR3	28.4±23.2	59.5±39.1
–	–	–	–	100	PL-Psub-IIa-PAR1	138.6±19.7	179.8±6.4
–	–	–	–	101	PL-Psub-IIa-PAR3	163.6±20.5	186.6±3.9
–	–	–	–	169	HCII-DER	134.5±6.7	161.6±4.7
–	–	–	–	170	HCII-DER-IIa	136.1±7.0	164.0±6.2

It is known that thrombi formed at low thrombin concentrations are composed of thick fibrin fibers and are highly susceptible to fibrinolysis; while thrombi formed at high thrombin concentrations are composed of thin fibers and are relatively resistant to fibrinolysis [218]. The addition of fXI in TF-initiated coagulation results in extra thrombin generation, which could protect fibrin clots from fibrinolysis [16] through the activation of thrombin activatable fibrionolysis inhibitor (TAFI) [210]. Thus, fXI deficiency does not seem to prevent the initiation of thrombi formation, but rather causes significant thrombi instability that prevents occlusion of the vessel. Moreover, fXI deficiency relates to only mild to moderate bleeding disorders and only has significant impact after trauma or surgery. The relative important impact on thrombosis and the relatively moderate impact on hemostasis make fXI an excellent target for the treatment of thrombotic disorders.

Intravital microscopy clearly demonstrated that platelet-rich thrombi form at sites of vessel injury in fXI-deficient mice [219, 220]. However, the platelet aggregates were unstable and undergo fragmentation, resulting a substantial reduction in thrombus growth and hence preventing injured vessels from occlusion [220]. Baird *et al.* studied platelet accumulation and fibrin deposition in fXI deficient mice after laser injury using digital fluorescence intravital microscopy [221]. As compared to wild-type mice, platelet accumulation was reduced by >90% and fibrin deposition at the site of injury by about 50% in fXI deficient mice after laser injury [219]. Renné *et al.* investigated the intrinsic pathway of coagulation on thrombus stability in mice and revealed that fXII- and fXI-deficient mice did not experience excessive injury-related bleeding. However, intravital fluorescence microscopy and blood flow measurements in three separate arterial beds revealed a severe defect in formation and stabilization

of platelet-rich occlusive thrombi induced by different methods of injury [220]. Infusion of human fXI or fXII into fXI or fXII null mice restored arterial thrombus formation following $FeCl_3$-induced injury of the carotid artery in the mouse [222, 220].

Yamashita *et al.* studied the role of fXI on arterial thrombus growth in the rabbit iliac artery in the presence of repeated balloon injury using a mouse monoclonal antibody XI-5108 to inhibit the auto-activation of FXIa. Intravenous administration of XI-5108 (3.0 mg kg^{-1}) remarkably reduced thrombus growth, and the activated partial thromboplastin time (APTT) was significantly prolonged; while prothrombin time (PT) and bleeding time (BT) remained unchanged [223]. Gruber *et al.* also showed in a baboon model when thrombosis was initiated by knitted dacron or TF-presenting teflon grafts deployed into arteriovenous shunts , intraluminal thrombus growth was markedly reduced in baboons treated with antihuman fXI antibody (aFXI) [224]. Compared with heparin at doses significantly prolonged the APTT, PT and BT, aFXI also prolonged the APTT, but the PT and BT were unaffected [224]. Recent studies showed that fXI deficient C57BL/6 mice in a carotid artery injury were protected from the formation of occlusive thrombi to a degree similar to fIX deficient mice after varied concentrations of ferric chloride were induced [225]. Carotid artery blood flow was completely blocked within 10 min in C57BL/6 mice by application of 3.5% $FeCl_3$. In contrast, fXI- and fIX-deficient mice were fully protected from occlusion induced by 5% $FeCl_3$, and partially protected against the effect of 7.5% $FeCl_3$. While fXI and fIX deficiencies were indistinguishable in the carotid artery injury model, there was a marked difference in tail-bleeding-time assay. The bleeding time in fXI-deficient mice, similar to that in and wild-type mice, were significantly shortened than that in fIX-deficient mice [225]. Lin *et al.* de-

signed and synthesized peptidomimetic inhimibitors of FXIa as novel anticoagulants [226], They showed that compound *32* caused a doubling of the APTT in human plasma and was efficacious in a rat model of venous thrombosis, which suggested that fXI played a significant role in venous thrombosis and could be a suitable target for the development of antithrombotic therapy.

Theoretical considerations and these experimental data [16, 210, 219, 220, 221, 222, 223, 224, 225, 226] suggested that fXI/FXIa could be excellent candidates as clinical targets in treatment of thrombotic disease. Inhibition of fXI/FXIa could potentially reduce the risk of occlusive thrombi formation without sacrificing hemostasis as deficiency of fXI results in bleeding manifestations only after trauma or surgery. Thus the use of sensitivity analysis could capture important mechanisms in a human-related cascade, and these mechanisms could be potentially excellent therapeutic targets in clinical treatments. Although experiments in animal models and clinical trials are always the most important steps in developing new drugs, mechanistic modeling and sensitivity analysis could be used as the first step in selecting potential drug targets.

5.5 Methods

5.5.1 Formulation of the model equations.

The reactions considered in the coagulation model have been compiled from literature [162, 204, 113, 69, 17, 205, 206, 16, 15, 60, 52, 146, 9, 8, 53]. Mass balance equations are written around each protein or protein complex yielding the set

of differential equations (vector-form):

$$\frac{d\mathbf{x}}{dt} = \mathbf{S}\mathbf{r}(\mathbf{x}, \mathbf{k}) = \mathbf{g}(\mathbf{x}, \mathbf{k}) \qquad \mathbf{x}(t_o) = \mathbf{x}_o \tag{5.1}$$

The symbol $\mathbf{S}$ denotes the connectivity matrix (193×301), while $\mathbf{x}$ denotes the 193-dimensional concentration vector of proteins or protein complexes and $\mathbf{r}(\mathbf{x}, \mathbf{k})$ denotes the 301-dimensional vector of reaction rates and $\mathbf{k}$ denotes the parameter vector. Each row in $\mathbf{S}$ describes a particular protein or protein complex while each column describes the stoichiometry associated with a specific interaction in the network. Thus, the (i, j) element of $\mathbf{S}$, denoted by σ_{ij}, describes how protein i is connected to rate process j. If $\sigma_{ij} < 0$, then protein i is consumed in r_j, conversely, if $\sigma_{ij} > 0$ protein i is produced by r_j and if $\sigma_{ij} = 0$ there is no connection between protein i and rate process j. We have assumed mass action kinetics for each interaction in the network; under the mass action assumption the rate expression for protein-protein interaction q:

$$\sum_{j \in \{\mathbf{R}_q\}} \sigma_{jq} x_j \rightarrow \sum_{p \in \{\mathbf{P}_q\}} \sigma_{pq} x_p \tag{5.2}$$

is given by:

$$r_q\left(\mathbf{x}, k_q\right) = k_q \prod_{j \in \{\mathbf{R}_q\}} x_j^{-\sigma_{jq}} \tag{5.3}$$

where $\left\{\mathbf{R}_q\right\}$ denotes the set of reactants for reaction q, $\left\{\mathbf{P}_q\right\}$ denotes the product set for reaction q, k_q denotes the rate constant governing the qth interaction and σ_{jq}, σ_{pq} denote stoichiometric coefficients (elements of the matrix $\mathbf{S}$). We have treated every protein-protein interaction and catalytic mechanism as non-negative. All reversible interactions were split into two irreversible steps, thus, every element of the reaction rate vector $\mathbf{r}(\mathbf{x}, \mathbf{k})$ took the form shown in Eqn. 5.3. The model equations were solved using the LSODE routine of the OCTAVE programming environment (v2.9.9; www.octave.org) on an Apple Computer

MacOSX (Cupertino, CA; v10.4.8) workstation. Initial conditions were taken from each experiment and roughly correspond to *in-vivo* physiological conditions (Table fXItbl-cases). Among the parameter ensemble, 100 parameter sets that resulted in CV of 2 were selected for the sensitivity analysis.

5.5.2 Error Analysis of the Coagulation Simulations.

The correlation between model simulations and experimental data was calculated using the relationship:

$$r^2 = \frac{\sum_{h=1}^{N} \left(Y_m(t_h) - \bar{Y} \right)^2}{\sum_{h=1}^{N} \left(\bar{Y}(t_h) - Y_m(t_h) \right)^2 + \sum_{h=1}^{N} \left(Y_m(t_h) - \bar{Y} \right)^2} \tag{5.4}$$

where $Y_m(t_h)$ denotes the model value at time point h, $\bar{Y}$ denotes the global average experimental value (average of experimental measurements over time) and $\bar{Y}(t_h)$ denotes the average experimental value at time point h (average of experimental trials). Eqn. 5.4 measures the fraction of variation captured by the model. In addition to correlation, the scaled standard error was used to measure the agreement between the model:

$$s_E = \frac{1}{\max_h \left(\bar{Y}(t_h) \right)} \left(\frac{\sum_{h=1}^{N} \left(\bar{Y}(t_h) - Y_m(t_h) \right)^2}{N} \right)^{1/2} \tag{5.5}$$

Both Eqn. 5.4 and 5.5 were taken from [147].

5.5.3 Computation of overall state sensitivity coefficients.

The sensitive or fragile interactions of the coagulation architecture were determined by computing Overall State Sensitivity Coefficients (OSSC) [89]. Because

each parameter corresponds directly to a particular molecular interaction in the cascade, OSSC values were used to gauge which interactions were qualitatively important. Large OSSC values for interactions relative to their peers indicated fragility or sensitivity while small OSSC values indicated robustness. The OSSC value for interaction j was defined as:

$$O_j(t) = \frac{k_j^*}{N_S}\left(\sum_{h=1}^{N_T}\sum_{i=1}^{N_S}\left[\frac{1}{x_i^*}\frac{\partial x_i}{\partial k_j}\bigg|_{t_h}\right]^2\right)^{1/2} \tag{5.6}$$

where N_T denotes the number of time points used in the simulation while N_S denotes the number of proteins/protein complexes in the model. The first-order sensitivity coefficients:

$$s_{ij}(t_h) = \frac{\partial x_i}{\partial k_j}\bigg|_{t_h} \tag{5.7}$$

were computed by solving the differential equation:

$$\frac{d\mathbf{s}_j}{dt} = \mathbf{A}(t)\,\mathbf{s}_j + \mathbf{b}_j(t) \qquad j = 1, 2, , N_P \tag{5.8}$$

subject to the initial condition $\mathbf{s}_j(t_0) = \mathbf{0}$. In Eqn. 5.8, the quantity j denotes the parameter index, N_P denotes the number of parameters, $\mathbf{A}$ denotes the Jacobian matrix of the model equations and $\mathbf{b}_j$ denotes the jth column of the matrix $\mathbf{B}$, which contains first-derivatives of the mass balances w.r.t. the parameter values. The quantity $\mathbf{s}_j$ denotes the vector of first-order sensitivity coefficients w.r.t parameter j. The Jacobian matrix ($\mathbf{A}$) and the matrix of first-derivatives of the mass balances w.r.t the parameter values ($\mathbf{B}$) are given by:

$$\mathbf{A} = \frac{\partial \mathbf{g}}{\partial \mathbf{x}}\bigg|_{(\mathbf{x}^*,\mathbf{k}^*)} \qquad \mathbf{B} = \frac{\partial \mathbf{g}}{\partial \mathbf{k}}\bigg|_{(\mathbf{x}^*,\mathbf{k}^*)} \tag{5.9}$$

where $(\mathbf{x}^*, \mathbf{k}^*)$ denotes a point along the *nominal* or *unperturbed* system solution. The matrices $\mathbf{A}$ and $\mathbf{B}$ were numerically estimated at each time step using a generalized gradient algorithm [148] while the sensitivity balances were solved using the LSODE routine of the OCTAVE programming environment

(v2.9.9; www.octave.org) on an Apple Computer MacOSX (Cupertino, CA; v10.4.8) workstation.

The connectivity matrix $\mathbf{S}$ (193×301) was used to rearrange the parameter OSSC values to the species OSSCs through the equation:

$$\mathbf{Q} = |\mathbf{S}|\mathbf{O} \tag{5.10}$$

The rank orders of the species OSSCs were used to access the fragility of different species in the model.

5.5.4 Statistical and clustering analysis of the shifts in overall state sensitivity coefficients.

Three different tests were performed to identify large statistically significant shifts in OSSC values between defective networks and the control. A Welch t-test [149] was used to find all statistically significant shifts resulting from the different structural perturbations and then a secondary test on the $z-$score of each shift was preformed to find only the most prominent. The OSSC values calculated over the family of parameter sets were assumed to follow normal distributions for all cases. The statistical significance of shifts in OSSC values relative to the control were determined by performing a Welch t-test with the null hypothesis that the means of the sensitivity coefficients were equal at a 1% significance level. The Welch t-test is similar to the student t-test with the exception that the two distributions being compared are not required to have equal variances. The list of significant OSSC values was further restricted to only those shifts with a magnitude larger than a specified z-score (0.1) away

from the squared mean displacement relative to the control:

$$d_{j,q} = \left(\bar{O}_j^q - \bar{O}_j^c\right)^2, \qquad j = 1, 2, , N_P \tag{5.11}$$

where $\bar{O}_j^c$ denotes the mean OSSC value over the family of parameter sets for parameter j in the control while $\bar{O}_j^q$ denotes the same quantity for defective case q. A significant shift in OSSC value was *accepted* if:

$$d_{j,q} > z\sigma_{d_q} + \mu_{d_q} \tag{5.12}$$

where z denotes a desired z-score, σ_{d_j} denotes the standard deviation of the total displacement over all significant OSSC values for the *qth* defective case and μ_{d_q} denotes the mean of the significant displacements for the structurally defective case q.

A large statistically significant shift in OSSC value, while indicative of the shifting importance of an interaction, does not guarantee that an interaction is ranked differently between cases. To this end, we used the Spearman rank correlation denoted by ρ and defined as:

$$\rho = 1 - \frac{6\sum_{i=1}^{N_P} d_i^2}{N\left(N^2 - 1\right)} \tag{5.13}$$

to measure the difference in qualitative ranking between cases. The quantity d_i denotes the difference in the ordinal rank of interaction i between a structurally defective network and the control, N denotes the number of pairs of values and N_P denotes the number of parameters considered. The Spearman rank is bounded by $-1 \leq \rho \leq 1$; a Spearman rank of one indicates that two ranked lists are identical, a Spearman rank equal to negative one indicates that two ranked lists are perfectly negatively correlated, while a Spearman rank of zero indicates that two ranked lists are uncorrelated.

The distributions of OSSC values obtained from monte-carlo sampling were clustered using a k-means algorithm [209]. The mean and standard deviation obtained from the monte-carlo sensitivity analysis was used to estimate the underlying OSSC distribution (N = 200 points) where the OSSC values were assumed to be normally distributed. Two hundred different clustering attempts were run for each model to control for clustering artifacts. The most probable configuration was reported.

CHAPTER 6

COMPUTATIONAL ANALYSIS OF THE EFFECT OF FLOW ON BLOOD CLOT FORMATION

6.1 Abstract

A mathematical model, that was validated for thrombin and fibrin formation in the absence of flow, was further refined to simulate blood clot formation under simple pressure-driven parabolic flow after being exposed to different sizes of tissue factors (TF) patches. The predicted clot times at various shear rates and TF patch sizes were generally consistent with experimental observations using microfluidic capillaries or parallel plate flow. Our numerical analysis elucidates two counteracting effects of flow on the formation of arterial clot under conditions of exposed TF: (1) inhibition of the initiation of blood clot formation by the flow-mediated transport of enzymes; (2) promotion of rapid formation of active factors and blood clots via shear induced platelet activation (SIPA) under high shear. Thresholds in shear rates or TF patch sizes were observed for the initiation of clot formation; the balance between the generation of active factors and the removal of those factors by flow was possibly the reason for the threshold phenomena. Extremely low shear, where the flow-mediated transport was insignificant, and extremely high shear, where the generation of active factors was significant, could both lead to the initiation of clotting; the shear rates, at which the blood clotting did not initiate within 1000 seconds, were found to be correlated with the normal physiological range of shear rates.

6.2 Introduction

When the delicate balance between the pro- and anti-coagulants in the blood is interrupted by plaque rupture, vessel damage, or dysfunctional endothelium, blood clots could form at the site to interfere with normal blood flow, which is central to cardiovascular diseases. The mechanisms underlying clot formation or thrombosis were first identified over a hundred years ago when Virchow proposed his triad of blood, surface, and flow. The local rheological flow conditions are pivotal for the hemostatic system and largely affect the blood coagulation and platelets activation and deposition [227]. The underlying chemical, physical, and biological processes culminated in clot formation in the presence of flow have been proven difficult to model in a systematic, quantitative fashion. In this paper, we built a mathematical model to study the effect of flow on the formation of blood clots. It encompassed the extrinsic and intrinsic pathways of thrombin generation, as well as the formation and lysis of fibrin clots; we studied the effect of flow, the wound size (TF patch size) and the shear-induced platelet activation (SIPA) on the time of clot formation under model simple flow.

6.2.1 The biology of clot formation and lysis:

Following injury, a family of proteins (coagulation factors) and a key group of blood cells (platelets), both of which are normally inactive in the circulation, are activated by several different interconnected mechanisms that eventually lead to thrombin generation and fibrin clot formation at the wound site. Thrombin is the terminal protease generated by the process of blood coagulation. There are two pathways in the coagulation cascade which lead to thrombin generation:

the intrinsic and extrinsic pathways [111, 108]. In the extrinsic pathway, the exposed TF at the site of injury binds with circulating factor VII/VIIa to form TF-FVIIa complex and initiates a series of enzymatic interactions that leads to the formation of thrombin. The details of the coagulation process could be found in many other articles [116, 117, 110, 111, 112, 108, 115, 162]. The protease thrombin not only plays a key role in the feedback activation of upstream factors and platelets, buts also activates the intrinsic protease factor XI (fXI) [13, 14, 16, 17, 206, 19, 15, 205]. The intrinsic pathway of coagulation joins up with the extrinsic pathway at the point where fIX is activated by FXIa to form FIXa.

Thrombin irreversibly activates platelets through a family of transmembrane receptors on the platelet surface called Protease-Activated Receptors (PARs) [113, 204]. Platelets, another key components for thrombus formation, are produced in the bone marrow from megakaryocytes as cytoplasmic fragments without genomic DNA [228]. The lack of genomic DNA makes platelets incapable of transcription of nuclear material, rather structural and biosynthetic proteins that are required for normal platelet function are translated from megakaryocyte derived RNA. Platelets are present as inactive forms in the circulation and remain inactive because of a series of signals emitted by normal endothelial cells. However, platelets are highly reactive in the presence of vascular injury; they respond to and interact with unique substances in the tissue fragments released by ruptured plaques. These materials, primarily collagen, fibronectin and von Willebrand factor (vWF), existing in the tissue fragments promote platelet binding with the plaque ruptures (platelet adhesion) through specific molecular recognition interactions. The adhered platelet is then activated by external signals such as Adenosine Diphosphate (ADP),Thromboxane A2 (TXA2) and thrombin.

Activated platelets have a different physical shape than their inactivate counterparts and transmit chemical and peptide signals into the blood stream. These signals attract additional platelets to the scene and promote further binding and activation. In particular, activated platelets secreted ADP and Thromboxane A2 (TXA2), both of which promote further activation. Jin *et al.* have explored the molecular mechanisms of ADP induced activation of platelets and have shown that the P2Yi receptor mediates ADP-induced shape change in activated platelets [229]. The shift in shape will expose key phospholipid binding sites that are required for the formation of the critical surface bound complexes in the coagulation response. In addition, activated platelets secrete fibrinogen, a linker-like substance which interacts with platelet glycoprotein surface receptors (Glycoprotein IIb/IIIa) to cross-link other activated platelets thereby forming a temporary platelet plug over the plaque ruptures. The platelet plug forms in seconds after exposure to the tissue fragments and serves as a necessary scaffold for the more permanent fibrin clot. Thrombin is a critical mediator between the formation of the platelet plug (platelet aggregation) and the fibrin clot (thrombus). Thrombin cleaves fibrinogen into fibrin monomers that form fibrin matrix on and between the aggregated platelet scaffold leading to the formation of insoluble fibrin clot [230, 231, 11]. Once a fibrin clot is formed, it serves as a cofactor for the activation of plasminogen to plasmin (PLA) by tissue-type plasminogen activator (tPA) or urokinase (uPA). Plasmin cleaves fibrin and leads to the breakdown of a fibrin clot, which is normally called fibrinolysis. Thrombin also plays a role in fibrinolysis by cleaving thrombin activatable fibrinolysis inhibitor (TAFI) to its active form activated TAFI (TAFIa), which will attenuate fibrinolysis by blocking the binding sites of plasmin to fibrin.

6.2.2 Review of flow effects on blood clot formation:

Arterial thrombosis usually occurs in flowing blood following the events such as plaque rupture, vessel damage, or dysfunctioning endothelium [232, 233, 227]. The roles of blood flow in coagulation and thrombosis have been rightly recognized more than a century ago by Virchow [42]. The flow behavior of blood may partly explain the localization and morphology of arterial, intracardiac and venous thrombi within the human circulation, and even why the increase in haematocrit, fibrinogen and other macromolecules, and rigid blood cells may increase the risk of ischaemic events [234, 42].

Under pressure-driven flow, in a laminar regime, shear stress is maximum at the vessel wall, and affects endothelial cell morphology and function. Fluid shear stress is the force of shearing motion of blood per unit area. Extremely low shear stress induces an intimal thickness of the arteries, which can develop into an early atherosclerotic plaque under certain circumstances such as excessive low density lipoprotein concentrations in blood [235]. The use of the non-invasive detection method such as Doppler ultrasound, enables investigators to localize atherosclerotic plaques in arteries as an indicator of atherosclerosis [235]. The correlation between early plaque localization in human subjects and areas of relative low and oscillatory wall shear stress implicates that this factor as the key to the role of fluid dynamics in atherogenesis [235, 236, 237, 238]. This intimal thickening can evolve into an early atherosclerotic plaque under certain circumstances such as excessive low density lipoprotein concentrations in blood [41]. Each early plaque exhibits an individual natural history of progression, regression, or stabilization. In the presence of certain local, systemic, and genetic factors, the local vascular wall might undergo excessive expansive remod-

eling. A self-perpetuating vicious cycle is established among local endothelial shear stress, excessive expansive remodeling, and plaque inflammation, transforming the early plaque to a thin cap fibroatheroma [41]. The stenotic plaques might either evolve with a phenotype promoting fibroproliferation consistently throughout their natural history course or represent a final stage of scarring in the setting of prior inflamed this cap fibroatheroma through repetitive microruptures and healing. Also, the stenotic plaques might infrequently undergo local erosion or develop calcified nodules and eventually lead to local thrombus formation and manifestation of an acute coronary syndrome [41].

Approximately 20 % of the early developed atherosclerotic plaques could grow to stenotic plaques through constrictive remodeling and result in a high local shear stress at the vessel wall [41]. High intra-stenotic shear stress may activate platelets, promoting the formation of initial platelet-rich "white-head" of arterial thrombi, while low post-stenotic shear stress may promote the formation of subsequent, fibrin- and red cell-rich"red tail" [3]. Blood viscosity, platelet microemboli, and activated leucocytes may each reduce post-stenotic microcirculatory blood flow, promoting infarction. Such mechanisms may explain the associations of increased levels of blood and plasma viscosity, haematocrit, white cell count, fibrinogen and vWF with risk and outcome of myocardial, cerebral and limb infarction [232, 233, 239, 42, 227, 41].

When blood with a parabolic velocity profile passes through a narrowing in the channel, it accelerates resulting in much higher wall shear stress near the apex of stenosis. Platelets are also concentrated at the vessel wall where they can be activated by high shear stress and well-placed to interact with vWF and subendothelium, resulting in platelet adhesion and activation

[240, 241, 39, 242, 243]. Shear-induced platelet activation (SIPA) and aggregation are important mechanisms of arterial thrombosis formation. In 1975, Brown used a cone and plate viscometer to demonstrate that exposing platelet-rich plasma to fluid shear stresses > 50 $dynes/cm^2$ resulted in changes in platelet morphology, along with secretion (ADP,ATP, serotonin) and aggregation [244]. Higher shear stresses (300, 750 and 1000 $dynes/cm^2$) were then proved to be able to induce activation of platelets in the average residence times of 25 to 1650 ms [245]. Early studies of SIPA in rotational viscometers focused on relative long exposure times to elevated shear stresses (50 to 100 $dynes/cm^2$) and a threshold response of platelet to shear stress is often addressed in these studies [246, 245, 247, 248, 249]. However, the threshold stress depends heavily on the time the platelets are subjected to the shear stress. Hellums et al. later showed that shear-induced platelet activation was a function of both the shear stress magnitude and the exposure time to shear by consolidating the finding from several groups using different flow devices [250]. Boreda further derived a platelet stimulation function defined by PSF = $\tau \times t^{0.452}$, where the activation state was linearly dependent on the magnitude of applied shear stress (τ) and somewhat less dependent on exposure time (t) [251]. Platelet activation state (PAS) measured in small diameter tubing directly increased with shear stress and time of exposure to shear, and elicited procoagulant activity on the platelet surface [252]. Thereby linking shear-mediated platelet responses to coagulation reactions. Thus, exposure of platelets to shear conditions causes platelet activation and that this activation is dependent on both shear stress and time of exposure. Using these relationships, Raz *et al.* used numerical models to study flow induced platelet activation resulting from stress histories along Langrangian trajectories in the flow field and validated using Digital Particle Image

Velocimetry (DPIV) in 84 % eccentric and axisymetric coronary stenosis model [253]. CFD, DPIV and PAS assay results in their study agreed well in predicting the level of platelet activation.

6.2.3 Review of the mathematical models:

Numerous models have been built to understand the underlying complex and intertwined chemical and biological processes that lead to blood coagulation [48, 20, 52, 12, 54, 60, 8, 9, 254]. In recent years, Mann and coworkers presented an model for thrombin generation via the extrinsic pathway [52, 12], and extended it to include the role of inhibitors [53]. Kuharsky and Fogelson [60] assumed the existence of a thin, well-mixed layer near the surface of the injured vessel. Transport of species from the bulk flow into this layer was quantified by an overall mass transfer coefficient. A more recent work by Anand *et al.* [8, 9] suggested a reaction-diffusion model of clot formation and lysis under flow conditions, using quasi-one-dimensional thrombus formation in a cylindrical vessel. Sorensen et al. [69, 70] proposed a set of coupled convection-reaction-diffusion equations to model platelet activation and deposition in flowing human blood. The equations were solved using finite element method in a two-dimensional flow and the results were compared with experimental results of platelet deposition onto collagen. In order to understand the complex biological system governing blood clotting, a simple chemical system was developed by Kastrup et. al [254, 255]. The group showed that the initiation of blood clotting on a 2-D surface in response to TF patches in the absence of flow depended not only on the size of individual patches [254], but also on the shape of the patch [255].

Most of the models focused on the reaction aspect of blood clotting. Only a few of them studied the effect of flow on clot formation. This is possibly due to the complexity arising from incorporating rheological aspects into the model, which lies not only in the influence of flow on the biochemical reactions but also the hemodynamic properties of blood flow itself. Even in the models that considered flow effect, they mostly focused on the low to medium shear range and ignored the effect of shear-induced platelet activation. In the present study, we built a mathematical model to study the formation of blood clot under low, medium, to high shear rates. We did a systematic research on the effect of flow-mediate transport and the effect of SIPA on clot formation.

6.3 Results

The mathematical model consisted 193 species and 301 interactions in the blood clotting system and it was developed to simulate blood clot formation in the simple 1-D flow conditions. We considered simple unidirectional, pressure driven flow, and shear rate in the boundary layer near the wall was used as the shear rate. The model was first validated for the formation of fibrin under quiescent conditions, shown in Figure 6.1, which worked as a supplement to the previous validation results for thrombin generations in the absence of flow (see Chapter 4 and 5); it was further developed to calculate clot time, which was a function of either thrombin or fibrin concentration, and the validations against experimental data were shown in Figure 6.2 and Figure 6.3 [256]. Since platelets could be activated by shear after exposure for critical time [252], we introduced platelet activation by different shear stresses at different exposure time; the shear rates, viscosities of blood, shear stress, exposure time required for SIPA,

and the rate of SIPA were shown in Table 6.1. The activation of platelets by shear was compared against the experimental observation [241] and the formation of fibrin and activated platelets (AP) were simulated under high shear conditions (Figure 6.4). Threshold effects were observed for the initiation of clot formation under various shear conditions and the shear rates, under which the blood clotting did not initiate in 1000 seconds, were found to be correlated with the normal physiological range of shear rates.

6.3.1 Model validation against the formation of fibrin in the absence of flow.

Our previous model validation focused on the generation of thrombin under quiescent conditions (see Chapter 4 and 5). However, generation of a stable blood clot requires thrombin-mediated conversion of fibrinogen to fibrin. Concentration of fibrin is another important marker for blood clot formation. Here in this part, we performed the simulation of fibrin formation after the addition of physiological amount of fibrinogen, and we simulated the process of fibrinolysis by tPA, uPA and plasmin in the presence and absence of TAFI [257, 258]. We compared our results against experimental data [257, 258] and we found that our model successfully predicted evolution of fibrin concentrations at different experiment conditions (Figure 6.1). Fibrin formed when fibrinogen was cleaved by thrombin; as shown in Figure 6.1A, after a lag phase of about 20 min, a burst of fibrin formation was observed. Our simulation well captured the experimentally observed time lag followed by surge in concentration in the formation of fibrin. When fibrin formed, plasmin that was activated by tPA or uPA could

cleave fibrin between its D and E domains and lead to the lysis of fibrin clots. Furthermore, TAFIa activated by thrombin prevented fibrin from fibrinolysis by competing with plasmin for fibrin binding sites. Figure 6.1B, 6.1C and 6.1D show the effect of TAFI in fibrinolysis when either plasmin or plasmin activator (tPA or uPA) was present. In all, the fibrin concentrations (blue curves) increased when TAFI was present, as the results of the inhibition of fibrinolysis by TAFI. Our model simulations are in good agreement with the experiments indicating that our model was not only capable in thrombin simulations but also able to predict fibrin formation.

6.3.2 Threshold response to shear rate and the size of TF patch for the generation of thrombin under the low to medium shear.

Thrombin generation in an 1-D flow field was simulated under mild shear conditions (5 to 50 s^{-1}) (Figure 6.2A). In all simulations, the TF patch started at position x = 600 μm. A TF patch of 200 μm, between position x of 600 and 800 μm, was used to initiate the coagulation cascade. The clot time was calculated as the time when more than 0.1 nM of thrombin was formed. In both simulation and experiment, in normal pooled plasma (NPP), the clot time remained constant near 200 s for shear rate below 20 s^{-1}, followed by a rapid increase in clot time to 800 - 1000 s around shear rate of 30 s^{-1}, yielding a threshold shear rate between 20 to 30 s^{-1}. For shear rates below the threshold, thrombin generation initiated with 200 seconds. While increasing shear rates resulted in a decrease in the initiation of thrombin formation; a clot time greater than 800 seconds was

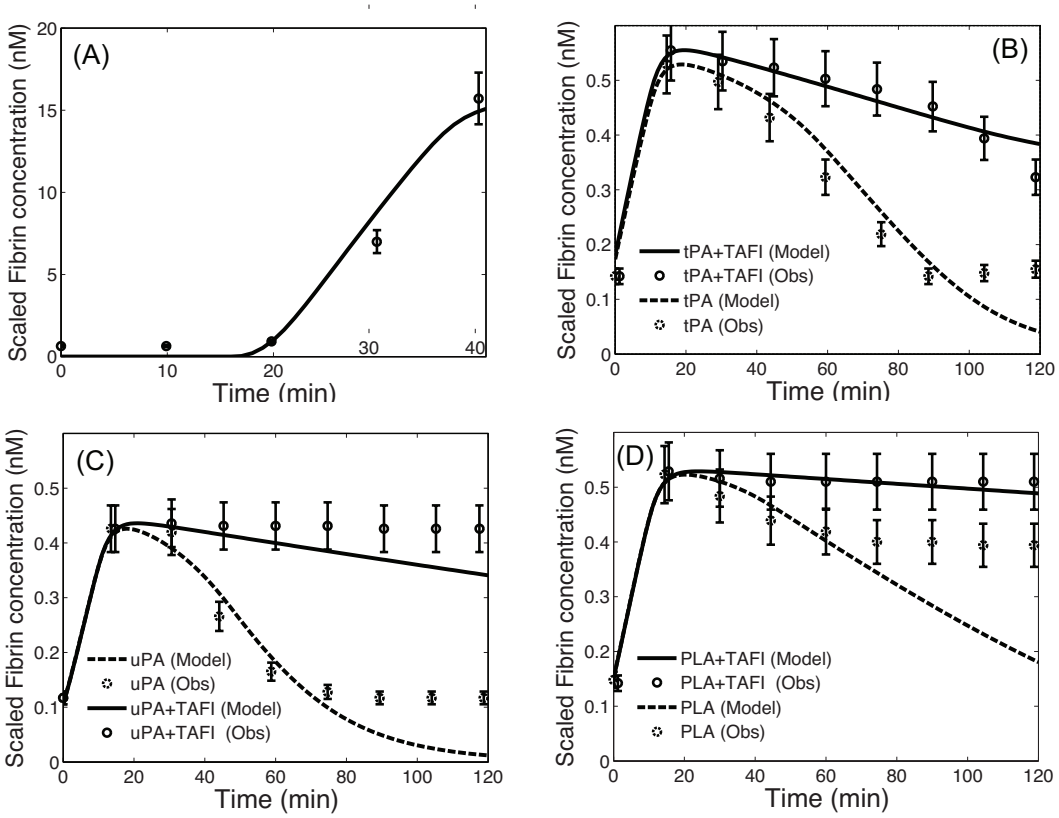

Figure 6.1: Model validation against experimental observations of the formation of fibrin in the absence of flow. (A) Computational simulation (solid line) is consistent with experimental observation of fibrin generation in time (shown as circles). The fibrin concentration was determined in diluted plasma samples by the ELISA [257]. (B-D) The fibrinolysis in time by tPA, uPA and plasmin (PLA) in the presence and absence of TAFI [258]. The fibrin concentrations were scaled by the maximum in each corresponding experiment.

observed for any shear rate greater than the threshold. This threshold effect is believed to be the result of competition between reaction and transport of activated coagulation factors [256]. The procoagulant factors got activated over the TF patch and these active factors could either react with other factors at the site or be transported from the site by the flow. Only when the concentration of activated factors exceeds a critical concentration at a position, thrombin generation could initiate. Therefore, when the shear rate is low, the effect of transport is not significant; the concentration of active factors could easily reach the critical value near the site of TF patch. This was proved by the generation of thrombin at shear rate of 5 s^{-1} (Figure 6.2C and 6.2E). It clearly shows that thrombin concentrations were much higher in positions near TF patch and it gradually decreased along the flow direction. While after the shear rate increased to 40 s^{-1}, thrombin generation initiated at the down-streams of the TF patch at time greater than 1000 seconds or 16 minutes (Figure 6.2D). This was because when the shear rate increased, the effect of flow-mediated removal of active factors from the TF patches became more significant. The active coagulation factors cumulated at at down-streams of the TF patch, which led to thrombin formation far from the patch.

Figure 6.2B shows the effect of TF patch size on clot formation at a constant shear rate. At a shear rate of 40 s^{-1}, increasing the size of TF patch from 100 to 1600 μm resulted in a substantial decrease in clot time around 200 to 400 μm of patch size. The threshold patch size between 200 and 400 μm observed in the model prediction is again consistent with the experimental observations. Similar mechanisms could apply in this case; the generation of active factors was much faster when the TF patch increased and the concentration of active factors could achieve the critical value at a much earlier stage, as depicted in

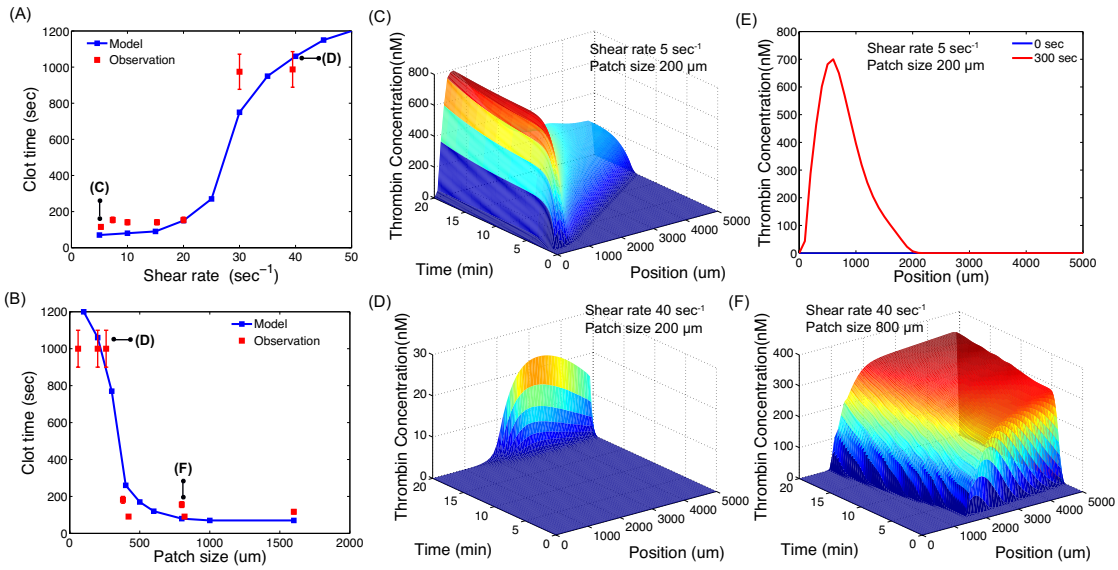

Figure 6.2: Model simulations of thrombin formation in normal pooled plasma (NPP). (A) and (B): Computational simulations are consistent with experiment observations that clot time in NPP displayed a threshold response to shear rate at a constant patch size of 200 μm (from 600 to 800 μm) (A) and to patch size at a constant shear rate of 40 s^{-1} (B) [256]. Clot time was determined as the time point at which $\geq$ 0.1 nM thrombin was generated in the simulation. In the experiment, the generation of thrombin was detected by fluorescence microscopy and the clot time was the time point when a burst of thrombin was generated or the initial formation of cross-linked fibrin appeared [256]. (C) and (D): Thrombin concentrations versus time and position with shear rates of 5 s^{-1} (C) and 40 s^{-1} (D) at a patch size of 200 μm. (E) Thrombin concentrations versus position at 0 and 300 sec at a shear rate of 5 s^{-1} and a patch size of 200 μm. Consistent with experiments at 300 sec [256], thrombin generation did not initiate at a shear rate of 40 s^{-1} (D), but did initiate at a shear rate of 5 s^{-1} (C and E). (F) Thrombin concentrations versus time and position at a shear rate of 40 s^{-1} and a patch size of 800 μm (from 600 to 1400 μm).

Figure 6.2B. We note that the initiation of thrombin generation occurred at position away from the TF patch for t he shear rate of 40 s^{-1} regardless of patch size (Figure 6.2D and F). This was possibly because the concentration of activated factors reached its critical concentration at somewhere down-streams of the TF patch as a result of increased flow-mediated removal effect.

6.3.3 Attenuation of fibrin clot formation by flow mediate transport of enzymes

The above simulations were performed to predict thrombin generation in normal pooled plasma (NPP) where small amount of platelets was present. However, given the importance of platelets and fibrinogen in blood clot formation, the experiments were also conducted in platelet rich plasma (PRP), where fibrinogen with fluorescence labels were also added in order to measure the formation of fibrin mesh [256]. Our calculation of clot time using the time for thrombin or fibrin $\geq$ 0.1 nM would return similar results; while here we used the time calculated for fibrin formation. As shown in Figure 6.3A, the threshold between shear rates of 70 to 100 s^{-1} was also observed in the PRP simulations. At low shear rates, the formation of clots started within 200 seconds, while after the shear rate increased to a value greater than the threshold, the simulated clot time increased to more than 400 seconds and continued to increase with shear rates. However, in the experiments, the threshold effect was much more distinct as the clot time sharply increased from 200 to about 1000 seconds right after crossing the threshold (In Figure 6.3A Observation). Such a high threshold value for clot time at shear rate between 70 and 100 s^{-1} in PRP correlated to the

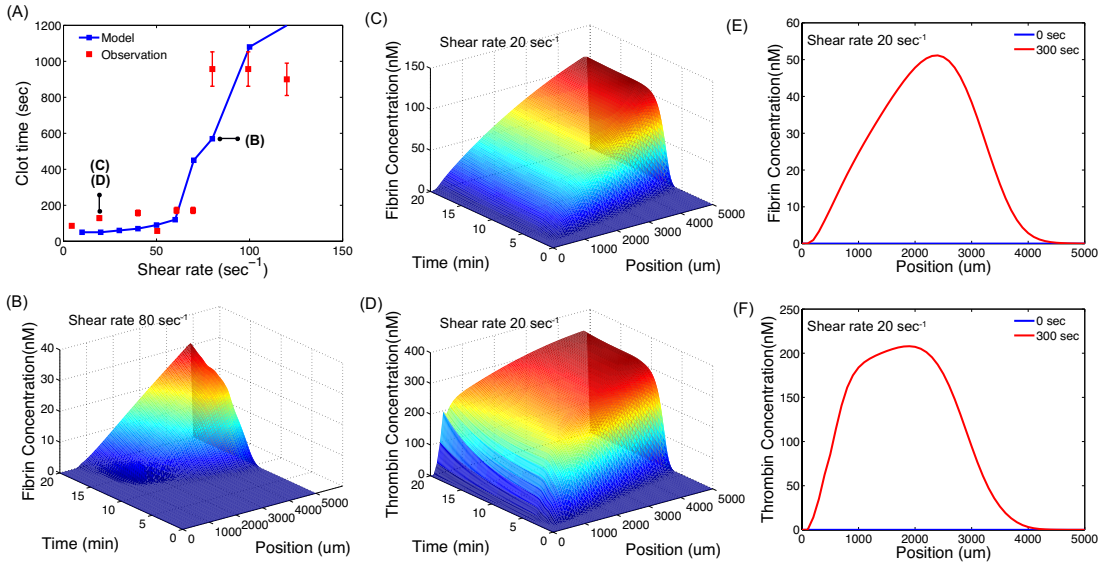

Figure 6.3: Model simulations of clot formation in platelet rich plasma (PRP). (A) Computational simulations are generally consistent with experiment observations that clot time in PRP displayed a threshold response to shear rate at a constant patch size of 200 μm [256]. The bright-field microscopy was used to detect the formation of fibrin mesh and aggregation of platelets [256]. In simulation, the clot time was calculated as the time point at which $\geq$ 0.1 nM fibrin was generated. (B) and (C) Fibrin concentrations versus time and position with shear rates of 80 s^{-1} (B) and 20 s^{-1} (C). (D) Thrombin concentrations versus time and position at a shear rate of 20 s^{-1}. (E) and (F): Fibrin and thrombin concentrations versus position at time of 0 and 300 sec at a shear rate of 20 s^{-1} and a patch size of 200 μm. Although TF patches located between 600 and 800 μm, the maximum fibrin and thrombin concentrations at 300 sec were found at downstream of the patches.

procoagulant phenotype at extremely low wall shear stress [256].

The 3-D plots of the fibrin concentrations versus time and position at two different shear rates 20 s^{-1} and 80 s^{-1} are shown in Figure 6.3B and 6.3C . The thrombin concentrations in time and position at shear rate of 20 s^{-1} is also depicted in Figure 6.3D. At high shear rate (80 s^{-1}), fibrin formation did not initiate

in about the first 600 s^{-1}, while fibrin formation initiated in the first 100 seconds at low shear rate (20 s^{-1}). The initiation of thrombin and fibrin formation occurred at about the same time as shown in Figure 6.3C and 6.3D. Figure 6.3E and 6.3F show the spatial evolution of concentrations of fibrin and thrombin at 0 and 300 seconds at shear rate 20 s^{-1}. The maximum fibrin and thrombin concentrations at 300 seconds were achieved at position about 2000 μm, which was the down-stream of the TF patch.

6.3.4 Acceleration of clot time via SIPA under high shear

Since the activation of platelets by shear was not only the function of shear rate, but also a weak function of time [252], we introduced platelet activation by different shear stresses at different time in PRP. The shear rates, viscosities of blood, shear stress, exposure time required for SIPA, and the rate of SIPA were summarized in Table 6.1. When the shear rate was below 100 s^{-1}, SIPA was not initiated druing the time span we considered. Hence the initiation time of fibrin formation at the shear rates lower than 100 s^{-1} would be the same as those in Figure 6.3A, and thus in Figure 6.4A, we only showed the clot times for shear rates $\geq$ 100 s^{-1}. With further increases in shear rates, the critical exposure time became smaller and smaller, and the activation rate of platelets became larger and larger. As a result, thus the activation of platelets increased drastically with increasing shear rate. The concentration profiles of activated platelets (AP) clearly show the impact of SIPA at different shear rates (Figure 6.4B), which were compared against experiments [241]. To be consistent with the experiment setup, the simulation was run over collagen patch as well; our model predicted apparent threshold activation of platelets by shear, while the experiments showed a

Table 6.1: Shear rate ($\dot{\gamma}$), and its corresponding blood viscosity (η), shear stress ($\tau = \eta\dot{\gamma}$), critical exposure time (t), SIPA rate (r) [7].

shear rate (sec^{-1})	viscosity (Newtonian/non-Newtonian) (poise)	shear stress ($dynes/cm^2$)	critical exposure time (sec)	SIPA rate (sec^{-1})
10	0.04/0.09	0.4/0.9	≥1200	–
20	0.04/0.08	0.8/1.6	≥1200	–
40	0.04/0.07	1.6/2.8	≥1200	–
60	0.04/0.06	2.4/3.6	≥1200	–
70	0.04/0.06	2.8/4.2	≥1200	–
80	0.04/0.06	3.2/4.8	≥1200	–
100	0.04/0.06	4.0/6	≥1200/780	0.1577
200	0.04	8	420	0.2133
500	0.04	20	60	0.5333
800	0.04	32	0	0.8533
1000	0.04	40	0	1.0667
1200	0.04	48	0	1.2800
1400	0.04	56	0	1.4933
1500	0.04	60	0	1.6000
3000	0.04	120	0	3.2000

more gradual increase of AP with increasing shear rates. When TF was present in the patch, the AP concentrations became a little higher because additional platelets were activated by thrombin that was initiated to form by TF.

Clots formation increased with the increase in shear rates when the effect of SIPA was considered, which was proved by the initiation times of clot for-

[7]The viscosities of blood at different shear rates were estimated from the apparent absolute steady shear blood viscosity of normal, healthy subjects [259]; the shear stresses were calculated from shear rates and viscosity for both Newtonian and non-Newtonian blood, in this study, the shear-thinning effect of non-Newtonian behavior of blood did not make much difference on the simulation results; the critical exposure time were estimated from the exposure time/shear stress plane and the derived platelet stimulation function ($PAS = \tau t^{0.452}$)[250, 252, 251]; the SIPA rates were estimated based on the experimental results [252] and by fitting with the experimental data [241].

mation for shear range from 100 to as high as 3000 s^{-1} (shown in Figure 6.4A). A threshold at shear rate between 800 to 1000 s^{-1} was observed as a competition result of SIPA and flow transport. When the shear rate increased to a value above the threshold, platelet activation by shear was significant enough to cope with the inhibitory effect of flow transport of active factors; in other words, the formation of active factors by SIPA was faster than the removal of those factors from the site by the flow. As a result, the concentration of active factors could achieve the critical value and led to the formation of clots. Taken together, in all cases with or without the effect of SIPA, the threshold effect on clot formation was observed. This threshold effect had its physiological importance and had been studied by several groups [60, 55, 260, 145, 261].

Furthermore, it is interesting to note that the threshold in the shear rates for initiating fibrin formation (Figure 6.4A) correlated with the shear rate at which the concentration of AP increased drastically (Figure 6.4B). Below the threshold, the fibrin clot did not form within 1000 seconds (Figure 6.4A) and the activation of platelet was also not observed at 1 minute (Figure 6.4A); while after the threshold, blood clotting initiated almost immediately and a large amount of platelets became activated after being sheared for 1 minute. The formation of fibrin and the activated platelet concentration were shown in Figure 6.4C and 6.4D, respectively. When the shear rate increased to 1500 s^{-1}, the concentrations of fibrin and AP versus time and position were shown in Figure 6.4E and 6.4F. At a shear rate of 100 s^{-1}, the induced activation of platelets took place after exposing to the shear stress for about 780 seconds (Figure 6.4D); while it was clear that the activation of platelets was much more quickly when the shear rate was as high as 1500 s^{-1} (Figure 6.4F).

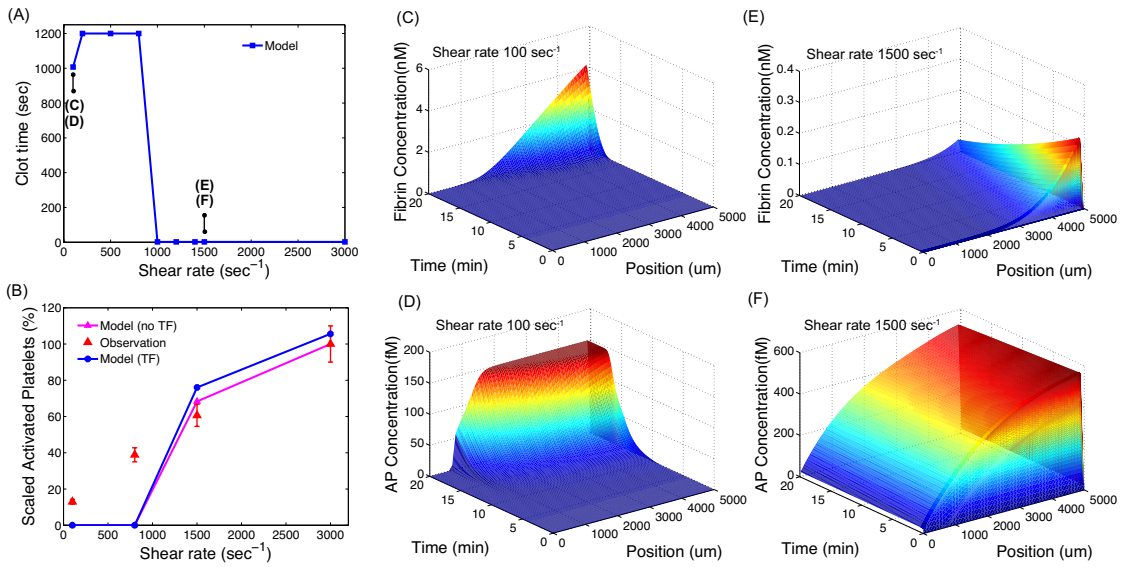

Figure 6.4: Model simulation of clot formation in high shear conditions. (A) Computational simulations of clot times under high shear conditions at a constant TF patch size of 200 μm. (B) Computational simulations and experimental observation of percentage platelet activation after exposed to shear rates of 100, 800, 1500 or 3000 s^{-1} for 1 minute. The simulations were conducted over 200 μm collagen patches with or without TF. The scaled platelet activation was calculated as all activated platelet (AP) concentrations scaled by the maximum AP concentration for simulation without TF. The experimental observations of platelet deposition over collagen were also scaled by its maximum amount of deposited platelets [241]. (C) and (D): Fibrin and AP concentrations versus time and position with a shear rate of 100 s^{-1} . (E) and (F): Fibrin and AP concentrations versus time and position with a shear rate of 1500 s^{-1}. The AP concentrations shown here were for the movable AP only.

The profiles of fibrin formation under different shear rates were quite different as well (Figure 6.4C and Figure 6.4E). At low shear (100 s^{-1}), fibrin concentration increased after a lag phase of about 1000 seconds; while at high shear (1500 s^{-1}), the formation of fibrin started almost immediately after exposure to shear and then degradation of fibrin, probably due to fibrinolysis, quickly showed up after the maximum amount of fibrin was formed. Our model also showed that SIPA could accelerate the burst of AP, which could contribute to the acute events happening after the rupture of plaque at stenotic regions (high shear range). This results indicated that at high shear conditions, e.g. stenosis, a platelet-rich fibrin clot (white head) may form; while at low shear, e.g. post stenosis recirculation region, a fibrin-rich clot was more preferred to form, which could possibly capture red blood cell and form the red tail [3, 8, 239, 42, 227].

6.4 Discussion

Blood flow could affect the formation of clot in different ways. Two counteracting effects of flow on the formation of arterial clotting under conditions of exposed tissue factors (TF) are: (1) flow-mediated transport of enzymes inhibit the initiation of blood clot formation; (2) high shear inducing platelet activation promotes rapid clot formation. Extremely low and high shear stresses could result in either the early formation of plaque or the activation and aggregation of platelets. Early formed plaque, when combining with other risk factors (e.g. excessive low density lipoprotein concentrations, etc), could grow into high-risk plaque and may induce various ischemic events when ruptured. On the other hand, the removal of active enzymes from the reactive vessel surface by flow could inhibit the generation of thrombin to some extent. Re-

searchers often concentrated one or the other effect of blood flow on clot formation [235, 262, 263, 42, 264, 227, 41, 265]. However, the competition between the 'procoagulant' effect of high shear stress and the 'anti-coagulant' effect of flow-mediated removal has not been systematically studied. Here we use the mathematical model to study the effect of flow with different shear rates on the formation of blood clots. Our results showed that when SIPA was not occurring in the model, the initiation of clot formation delayed with increasing shear rates as a result of enhanced flow transport; however, when the shear rates were high enough to induce platelet activation in a short time, the initiation of blood clotting rapidly increased with shear rates.

Threshold effects were observed for the initiation of clot formation under different shear conditions. A threshold regulation in the blood clotting systems has been observed by many other researchers [60, 55, 260, 145, 261]. Jesty et. al. proposed that the threshold regulation could play a major role among the various mechanisms of regulation in blood clotting; they believed that the threshold system was the result of the kinetic balance of formation and inhibition of the feedback enzymes in clotting [260]. Both experimental evidence [254, 117] and computational validation [60, 254] could be found in literature for the presence of threshold under quiescent conditions. Okorie et. al. further provided both experimental and computation evidence for the TF thresholds that triggered clotting under flow with different shear rates; different critical TF concentrations were determined at wall shear rates of 100, 500 and 1000 s^{-1} [261]. For given systems of particular kinetic properties, Beltrami et. al. found that lower flow rates or larger active patches could result in exceeding the activation threshold using a partial differential equation model of an archetypal feedback loop [55]. In our model, we found thresholds in both the shear rate and the TF patch size.

The threshold here could be considered as the balance between the rates for the generation of active factors and the rates for the removal of those active factors by flow. Lower shear rates or larger active patches could result in exceeding the activation threshold of clotting system; while extremely high shear rates could also result in exceeding the activation threshold because of the effect of SIPA.

The shear rates we studied in this paper could be categorized, based on the different thresholds, into three regions: low shear (shear rate $< 100\ s^{-1}$), moderate shear ($100\ s^{-1} \leq$ shear rate $< 1000\ s^{-1}$) and high shear (shear rate $\geq 1000\ s^{-1}$). It is interesting to note that the moderate shear region corresponded to the physiological shear range ($\approx 10^2$ to $10^3\ s^{-1}$) [256]; these physiologically preferred shear rates not only related to the minimization work and the optimization of efficient oxygen transport according to Murray's law [266], but also related to the prevention or inhibition of blood clotting. In the low shear region, the inhibitory effect of flow-mediated removal of active factors, which was proposed and studied using a mathematical model of intravascular coagulation by Fogelson et al [264], was not significant enough; therefore the concentrations of active factors could exceed the threshold. This finding was also consistent with the experimental observation that the initiation of clotting was increased with decreasing shear rates from $110\ s^{-1}$ to $17\ s^{-1}$ in the junction micro-fluidic flow vessel system [265]. The activation and aggregation of platelets by high shear have been observed many years ago by a number of researchers [244, 246, 245, 247, 248, 240, 241, 39, 242, 243], which were believed to contribute to the onset of artery thrombosis [267] and correlated with thrombin generation [40]. Our model proved that extremely high shear rates would also result in active factors concentration exceeding the activation threshold due to SIPA. Other interesting findings included that the concentration of AP was

much higher when the shear rates were high, which could lead to the formation of platelet-rich thrombi under high shear.

Our mathematical model successful predicted blood clot formation in the absence and presence of flow. While there are limitations in the model: the model was only used to simulate blood clotting in a simple, model 1-D flow system with constant shear rates, the physiological flow conditions in arteries is more complex, e.g. the oscillation flow when the shear rate and stress at the wall are continuously changing in time; and the concentrations of factors in the model were assumed constants across the radius, while the diffusion in radius direction could also be important. Given all these limitations, our model was able to combine the complex interactions in the clotting system with the effect of flow and to the best of our knowledge, our model is the first mathematical model that did a systematic study of the effect of shear rates from really low shear (10 s^{-1}) to really high one (3000 s^{-1}). Therefore, we believe this model could provide insights into the blood clotting system under flow conditions.

6.5 Methods

The mathematical model of this study was designed to describe spatial dynamics of clot formation initiated over a patch of tissue factor (TF). The species conservation equation was written around around each protein or protein complex:

$$\frac{D\mathbf{c}}{Dt} = \mathbf{D}\nabla^2\mathbf{c} + \mathbf{R} \tag{6.1}$$

where $\mathbf{c}$ (193×1) denotes the concentration vector of proteins or protein complexes. The symbol $\mathbf{D}$ denotes the diffusion coefficients of all proteins or protein

complexes. Except for platelets or platelet-bound species, the diffusion coefficients of other proteins were assumed to be $5\times10^{-7}cm^2/s$ (approximate value for a solution-phase protease in blood clotting, such as thrombin [254, 268, 227]); the diffusion coefficients of platelets or platelet-bound species were given as $5\times10^{-9}cm^2/s$ [60]. The reactions were assumed to occur within a boundary layer of 2-3 μm (the distance over which platelets can attach to one another because of their pseudopodia [269, 60]) in 1-dimensional (or pseudo-2D) flow field where x is the direction of flow. The above convection-diffusion-reaction equation could be simplified as:

$$\frac{\partial \mathbf{c}}{\partial t} = \mathbf{D}\frac{\partial^2 \mathbf{c}}{\partial x^2} - v_x\frac{\partial \mathbf{c}}{\partial x} + \mathbf{R} \tag{6.2}$$

where the velocity v_x is calculated by multiplying the wall shear (sh) with one-half of the boundary layer thickness (h) ($v_x = sh \times \frac{h}{2}$).

The details for the reaction equation (**R**) and model parameters can be found in the our previous work [162]. The initial concentrations were taken from each experiment and roughly correspond to *in-vivo* physiological conditions. TF patch in each simulation was located at the spatial grid started from x = 600 μm and the initial conditions of platelets and fibrinogen concentrations were determined to be consistent to the NPP and PRP environments. All other parameters and initial conditions held constant.

Given the large scale of the partial differential equation, it was solved using a time-splitting method [270]. The key of the method is to separate chemical species transport (i.e., convection and diffusion) from chemical reaction. At time $t = t_i$ to $t = t_{i+\frac{1}{2}}$, we solve the convection-diffustion reactions only:

$$\frac{\partial \mathbf{c}}{\partial t} = \mathbf{D}\frac{\partial^2 \mathbf{c}}{\partial x^2} - v_x\frac{\partial \mathbf{c}}{\partial x} \qquad \mathbf{c}\,(t_i) = \mathbf{c}\,|_{t=t_i} \tag{6.3}$$

At time $t = t_{i+\frac{1}{2}}$ to $t = t_{i+1}$:

$$\frac{d\mathbf{c}}{dt} = \mathbf{Sr}(\mathbf{c}, \mathbf{k}) = \mathbf{R}(\mathbf{c}, \mathbf{t}) \qquad \mathbf{c}\left(t_{i+\frac{1}{2}}\right) = \mathbf{c}\mid_{t=t_{i+\frac{1}{2}}} \tag{6.4}$$

Equation 6.3 was solved using the method of lines (MOL) [271] in the OCTAVE programming environment (v2.9.9; www.octave.org), and the solutions at this time step were used as the initial conditions of the next time step. Equation 6.4 was solved using the LSODE routine of the OCTAVE programming environment on an Apple Computer MacOSX (Cupertino, CA; v10.4.8) workstation.

6.6 Limitations and Future Directions

6.6.1 Limitations

Plasma flowing parallel to the wall convectively transports coagulation factors from upstream to a region close to the reactive site (TF patch), and Brownian motion mediates the radial movement toward the reactive wall. Local flow conditions near the wall can significantly enhance or impede the transport of molecule to (and away from) a reactive surface and are typically characterized by the wall shear rate (γ_w), which is the rate at which the axial flow velocity increases as one moves directly away from the vessel wall toward the center of the vessel. Because the velocity profile across the vessel is roughly parabolic, the γ_w approximates the flow velocities only near the wall. For fully developed, laminar flow through a rigid tube the velocity at distance h ($h \ll 2r$) from the wall can be γ_w can be calculated as $V_x(h) = \gamma_w h$. Because the coagulation reactions are initiated by the reactive TF surface and diffusion is only an effective means

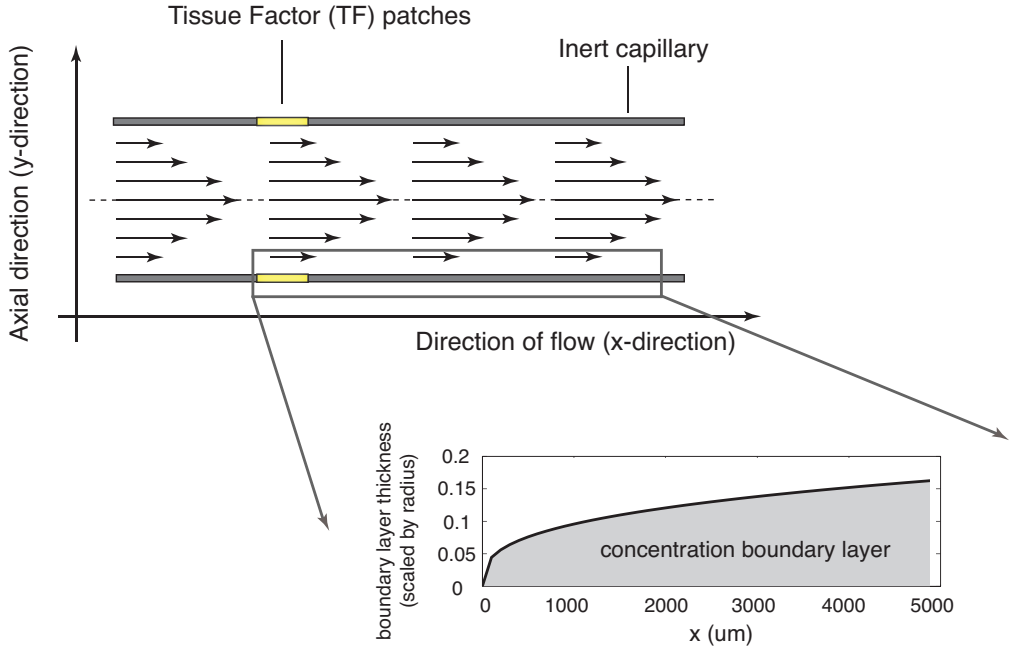

Figure 6.5: Illustration of the capillary with TF patch.

of transport over short distances, the reactions are assumed to occur within a concentration boundary layer from the wall (Figure 6.5).

In this study, we assumed the species in a thin boundary near the vessel wall were well-mixed and ignored the diffusion along y-direction. However, by calculating the squared Thiele modulus for species *l*:

$$\phi^2{}_l = \sum_{k=1}^{M} \frac{H^2 \sigma_{lq} r_q(c^*, k)}{D^* c_l^*} \tag{6.5}$$

where H is the characteristic length, i.e. the boundary layer thickness, D^* is the characteristic diffusion coefficient, c_l^* is the characteristic concentration for species *l* (we used the concentration vector at the centerline), M is the number

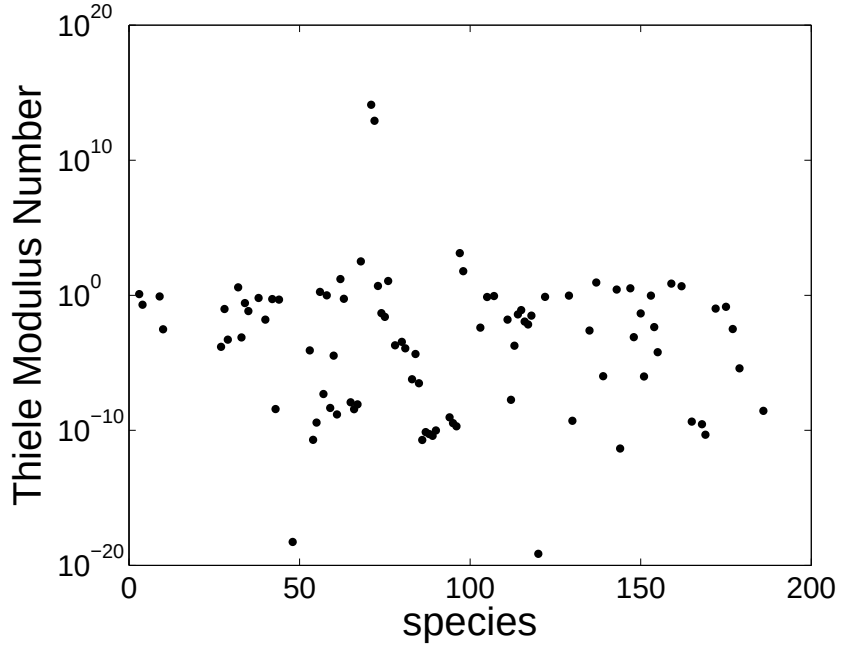

Figure 6.6: Thiele modulus numbers for all species in the model.

of reactions, r_q is the reaction rate and σ_{lq} denote stoichiometric coefficients (elements of the connectivity matrix $\mathbf{S}$). The distribution of Thiele modulus was shown in Figure 6.6.

The squared Thiele modulus is the ratio of two characteristic times, diffusion to reaction. If the reaction is very fast, its characteristic time is small and the Thiele modulus is large ($\phi^2 \gg 1$), the concentration on the TF patch may be small because the reaction is so fast that the material cannot diffuse to the surface before it is reacted. Likewise, if the diffusion is very fast, its characteristic time is small and the Thiele modulus is small ($\phi^2 \ll 1$), now the concentration may not vary very much within the boundary layer because the diffusion is fast enough to keep the boundary filled with reactants. If the reaction and diffusion have similar characteristic time, the Thiele modulus approaches 1 ($\phi^2 \approx 1$), the diffusion and reaction phenomena have comparable importance.

Most of the species have shown small Thiele modulus numbers, indicating fast diffusion and slow reactions. However, for the species related to platelets activation on the surface, large Thiele modulus was observed. These results indicated that the well-mixed assumption in the boundary layer was not valid for all species in the model. Furthermore, the Peclet number $Pe = UH/D$ in the model ranged from O(1) to O(10^3) for shear rates from 10 to 3000 s^{-1}. Thus, some characteristic behavior of flow on clot formation may be missed because of this well-mixed assumption. Hence we proposed two solutions for the situation in order to get more suitable model in Future Directions.

6.6.2 Future Directions

The main problem with the current model is related to the diffusion along y-direction. Equation 6.2 can be re-written as:

$$\frac{\partial \mathbf{c}}{\partial t} = \mathbf{D}(\frac{\partial^2 \mathbf{c}}{\partial x^2} + \frac{\partial^2 \mathbf{c}}{\partial y^2}) - v_x \frac{\partial \mathbf{c}}{\partial x} + \mathbf{R} \tag{6.6}$$

with the boundary conditions:

$$\mathbf{c}(\infty, y) = \mathbf{c_b} \tag{6.7}$$

$$\frac{\partial \mathbf{c}}{\partial t}(-\infty, y) = 0 \tag{6.8}$$

where $x = \infty$ denotes far away from the TF patch at downstream and $x = \infty$ denotes upstream far away from the patch. One solution for this is to average the concentrations $\mathbf{c}(x, y)$ along y-direction to get average concentration in the boundary layer at a given position x, which is defined as:

$$\bar{\mathbf{c}}(x) = \frac{1}{H} \int_0^H \mathbf{c}(x, y) dy \tag{6.9}$$

The velocity v_x within the boundary layer can be estimated by multiplying the wall shear (γ_w) with one-half of the boundary layer thickness (H) ($\bar{v}_x = \frac{\gamma_w H}{2}$). The boundary conditions in y-directions are:

$$\frac{\partial \mathbf{c}}{\partial y}(x, H) = 0 \qquad -\infty < x < \infty \tag{6.10}$$

$$\frac{\partial \mathbf{c}}{\partial y}(x, 0) = 0 \qquad x < 0 \qquad or \qquad x > L \tag{6.11}$$

$$\frac{\partial \mathbf{c}}{\partial y}(x, 0) = \frac{\mathbf{c_b} - \mathbf{c}}{H} \qquad 0 \le x \le L \tag{6.12}$$

where $\mathbf{c_b}$ is the bulk concentration and L is the length of the TF patch. At the top surface ($y = H$) of the boundary, no flux along y-direction. At the bottom of the boundary (the vessel wall), for places without TF patch, no flux along y-direction, while over the patch, the concentration change within the volume (V) equals the diffusion along y-direction across the area (A), thus, $(c_b - c)V = A\frac{\partial \mathbf{c}}{\partial y}(x, 0)$ and $H = V/A$.

The boundary layer is defined using the same methodology from [60]. The averaged boundary thickness can be estimated using:

$$H = \frac{3}{4}(\frac{rLD}{V})^{1/3} \tag{6.13}$$

where r is the radius of the capillary, L is the length of TF patch, D is the diffusion coefficient of a protein, and V is the velocity at the centerline. If the boundary layer is thinner than the typical distance at which platelets can attached to other platelets ($2 - 3\mu m$), then we set $H = 2.5\mu m$.

The ordinary differential equation governing $\bar{\mathbf{c}}(x)$ is obtained by averaging each term in Equation 6.6 and can be solved using a time-splitting method as stated in Methods [270].

$$\frac{\partial \bar{\mathbf{c}}}{\partial t} = \mathbf{D}\frac{\partial^2 \bar{\mathbf{c}}}{\partial x^2} + \frac{\mathbf{D}}{H}\frac{\partial \mathbf{c}}{\partial y}\Big|_{y=0}^{y=H} - \bar{v}_x \frac{\partial \bar{\mathbf{c}}}{\partial x} + \mathbf{R} \tag{6.14}$$

or, using the boundary conditions at the top and bottom of the boundary layer:

$$\frac{\partial \bar{\mathbf{c}}}{\partial t} = \mathbf{D}\frac{\partial^2 \bar{\mathbf{c}}}{\partial x^2} - \bar{v}_x \frac{\partial \bar{\mathbf{c}}}{\partial x} + \mathbf{R} \qquad x < 0 \qquad or \qquad x > L \tag{6.15}$$

$$\frac{\partial \bar{\mathbf{c}}}{\partial t} = \mathbf{D}\frac{\partial^2 \bar{\mathbf{c}}}{\partial x^2} - \frac{\mathbf{D}(\mathbf{c_b} - \bar{\mathbf{c}})}{H^2} - \bar{v}_x \frac{\partial \bar{\mathbf{c}}}{\partial x} + \mathbf{R} \qquad 0 \le x \le L \tag{6.16}$$

Another solution to capture diffusion of material in the y-direction is to model the flow effect in two dimensional space using Finite Element Methods. In this way, we can incorporate the diffusion along y-direction. However, because of the limited time, these two solutions were not included in this dissertation.

APPENDIX A

CHAPTER 1 APPENDIX

Table A.1: Nomenclature

fI	fibrinogen
FIa	fibrin
fII	prothrombin
FIIa	thrombin
fVII	factor VII
FVIIa	activated factor VII
fV	factor V
FVa	activated factor V
fVIII	factor VIII
FVIIIa	activated factor VIII
fIX	factor IX
FIXa	activated factor IX
fX	factor X
FXa	activated factor X
TF	Tissue Factor
TFPI	Tissue Factor Pathway Inhibitor
ATIII	Antithrombin III
PC	Protein C
APC	activated Protein C
TM	Thrombomodulin
PL	resting platelets
AP	activated platelets

Table A.2: Initial Conditions for different cases in Figure 2.2

cases	A	B	C and D	E	F
fII	1700/2000 nM	1700 nM	1400 nM	1400 nM	1400 nM
fVII	–	–	–	–	10 nM
FVIIa	–	–	–	–	0.5 nM
TF	–	–	–	–	1 pM
TF-FVIIa	1.25 pM	1.25 pM	1.25 pM	5/10/50/500/5000 pM	–
fV	20 nM	20 nM	20 nM	20 nM	20 nM
fVIII	0.7 nM	0.7 nM	0.7 nM	0.7 nM	0.3 nM
fIX	90 nM	90 nM	90 nM	90 nM	70 nM
fX	170 nM	170 nM	170 nM	170 nM	135 nM
TFPI	0/1/2.5/5 nM	0/2.5 nM	2.5 nM	–	3 nM
ATIII	–	0/3400 nM	–	–	3000 nM
PC	–	–	65 nM	–	–
TM	–	–	0/1/10 nM	–	–
number of PL	150	150	150	150	150
number of PL binding sites on subendothelium	100	100	100	100	100
number of fII/FIIa binding sites on AP surfaces	50	50	50	20	0.5
number of fV/FVa binding sites on AP surfaces	50	50	50	20	50
number of fVIII/FVIIIa binding sites on AP surfaces	5×10^{-10}	5×10^{-10}	5×10^{-10}	5×10^{-10}	5×10^{-6}
number of fIX/FIXa binding sites on AP surfaces	50	50	50	20	5×10^{-8}
number of specific fIX/FIXa binding sites on AP surfaces	50	50	50	20	5×10^{-8}
number of fX/FXa binding sites on AP surfaces	50	50	50	20	150

Table A.3: Reactions and parameter values used in the extrinsic coagulation model [1].

p-index	case A	case B	case C	case D
Description				
VII+TF ⇌ VII-TF	5×10^{-2}	5×10^{-3}	–	[60]
VIIa+TF ⇌ VIIa-TF	5×10^{-2}	5×10^{-3}	–	[60]
Xa+VII-TF ⇌ Xa-VII-TF	5×10^{-3}	1.0	–	[60]
Xa-VII-TF→ VIIa-TF + Xa	–	–	5×10^{-3}	[60]
IIa+VII-TF ⇌ IIa-VII-TF	3.92×10^{-4}	1.0	–	[60]
IIa-VII-TF → VIIa-TF +IIa	–	–	3.92×10^{-4}	[60]
X+VII-TF ⇌ X-VIIa-TF	0.1	5.5	–	[54]
X-VII-TF → VIIa-TF + Xa	–	–	1.4	[54]
IX+VIIa-TF ⇌ IX-VIIa-TF	0.1	2.2	–	[54]
IX-VII-TF → VIIa-TF + IXa	–	–	0.47	[54]
VII+Xa ⇌ VII-Xa	0.1	1.0	–	[60, 53]
VII-Xa → VIIa + Xa	–	–	0.5	[60, 53]
VII+IIa ⇌ VII-IIa	0.1	10	–	[60, 53]
VII-IIa → VIIa + IIa	–	–	0.5	[60, 53]
V+IIa ⇌ V-IIa	0.1	7.2[1]	–	[54]
V-IIa → V + IIa	–	–	0.26	[54]
VIII+IIa ⇌ VIII-IIa	0.1	15[2]	–	[54]
VIII-IIa → VIIIa + IIa	–	–	0.9	[54]
Xa + IX ⇌ Xa-IX	0.1	1.5	–	[52]
Xa-IX → Xa + IXa	–	–	2.3×10^{-2}	[52]
Xa + V ⇌ Xa-V	0.1	1.0	–	[52, 54]
Xa-V → Xa + Va	–	–	4.3×10^{-2}	[52, 54]
Xa + VIII ⇌ Xa-VIII	0.1	2.1	–	[52, 54]
Xa-VIII → Xa + VIIIa	–	–	2.3×10^{-2}	[52, 54]
Xa + II ⇌ Xa-II	7.5×10^{-6}	1.0×10^{-9}	–	[53]
Xa-II ⇌ IIa + Xa	–	–	7.5×10^{-6}	[53]
IX + P9s ⇌ IX-P9s	1.0×10^{-2}	2.5×10^{-2}	–	[60]

Continued on next page

Reaction	k^+ ($nM^{-1}s^{-1}$)	k^- (s^{-1})	k_c (s^{-1})	Source
IXa + P9s ⇌ IXa-P9s	1.0×10^{-2}	2.5×10^{-2}	–	[60]
IXa + P9s* ⇌ IXa-P9s*	1.0×10^{-2}	2.5×10^{-2}	–	[60]
X + P10s ⇌ X-P10s	0.1	2.5×10^{-2}	–	[60]
Xa + P10s ⇌ Xa-P10s	0.1	2.5×10^{-2}	–	[60]
V + P5s ⇌ V-P5s	5.7	0.17	–	[60]
Va + P5s ⇌ Va-P5s	5.7	0.17	–	[60]
VIII + P8s ⇌ VIII-P8s	5.0×10^{-2}	0.17	–	[60]
VIIIa + P8s ⇌ VIIIa-P8s	5.0×10^{-2}	0.17	–	[60]
II + P2s ⇌ II-P2s	1.0×10^{-2}	5.9	–	[60]
IIa + P2s ⇌ IIa-P2s	1.0×10^{-2}	2.042	–	[60]
PL + Psub → AP-Psub	–	–	0.9	[60]
PL + Psub → PL-Psub	–	–	20	[60]
AP + Psub → AP-Psub	–	–	0.2	[60]
PL + AP ⇌ PL-AP	5×10^{-7}	1.0	–	[60]
PL-AP ⇌ 2AP	–	–	5×10^{-7}	[60]
PL + AP-Psub ⇌ PL-AP-Psub	5×10^{-7}	1.0	–	[60]
PL-AP-Psub → AP+ AP-Psub	–	–	5×10^{-7}	[60]
PL + IIa ⇌ PL-IIa	3×10^{-7}	1.0	–	[60]
PL-IIa → AP + IIa	–	–	3×10^{-7}	[60]
PL-Psub + IIa ⇌ PL-Psub-IIa	3×10^{-2}	1.0×10^{-2}	–	[60]
PL-Psub-IIa → AP-Psub + IIa	–	–	9×10^{-3}	[60]
V-P5s + Xa-P10s ⇌ V-P5s-Xa-P10s	0.1	1.0	–	[60, 54]
V-P5s-Xa-P10s → Va-P5s + Xa-P10s	–	–	4.6	[60, 54]
V-P5s + IIa-P2s ⇌ V-P5s-IIa-P2s	1.73×10^{-2}	1.0	–	[60, 54]
V-P5s-IIa-P10s → Va-P5s + IIa-P10s	–	–	4.6	[60, 54]
X-P10s+VIIIa-P8s-IXa-P9s ⇌ X-P10s-VIIIa-P8s-IXa-P9s	0.1	1.0×10^{-2}	–	[60, 54]
X-P10s-VIIIa-P8s-IXa-P9s → Xa-P10s + VIIIa-P8s-IXa-P9s	–	–	20.0	[60, 54]
X-P10s+VIIIa-P8s-IXa-P9s* ⇌ X-P10s-VIIIa-P8s-IXa-P9s*	0.1	0.01	–	[60, 54]
X-P10s-VIIIa-P8s-IXa-P9s* → Xa-P10s + VIIIa-P8s-IXa-P9s*	–	–	20.0	[60, 54]

Continued on next page

Reaction	k^+ ($nM^{-1}s^{-1}$)	k^- (s^{-1})	k_c (s^{-1})	Source
VIII-P8s + Xa-P10s ⇌ VIII-P8s-Xa-P10s	0.1	2.1	-	[60, 54]
VIII-P8s-Xa-P10s → VIIIa-P8s + Xa-P10s	–	–	0.023[2]	[60, 54]
VIII-P8s + IIa-P2s ⇌ VIII-P8s-IIa-P2s	0.1	15[2]	–	[60, 54]
VIII-P8s-IIa-P10s → VIIIa-P8s + IIa-P10s	–	–	0.9	[60, 54]
II-P2s + Va-P5s-Xa-P10s ⇌ II-P2s-Va-P5s-Xa-P10s	0.1	0.05[1]	–	[60, 54]
II-P2s-Va-P5s-Xa-P10s → IIa-P2s + Va-P5s-Xa-P10s	–	–	30[1]	[60, 54]
VIIIa-P8s + IXa-P9s ⇌ VIIIa-P8s-IXa-P9s	0.1	0.4	–	[60, 54]
VIIIa-P8s + IXa-P9s* ⇌ VIIIa-P8s-IXa-P9s*	0.1	0.4	–	[60, 54]
Va-P5s + Xa-P10s ⇌ Va-P5s-Xa-P10s	1.0	1.0	–	[60, 54]
Xa-P10s + IX-P9s ⇌ Xa-P10s-IX-P9s	1.0×10^{-3}	1.5	–	[52]
Xa-P10s-IX-P9s → Xa-P10s + IX-P9s	–	–	2.3×10^{-2}	[52]
APC + VIIIa-P8s ⇌ APC-VIIIa-P8s	0.12	1.0	–	[60]
APC-VIIIa-P8s → APC+VIIIa-P8s-i	–	–	0.5	[60]
APC + Va-P8s ⇌ APC-Va-P8s	0.12	1.0	–	[60]
APC-Va-P8s → APC+Va-P8s-i	–	–	0.5	[60]
APC + Va-P5s-Xa-P10s ⇌ APC-Va-P5s-Xa-P10s	0.12	1.0	–	[60, 8]
APC-Va-P5s-Xa-P10s → APC + Va-P5s-Xa-P10s-i	–	–	0.5	[60, 8]
APC + VIIIa-P8s-IXa-P9s ⇌ APC-VIIIa-P8s-IXa-P9s	0.12	1.0	–	[60, 8]
APC-VIIIa-P8s-IXa-P9s → APC + VIIIa-P8s-IXa-P9s-i	–	–	0.5	[60, 8]
APC + VIIIa-P8s-IXa-P9s* ⇌ APC-VIIIa-P8s-IXa-P9s*	0.12	1.0	–	[60, 8]
APC-VIIIa-P8s-IXa-P9s* → APC + VIIIa-P8s-IXa-P9s*-i	–	–	0.5	[60, 8]
TFPI + Xa ⇌ TFPI-Xa	1.6×10^{-3}	3.3×10^{-4}	–	[54, 60]
TFPI-Xa + VIIa-TF ⇌ TFPI-Xa-VIIa-TF	1.0×10^{-3}	1.1×10^{-3}	–	[60]
TFPI + Xa-VIIa-TF ⇌ TFPI-Xa-VIIa-TF	0.32	1.1×10^{-4}	–	[53]
IIa → IIa-i	–	–	1.35×10^{-4}	[53]
ATIII + IXa ⇌ ATIII-IXa	4.9×10^{-7}	1.0×10^{-9}	–	[60, 53]
ATIII-IXa →ATIII+IXa-i	–	–	4.9×10^{-7}	[60, 53]
ATIII + Xa ⇌ATIII-Xa	2×10^{-4}	1.0×10^{-9}	–	[60, 53]
ATIII-Xa → ATIII+Xa-i	–	–	1.5×10^{-6}	[60, 53]

Continued on next page

Reaction	k^+ ($nM^{-1}s^{-1}$)	k^- (s^{-1})	k_c (s^{-1})	Source
ATIII + IIa ⇌ ATIII-IIa	1.5×10^{-5}	1.0×10^{-9}	–	[60, 53]
ATIII-IIa → ATIII+IIa-i	–	–	4.75×10^{-6}	[60, 53]
ATIII + VIIa-TF ⇌ VIIIa-TF-ATIII	2.5×10^{-7}	1.0×10^{-9}	–	[53]
PC + IIa ⇌ PC-IIa	1.003×10^{-6}	1.0×10^{-9}	–	[8, 116]
PC-IIa → APC + IIa	–	–	1.67×10^{-4}	[8, 116]
IIa + TM ⇌ IIa-TM	3.0×10^{-2}	4.5×10^{-2}	–	[116]
IIa-TM + PC ⇌ IIa-TM-PC	1.4×10^{-4}	0.5	–	[116]
IIa-TM-PC → IIa-TM + APC	–	–	40	[116]

[1]The mode consists of 92 protein or protein complexes and 148 interactions. The kinetics of binding and reaction interactions are assumed to follow mass action rate laws where k^+ denotes the on-rate constant, k^- denotes the off-rate constant and k_c denotes the catalytic rate constants. All binding interactions are assumed to be reversible. Values for the kinetic parameters and network structure were taken from the literature, see [52, 54, 116, 60, 53, 8]. Of the 148 parameters in the model, 138 were taken directly from literature or have a literature basis. Only 10 of 148 parameters have no direct literature source: of these, nine of ten parameters correspond to interactions of APC with the FVIIIa-FIXa and FVa-FXa surface complexes. The parameter values governing the interaction of APC with FVIIIa-FIXa/FVa-FXa were approximated by literature values describing the interaction of APC with FVa and FVIIIa in plasma. The remaining unknown parameter was the rate constant governing the nonspecific inactivation of FIIa (IIa→IIa-i); we have assumed an arbitrary small value for this parameter. Last, there were differences in *in vitro* assay temperatures from which parameters were taken; parameter values were adjusted to the assay temperature of Mann and coworker (T1 = 37^oC). (1) Rate constant adjusted to $T_1 = 37^oC$ from $T_2 = 25^oC$ using Arrhenius rate law, where $Ea = 21kJ$,$R = 8.314gmol/K$; (2) Rate constant adjusted to $T_1 = 37^oC$ from $T_2 = 22^oC$using Arrhenius rate law.

APPENDIX B

CHAPTER 4 APPENDIX

Table B.1: Extended reactions and parameter values used in this coagulation model.

p-index	case A	case B	case C	case D
Description				
IIa + PAR1-PL ⇌ IIa-PAR1-PL	0.71	8.67	–	[204, 113]
IIa + PAR1-PL-Psub ⇌ IIa-PAR1-PL-Psub	0.13	6.46	–	[204, 113]
IIa-PAR1-PL → AP + IIa	–	–	0.03	[204, 113]
IIa-PAR1-PL-Psub → AP-Psub + IIa	–	–	0.04	[204, 113]
IIa + PAR3-PL ⇌ IIa-PAR3-PL	0.03	1.01	–	[204, 113]
IIa + PAR3-PL-Psub ⇌ IIa-PAR3-PL-Psub	0.10	8.74	–	[204, 113]
IIa-PAR3-PL → AP + IIa	–	–	0.82	[204, 113]
IIa-PAR3-PL-Psub → AP-Psub + IIa	–	–	0.42	[204, 113]
IIa + PAR4-PL ⇌ IIa-PAR4-PL	0.22	4.39	–	[204, 113]
IIa + PAR4-PL-Psub ⇌ IIa-PAR4-PL-Psub	0.88	1.59	–	[204, 113]
IIa-PAR4-PL → AP + IIa	–	–	0.24	[204, 113]
IIa-PAR4-PL-Psub → AP-Psub + IIa	–	–	0.93	[204, 113]
AP → APs + ADP	–	–	1×10^{-6}	[69]
AP → APs + TXA2	–	–	1×10^{-6}	[69]
AP → APs + I	–	–	1×10^{-6}	[69]
AP-Psub → APs + ADP	–	–	1×10^{-3}	[69]
AP-Psub → APs + TXA2	–	–	1×10^{-3}	[69]
AP-Psub → APs + I	–	–	1×10^{-3}	[8]
ADP + PL ⇌ ADP-PL	3×10^{-7}	1.0	–	[69]
ADP-PL → AP + ADP	–	–	3×10^{-7}	[69]
TXA2 + PL ⇌ TXA2-PL	1.61×10^{-2}	1.0	–	[69]
TXA2-PL → AP + TXA2	–	–	1.61×10^{-2}	[69]
ADP + PL-Psub ⇌ ADP-PL-Psub	3×10^{-2}	0.01	–	[69]
ADP-PL-Psub → AP-Psub + ADP	–	–	3×10^{-3}	[69]
TXA2 + PL-Psub ⇌ TXA2-PL-Psub	1.61×10^{-2}	1.0	–	[69]
TXA2-PL-Psub → AP-Psub + TXA2	–	–	1.61×10^{-2}	[69]
IIa + I ⇌ IIa-I	1.898×10^{-2}	1.0	–	[8]

Continued on next page

Reaction	k^+ ($nM^{-1}s^{-1}$)	k^- (s^{-1})	k_c (s^{-1})	Source
IIa-I → IIa + Ia	–	–	59×10^{-4}	[8]
XII+Surface ⇌ XII-Surface	0.1	0.1	–	[17, 14]
XII-Surface → XIIa+Surface	–	–	0.1	[17, 14]
XIIa+PK ⇌ XIIa-PK	0.1	0.1	–	[17, 14]
XIIa-PK → XIIa+ K	–	–	0.1	[17, 14]
XII+K ⇌ XII-K	0.1	0.1	–	[17, 14]
XII-K → XIIa+ K	–	–	0.1	[17, 14]
XIIa+ XII ⇌ XIIa-XII	0.1	0.1	–	[17, 14]
XIIa-XII → 2XIIa	–	–	0.1	[17, 14]
XIIa+ XI ⇌ XIIa-XI	0.3×10^{-3}	0.1	–	[17, 14]
XIIa-XI → XIIa+XIa	–	–	0.35	[17, 14]
XIa + XI ⇌ XIa-XI	1.3×10^{-3}	0.1	–	[17]
XIa-XI → 2*XIa	–	–	0.13	[17]
XI + P11s ⇌ XI-P11s	0.04	1.0	–	[205, 206]
XIa + P11s* ⇌ XIa-P11s*	0.06	1.0	–	[205, 206]
IIa-P2s + XI-P11s ⇌ IIa-P2s-XI-P11s	0.0125	0.1	–	[17, 16, 15]
IIa-P2s-XI-P11s → IIa-P2s + XIa-P11s*	–	–	1.43	[17, 16, 15]
XIa + IX ⇌ XIa-IX	0.016	0.1	–	[206]
XIa-IX → XIa + IXa	–	–	7.7	[206]
XIa-P11s* + IX ⇌ XIa-P11s*-IX	0.016	0.1	–	[206]
XIa-P11s*-IX → XIa-P11s* + IXa	–	–	7.7	[206]
tPA+PAI1 ⇌ tPA-PAI1	0.02	2×10^{-3}	–	[272, 273, 274, 275]
uPA+PAI1 ⇌ uPA-PAI1	1.8×10^{-2}	1.0×10^{-3}	–	[272, 273]
tPA+PAI2 ⇌ tPA-PAI2	1.2×10^{-4}	1.0×10^{-6}	–	[274, 34]
uPA+PAI2 ⇌ uPA-PAI2	2.1×10^{-3}	1.0×10^{-5}	–	[34]
PLG+tPA ⇌ PLG-tPA	1.67×10^{-2}	0.1	–	[276, 277, 275]
PLG-tPA → PLA+tPA	–	–	2.0	[276, 277, 275]
PLG+uPA ⇌ PLG-uPA	3.3×10^{-3}	0.1	–	[278]
PLG-uPA → PLA+uPA	–	–	73	[278]

Continued on next page

Reaction	k^+ ($nM^{-1}s^{-1}$)	k^- (s^{-1})	k_c (s^{-1})	Source
PLA+A2AP ⇌ PLA-A2AP	3.8×10^{-2}	7.22×10^{-3}	–	[279, 280, 281, 282, 283, 284]
PLA-A2AP → PLA+A2AP-inactive	–	–	4.2×10^{-3}	[279, 280, 281, 282, 283, 284]
PLA+A2M ⇌ PLA-A2M	5.0×10^{-4}	1.0×10^{-5}	–	[283, 284, 285]
PLA-A2M → PLA+A2M-inactive	–	–	1.0×10^{-5}	[283, 284, 285]
FDPs+PLA ⇌ FDPs-PLA	0.01	0.1	–	[286, 287]
IIa+TAFI ⇌ IIa-TAFI	1.29×10^{-3}	0.1	–	[258, 288]
IIa-TAFI → IIa+TAFIa	–	–	61	[258, 288]
Ia+PLA ⇌ Ia-PLA	7.45×10^{-5}	0.1	–	[257]
Ia-PLA → Ddimer+FDPs+PLA	–	–	1.16×10^{-4}	[257]
Ia+FDPs-PLA ⇌ Ia-FDPs-PLA	7.45×10^{-5}	0.1	–	[257]
Ia-FDPs-PLA → Ddimer+FDPs+FDPs-PLA	–	–	1.16×10^{-3}	[257]
TAFIa+FDPs ⇌ TAFIa-FDPs	100	1.0×10^{-4}	–	[286, 287]
H5+ATIII ⇌ H5-ATIII	3.7×10^{-2}	0.9	–	[124, 289]
H5-ATIII+Xa ⇌ H5-ATIII-Xa	2.0×10^{-2}	1.0×10^{-9}	–	[124, 289]
H5-ATIII-Xa → H5-ATIII+Xa-inactive	–	–	0.6×10^{-3}	[124, 289]
H5-ATIII+IIa ⇌ H5-ATIII-IIa	1.5×10^{-5}	1.0×10^{-9}	–	[124, 289]
H5-ATIII-IIa → H5-ATIII+IIa-inactive	–	–	0.5×10^{-5}	[124, 289]
HCII+IIa ⇌ HCII-IIa	4.5×10^{-7}	1.0×10^{-9}	–	[290, 291, 292]
HCII+IIa-P2s ⇌ HCII-IIa-P2s	4.5×10^{-7}	1.0×10^{-9}	–	[290, 291, 292]
HCII+DER ⇌ HCII-DER	0.9	1.0×10^{-9}	–	[290, 291, 292]
HCII-DER+IIa ⇌ HCII-DER-IIa	0.02	1.0×10^{-9}	–	[290, 291, 292]
HCII-DER+IIa-P2s ⇌ HCII-DER-IIa-P2s	0.02	1.0×10^{-9}	–	[290, 291, 292]
ARG +IIa ⇌ ARG-IIa	0.033	0.33	–	[290, 291]
ARG +IIa-P2s ⇌ ARG-IIa-P2s	0.033	0.33	–	[290, 291]
BIV+IIa ⇌ BIV-IIa	0.43	0.82	–	[290, 291]
BIV-IIa → BIV-inactive+IIa	–	–	1.0×10^{-2}	[290, 291]
BIV+IIa-P2s ⇌ BIV-IIa-P2s	0.43	0.82	–	[290, 291]
BIV-IIa-P2s → BIV-inactive+IIa-P2s	–	–	1.0×10^{-2}	[290, 291]
LEP+IIa ⇌ LEP-IIa	0.29	1.7×10^{-5}	–	[290, 291]

Continued on next page

Reaction	k^+ ($nM^{-1}s^{-1}$)	k^- (s^{-1})	k_c (s^{-1})	Source
LEP+IIa-P2s ⇌ LEP-IIa-P2s	0.29	1.7×10^{-5}	–	[290, 291]
H5-ATIII+VIIa ⇌ H5-ATIII-VIIa	1.7×10^{-7}	1.0×10^{-9}	–	[293]
H5-ATIII+VIIa-TF ⇌ H5-ATIII-VIIa-TF	4.5×10^{-7}	1.0×10^{-9}	–	[293]
X+VIIa ⇌ X-VIIa	4.0×10^{-5}	0.1	–	[28, 196]
X-VIIa → Xa+VIIa	–	–	5.0×10^{-4}	[28, 196]
IX+VIIa ⇌ IX-VIIa	5.0×10^{-5}	0.1	–	[28, 196]
IX-VIIa → IXa+VIIa	–	–	1.5×10^{-5}	[28, 196]
APC+PCI ⇌ APC-PCI	6.5×10^{-6}	1.0×10^{-9}	–	[294]
IIa+PCI ⇌ IIa-PCI	6.1×10^{-6}	1.0×10^{-9}	–	[294]
Xa+PCI ⇌ Xa-PCI	2.01×10^{-5}	1.0×10^{-9}	–	[294]
XIa+PCI ⇌ XIa-PCI	9.03×10^{-5}	1.0×10^{-9}	–	[294]
uPA +PCI ⇌ uPA-PCI	2.2×10^{-6}	1.0×10^{-9}	–	[294]
tPA +PCI ⇌ tPA-PCI	0.8×10^{-6}	1.0×10^{-9}	–	[294]
K +PCI ⇌ K-PCI	6.5×10^{-5}	1.0×10^{-9}	–	[294]

BIBLIOGRAPHY

[1] World Health Organization: *World Health Statistics 2008*. STYLUS PUBLISHING LLC 2008.

[2] Ross R: **Atherosclerosis - an Inflammatory Disease**. *N. Engl. J. Med.* 1999, **340**:115–126.

[3] Diamond SL: **Engineering design of optimal strategies for blood clot dissolution**. *Annu. Rev. Biomed. Eng.* 1999, **01**:427–461.

[4] Hansson GK: **Inflammation, Atherosclerosis and Coronary Artery Disease**. *N. Engl. J. Med.* 2005, **352**:1685 – 1695.

[5] Bagot CN, Arya R: **Virchow and his triad: a question of attribution.** *Br. J. Haematol.* 2008, **143**(2):180–190.

[6] Chung I, Lip GYH: **Virchow's Triad Revisited: Blood Constituents.** *Pathophysiol Haemost. Thromb.* 2003/2004, **33**:449–454.

[7] Guyton AC, Hall JE: *Textbook of Medical Physiology, 9th Edition. Chapter 36: Hemostasis and Blood Coagulation.* Philadelphia: W.B. Saunders Co. 1996.

[8] Anand M, Rajagopal K, Rajagopal KR: **A Model Incorporating Some of the Mechanical and Biochemical Factors Underlying Clot Formation and Dissolution in Flowing Blood**. *J. Theor. Med.* 2003, **5**:183–218.

[9] Anand M, Rajagopal K, Rajagopal KR: **A Model for the Formation and Lysis of Blood Clots**. *Pathophysiol. Haemost. Thromb.* 2005, **34**:109–120.

[10] Butenas S, Veer C, Mann KG: **Evaluation of the Initiation Phase of Blood Coagulation Using Ultrasensitive Assays for Serine Proteases**. *J. Biol. Chem.* 1997, **272**:21527–21533.

[11] Lane DA, Philippou H, Huntington JA: **Directing thrombin**. *Blood* 2005, **106**:2605–2612.

[12] Lawson JH, Kalafatic M, Stram S, Mann KG: **A Model for the Tissue Factor Pathway to Thrombin: I An Empirical Study**. *J. Biol. Chem.* 1994, **269**:23357–23366.

[13] Gailani D, Broze Jr GJ: **Factor XI Activation in a Revised Model of Blood Coagulation**. *Science* 1991, **25**:909–912.

[14] Naito K, Fujikawa K: **Activation of Human Blood Coagulation Factor XI Independent of Factor XII**. *J. Biol. Chem.* 1991, **266**(12):7353–7358.

[15] Wielders SJH, Béguin S, Hemker H, Lindhout T: **Factor XI-dependent Reciprocal Thrombin Generation Consolidates Blood Coagulation when Tissue Factor is not Available**. *Arterioscler. Thromb. Vasc. Biol.* 2004, **24**:1138–1142.

[16] Kr von dem Borne PA, Meijers JCM, Bouma BN: **Feedback Activation of Factor XI by Thrombin in Plasma Results in Additional Formation of Thrombin that Protects Fibrin Clots from Fibrinolysis**. *Blood* 1995, **86**(8):3035–3042.

[17] Baglia FA, Walsh PN: **Thrombin-mediated Feedback Activation of Factor XI on the Activated Platelet Surface is Preferred over Contact Activation by Factor XIIa or Factor XIa**. *J. Biol. Chem.* 2000, **275**(27):20514–20519.

[18] Walsh PN: **Roles of Platelets and Factor XI in the Initiation of Blood Coagulation by Thrombin**. *Thromb. Haemost.* 2001, **86**:75–82.

[19] Walsh PN: **Roles of factor XI, platelets and tissure factor-initiated blood coagulation**. *J. Thromb. Haemost.* 2003, **1**:2081–2086.

[20] Solymoss S, Tucker MM, Tracy PB: **Kinetics of Inactivation of Membrane-bound Factor Va by Activated Protein C**. *J. Biol. Chem.* 1988, **263**:14881–14890.

[21] Rosenberg JS, McKenna PW, Rosenberg RD: **Inhibition of Human Factor IXa by Human Antithrombin**. *J. Biol. Chem.* 1975, **250**:8883–8888.

[22] Mann KG, Nesheim ME, Church WR, Haley P, Krishnaswamy S: **Surface-dependent reactions of Vitamin K-dependent enzyme complexes**. *Blood* 1990, **76**:1–16.

[23] Esmon CT: **The Roles of Protein C and Thrombomodulin in the Regulation of Blood Coagulation**. *J. Biol. Chem.* 1989, **264**:4743 – 4746.

[24] Mannucci MP, Tuddenham EGD: **The Hemophilias - from royal genes to gene therapy**. *N. Engl. J. Med.* 2001, **344**:1773 – 1780.

[25] Mitchell J, Phillott A: **Haemophilia and inhibitors 1: diagnosis and treatment.** *Nursing Times* 2008, **104**(26):26–27.

[26] Mathew P, Bolton-Maggs PHB: **Hemophilia C.** *Hematology* 2008.

[27] Rodeghiero F, Tosetto A, Castaman G: **How to estimate bleeding risk in mild bleeding disorders**. *J. Thromb. Haemost.* 2007, **5**:157–166.

[28] Tomokiyo K, Nakatomi Y, Araki T, Teshima K, Nakano H, Nakagaki T, Miyamoto S, Funatsu A, Iwanaga S: **A novel therapeutic approach combining human plasma-derived factors VIIa and X for haemophiliacs with inhibitors: evidence of a higher thrombin generation rate in vitro and more sustained haemostatic activity in vivo than obtained with factor VIIa alone**. *Vox Sanguinis* 2003, **85**:290–299.

[29] Allen GA, Hoffman M, Roberts HR, Monroe DM: **Manipulation of prothrombin concentration improves response to high-dose factor VIIa in a cell-based model of haemophilia**. *Br. J. Haematology* 2006, **134**:314 – 319.

[30] Schneiderman J, Rubin E, Nugent DJ, Young G: **Sequential therapy with activated prothrombin complex concentrates and recombinant FVIIa in patients with severe haemophilia and inhibitors: update of our previous experience**. *Haemophilia* 2007, **13**:244–248.

[31] Chavin SI, Siegel DM, Rocco TA, Olson JP: **Acute mycardial infarction during treatment with an activated prothrombin complex concentrate in a patient with factor VIII deficiency and a factor VIII inhibitor.** *Am. J. Med.* 1988, **85**:245–249.

[32] Roberts HR, Monroe DM, White GC: **The use of recombinant factor VIIa in the treatment of bleeding disorders**. *Blood* 2004, **104**:3858–3864.

[33] Gill R, Herbertson M: **Recombinant Factor VIIa: A Universal Haemostatic Agent?** *Annals of Cardiac Anaesthesia* 2006, **9**:97–99.

[34] Thorsen S, Philips M, Selmer J, Lecander I, Astedt B: **Kinetics of inhibition of tissue-type and urokinase-type plassminogen activator by plasminogen-activator inhibitor type 1 and type 2**. *Eur. J. Biochem.* 1988, **175**:33–39.

[35] Nielsen VG, Steenwyk BL, Gurley WQ: **Contact activation prolongs clot**

lysis time in human plasma: Role of Thrombin-activatable fibrinolysis inhibitors and factor XIII. *J. Heart Lung Transplant* 2006, **25**:1247–1252.

[36] Blann AD: **How a damaged blood vessel wall contributes to thrombosis and hypertension.** *Pathophysiol. Haemost. Thromb.* 2003/2004, **33**:445–448.

[37] Guo Z, Bussard KM, Chatterjee K, Miller R, Vogler EA, Siedlecki CA: **Mathematical modeling of material-induced blood plasma coagulation.** *Biomaterials* 2006, **27**:796–806.

[38] Brash JL: **The fate of fibrinogen following adsorption at the blood-biomaterial interface.** *Ann. NY Acad. Sci.* 1987, **516**:206–222.

[39] Moroi M, Jung SM, Nomura S, Sekiguchi S, Ordinas A, Diaz-Ricart M: **Analysis of the involvement of the von Willebrand factor-glycoprotein Ib interaction in platelet adhesion to a collagen-coated surface under flow conditions.** *Blood* 1997, **90**:4413–4424.

[40] Pontiggia L, Steiner B, Ulrichts H, Deckmyn H, Forestier M, Beer JH: **Platelet microparticle formation and thrombin generation under high shear are effectively suppressed by a monoclonal antibody against GPIbα.** *Thromb. Haemost.* 2006, **96**:774–780.

[41] Chatzizisis YS, Coskun AU, Jonas M, Edelman ER, Feldman CL, Stone PH: **Role of endothelial shear stress in the natural history of coronary atherosclerosis and vascular remodeling**. *J. Am. Coll. Cardiol.* 2007, **49**:2379–2393.

[42] Lowe GDO: **Virchow's triad revisited: abnormal flow**. *Pathophysiol. Haemost. Thromb.* 2003/2004, **33**:455–457.

[43] Goldsmith HL, Skalak R: **Hemodynamics.** *Annu. Rev. Fluid Mech.* 1975, **7**:213–247.

[44] Barbee JH, Cokelet GR: **The Fahraeus effect.** *Microvasc. Res.* 1971, **3**:6–16.

[45] Aarts PA, van den Broek SA, Prins GW, Kuiken GD, Sixma JJ, Heethaar RM: **Blood platelets are concentrated near the wall and red blood cells, in the center in flowing blood.** *Arteriosclerosis* 1988, **8**:819–824.

[46] Lee AJ, Mowbray PI, Lowe GDO, Rumley A, Fowkes FGR, Allen PL:

Blood viscosity and delevated carotid intima-media thickness in men and women: the Edinburgh Arter Study. *Circulation* 1998, **97**:1467–1473.

[47] Danesh J, Collins R, Peto R, Lowe GDO: **Haematocrit, viscosity, erthryocyte sedimentation rate: meta-analyses of prospective studies of coronary heart disease.** *Europ. Heart. J.* 2000, **21**:515–520.

[48] Davie EW, Ratnoff OD: **Waterfall Sequence for Intrinsic Blood Clotting**. *Science* 1964, **145**:1310–1312.

[49] Levine SN: **Enzyme Amplifier Kinetics**. *Science* 1966, **152**:651–653.

[50] Khanin MA, Semenov VV: **A mathematical model of the kinetics of blood coagulation.** *J. Theroret. Biol.* 1989, **136**(2):127–134.

[51] Willems GM, Lindhout T, Hermens WT, Hemker HC: **Simulation model for thrombin generation in plasma.** *Haemostasis* 1991, **21**(4):197–207.

[52] Jones KG, Mann KG: **A Model for the Tissue Factor Pathway to Thrombin: II A Mathematical Simulation**. *J. biol. Chem.* 1994, **269**:23367–23373.

[53] Hockin MF, Jones KC, Everse SJ, Mann KG: **A Model for the Stoichiometric Regulation of Blood Coagulation**. *J. Biol. Chem.* 2002, **277**:18322–18333.

[54] Leipold RJ, Bozarth TA, Racanelli AL, Dicker IB: **Mathematical Model of Serine Protease Inhibition in the Tissue Factor Pathway to Thrombin**. *J. Biol. Chem.* 1995, **270**:25383 – 28387.

[55] Beltrami E, Jesty J: **The role of membrane patch size and flow in regulating a proteolytic feedback threshold on a membrane: possible application in blood coagulation**. *Mathematical Biosciences* 2001, **172**:1–13.

[56] Baldwin SA, Basmadjian D: **A mathematical model of thrombin production in blood coagulation, part I: The sparsely covered membrane case.** *Annals of Biomedical Engineering* 1994, **22**(4):357–370.

[57] Basmadjian D, Sefton MV, Baldwin SA: **Coagulation on biomaterials in flowing blood: some theretical considerations.** *Biomaterials* 1997, **18**(23):1511–1522.

[58] Gregory K, Basmadjian D: **An analysis of the contact phase of blood**

coagulation: Effects of shear rate and surface are entwined. *Annals of Biomedical Engineering* 1994, **22**(2):184–193.

[59] Khanin MA, Rakov DV, Kogan AE: **Mathematical model for the blood coagulation prothrombin time test.** *Thromb. Res.* 1998, **89**(5):227–232.

[60] Kuharsky AL, Fogelson AL: **Surface-Mediated control of blood coagulation: The role of binding site densities and platelet deposition**. *Biophys. J.* 2001, **80**:1050–1074.

[61] Wagner WR, Hubbell JA: **Local thrombin synthesis and fibrin formation in an in vitro thrombosis model result in platelet recruitment and thrombus stabilization on collagen in heparinized blood.** *J. Lab. Clin. Med.* 1990, **116**:636–650.

[62] Badimon L BJ: **Mechanisms of arterial thrombosis in nonparallel streamlines: platelet thrombi grow on the apex of stenotic severely injured vessel wall. Experimental study in the pig model.** *J. Clin. Invest.* 1989, **84**:1134–1144.

[63] Xu CQ, Zeng YJ, Gregersen H: **Dynamic model of the role of platelets in the blood coagulation system.** *Medical Engi. Physics* 2002, **24**:587–593.

[64] Ataullakhanov FI, Panteleev MA: **Mathematical modeling and computer simulation in blood coagulation.** *Pathophysiol. Haemost. Thromb.* 2005, **34**:60–70.

[65] Basmadjian D: **Embolization: critical thrombus height, shear rates, and pulsatility. Patency of blood vessels.** *J. Biomed. Matls. Res.* 1989, **23**:1315–1326.

[66] Zarnitsina VI, Pokhilko AV, Ataullakhanov FI: **A mathematical model for the spatio-temporal dynamics of intrinsic pathway of blood coagulation. I The model description.** *Thromb. Res.* 1996, **84**(4):225–236.

[67] Zarnitsina VI, Pokhilko AV, Ataullakhanov FI: **A mathematical model for the spatio-temporal dynamics of intrinsic pathway of blood coagulation. II results.** *Thromb. Res.* 1996, **84**(5):333–344.

[68] Panteleev MA, Ovanesov MV, Kireev DA, Shibeko AM, Sinauridze EI, Ananyeva NM, Butylin AA, Saenko EL, Ataullakhanov FI: **Spatial prop-**

agation and localization of blood coagulation are regulated by intrinsic and protein C pathways, respectively. *Biophys. J.* 2006, **90**:1489–1500.

[69] Sorensen EN, Burgreen GW, Wagner WR, Antaki JF: **Computational Simulation of Platelet Deposition and Activation I. Model Development and Properties**. *Ann. Biomed. Eng.* 1999, **27**:436 – 448.

[70] Sorensen EN, Burgreen GW, Wagner WR, Antaki JF: **Computational Simulation of Platelet Deposition and Activation II. Results for Poiseuille Flow over Collagen**. *Ann. Biomed. Eng.* 1999, **27**:449 – 458.

[71] David T, Thomas S, Walker PG: **Platelet deposition in stagnation point flow: an analytical and computational simulation.** *Med. Eng. Phys.* 2001, **23**:299–312.

[72] Wootton DM, Markou CP, Hanson SR, Ku DN: **A mechanistic model of acute platelet accumulation in thrombogenic stenoses.** *Ann. Biomed. Eng.* 2001, **29**:321–329.

[73] Kitano H: **Computational systems biology**. *Nature* 2002, **420**:206 – 210.

[74] Kriete A, Eils R (Eds): *Computational systems biology.* Elsevier 2005.

[75] Hood L, Heath JR, Phelps EW, Lin B: **Systems biology and new technologies enable predictive and preventive medicine.** *Science* 2004, **306**:640–643.

[76] Assmus HE, Herwig R, Cho KH, Wolkenhauer O: **Dynamics of biological systems: role of systems biology in medical research**. *Exp. Rev. Molec. Diagn.* 2006, **6**:891 – 902.

[77] Arnaud CA: **Systems Biology's Clinical Future**. *Chem. Eng. News* 2006, **84**:17 – 26.

[78] Kitano H: *Foundations of systems biology.* Cambridge, MA: MIT press 2001.

[79] Turanyi T: **Sensitivity Analysis of Complex Kinetic Systems. Tools and Applications.** *J. Math. Chem* 1990, **5**(3):203–248.

[80] Cho KH, Shin SY, Kolch W, Wolkenhauer O: **Experimental Design in Systems Biology, Based on Parameter Sensitivity Analysis Using a**

Monte Carlo Method: A Case Study for the TNFα-Mediated NF-β-Signal Transduction Pathway. *Simulation* 2003, **79**:726 – 739.

[81] Saltelli A, Tarantola S, Chan KPS: **A Quantitative Model-Independent Method for Global Sensitivity Analysis of Model Output.** *Tech- nometrics* 1999, **41**:39–56.

[82] Saltelli A, Chan K, Scott E (Eds): *Sensitivity Analysis.* New York, NY: Wiley 2000.

[83] Saltelli A, Ratto M, Tarantola S, Campolongo F: **Sensitivity Analysis for Chemical Models.** *Chem. Rev.* 2005, **105**(7):2811–2828.

[84] Stelling J, Sauer U, Szallasi Z, Doyle III FJ, Doyle J: **Robustness of Cellular Functions**. *Cell* 2004, **118**:675 – 685.

[85] Carlson JM, Doyle J: **Complexity and robustness**. *Proc. Natl. Acad. Sci. USA* 2002, **99**(2358 - 2545).

[86] Barkai N, Leibler S: **Robustness in simple biochemical networks**. *Nature* 1997, **387**:913 – 917.

[87] Alon U, Surette MG, Barkai N, Leibler S: **Robustness in bacterial chemotaxis**. *Nature* 1999, **397**:168 – 171.

[88] Eißing T, Allgöwer F, Bullinger E: **Robustness properties of apoptosis models with respect to parameter variations and intrinsic noise**. *IEE Proc. Sys. Biol.* 2005, **152**:221 – 228.

[89] Stelling J, Gilles ED, Doyle III FJ: **Robustness properties of circadian clock architectures**. *Proc. Natl. Acad. Sci. USA* 2004, **101**:13210 – 13215.

[90] Alm E, Arkin A: **Biological Networks**. *Curr. Opin. Struct. Biol.* 2003, **13**:193 – 202.

[91] Uetz P, Giot L, Cagney G, Mansfield TA, Judson RS, Knight JR, Lockshon D, Narayan V, Srinivasan M, Pochart P, Qureshi-Emili A, Li Y, Godwin B, Conover D, Kalbfleisch T, Vijayadamodar G, Yang M, Johnston M, Fields S, Rothberg JM: **A comprehensive analysis of protein–protein interactions in *Saccharomyces cerevisiae***. *Nature* 2000, **420**:623 – 627.

[92] Ito T, Chiba T, Ozawa R, Yoshida M, Hattori M, Sakaki Y: **A comprehensive two-hybrid analysis to explore the yeast protein interactome**. *Proc. Natl. Acad. Sci. USA* 2001, **98**:4569 – 4574.

[93] Gavin A, Bosche M, Krause R, Grandi P, Marzioch M, Bauer A, Schultz J, Rick J, Michon A, *et al*, CC: **Functional organization of the yeast proteome by systematic analysis of protein complexes**. *Nature* 2002, **415**:141 – 147.

[94] Ho Y, Gruhler A, Heilbut A, Bader G, Moore L, Adams S, Millar A, Taylor P, Bennett K, *et al* KB: **Systematic identification of protein complexes in *Saccharomyces cerevisiae* by mass spectrometry**. *Nature* 2002, **415**:180 – 183.

[95] Lee TI, Rinaldi NJ, Robert F, Odom DT, Bar-Joseph Z, Gerber GK, Hannett NM, Harbison CT, Thompson C, ISimon, JZeitlinger, Jennings E, Murray H, Gordon DB, BRen, Wyrick J, Tagne JB, Volkert T, EFraenkel, Gifford D, Young RA: **Transcriptional Regulatory Networks in *Saccharomyces cerevisiae***. *Science* 2002, **298**:799 – 804.

[96] Arkin A, Ross J: **Statistical construction of chemical reaction mechanisms from measured time series**. *J. Phys. Chem.* 1995, **99**:970 – 979.

[97] Arkin A, Shen P, Ross J: **A Test Case of Correlation Metric Construction of a Reaction Pathway from Measurements**. *Science* 1997, **277**:1275 – 1279.

[98] Koza JR, Mydlowec W, Lanza G, Yu J, Keane MA: **Reverse engineering of metabolic pathways from observed data using genetic programming**. In *Proceedings of the 6th Pacific Symposium on Biocomputing*. Edited by Altmann R, Dunker A, World Scientific Publishing Company. 2001:434 – 445.

[99] van Riel NAW, Sontag ED: **Parameter estimation in models combining signal transduction and metabolic pathways: the dependent input approach**. *IEE Proc. Sys. Biol.* 2006, **153**:263 – 274.

[100] Kholodenko BN, Kiyatkin A, Bruggeman FJ, Sontag E, Westerhoff HV, Hoek JB: **Untangling the wires: a strategy to trace functional interactions in signaling and gene networks**. *Proc. Natl. Acad. Sci. USA* 2002, **99**:12841 – 12846.

[101] Sontag E, Kiyatkin A, Kholodenko BN: **Inferring dynamic architecture of cellular networks using time series of gene expression, protein and metabolite data**. *Bioinformatics* 2004, **20**:1877 – 1886.

[102] Cho K, Choo SM, Wellstead P, Wolkenhauer O: **A Unified Framework for Unraveling the Functional Interaction Structure of a Biomolecular Network Based on Stimulus-Response Experimental Data**. *FEBS Letters* 2005, **579**:4520 – 4528.

[103] Kremling A, Fischer S, Gadkar K, Doyle III FJ, Sauter T, Bullinger E, Allgöwer F, Gilles ED: **A Benchmark for Methods in Reverse Engineering and Model Discrimination: Problem Formulation and Solutions**. *Genome Res.* 2004, **14**:1773 – 1785.

[104] Gadkar KG, Varner J, Doyle III FJ: **Model Identification of Signal Transduction Networks from Data Using a State Regulator Problem**. *Syst. Biol.* 2005, **2**:17–30.

[105] Gadkar K, Gunawan R, Doyle III FJ: **Iterative approach to model identification of biological networks**. *BMC Bioinformatics* 2005, **6**:155 – 175.

[106] Somogyi R, Greller LD: **The Dynamics of Molecular Networks: Applications to Therapuetic Discovery**. *Drug Discov. Today* 2001, **6**:1267 – 1277.

[107] Tuddenham EGD, Cooper DN: *The molecular genetics of haemostasis and its inherited disorders*, *Volume 25 of* Oxford monographs in medical genetics. Oxford University Press 1994.

[108] Butenas S, Mann KG: **Blood Coagulation**. *Biochemistry* 2002, **67**:5–15.

[109] Schenone M, Furie BC, Furie B: **The blood coagulation cascade**. *Curr. Opin. Hematol.* 2004, **11**:272 – 277.

[110] Roberts HR, Monroe DM, Oliver JA, Chang JY, Hoffman M: **Newer Concepts of Blood Coagulation**. *Haemophilia* 1998, **4**:331–334.

[111] Mann K: **Biochemistry and Physiology of Blood Coagulation**. *Thromb. Haemost.* 1999, **82**:165–174.

[112] Giesen PL, Rauch U, Bohrmann B, Kling D, Roque M, Fallon JT, Badimon JJ, Himber J, Riederer MA, Nemerson Y: **Blood-borne tissue factor: another view of thrombosis**. *Proc. Natl. Acad. Sci. USA* 1999, **96**:2311 – 2315.

[113] Coughlin SR: **Thrombin signalling and protease-activated recpetors**. *Nature* 2000, **407**:258–264.

[114] Coughlin SR: **How the protease thrombin talks to cells**. *Proc. Natl. Acad. Sci. USA* 1999, **96**:11023–11027.

[115] Roberts HR, Hoffman M, Monroe DM: **A Cell-Based Model of Thrombin Generation**. *Semin. Thromb. Hemost.* 2006, **32**:32 – 38.

[116] Veer C, Golden NJ, Kalafatis M, Mann KG: **Inhibitory Mechanism of the Protein C Pathway on Tissue Factor-induced Thrombin Generation**. *J. Biol. Chem.* 1997, **272**:7983–7994.

[117] Veer C, Mann KG: **Regulation of Tissue Factor Initiated Thrombin Generation by the Stoichiometric Inhibitors Tissue Factor Pathway Inhibitor, Antithrombin-III, and Heparin Cofactor-II**. *J. Biol. Chem.* 1997, **272**:4367–4377.

[118] Bauer KA, Eriksson BI, Lassen MR, Turpie AGG: **Fondaparinux Compared with Enoxaparin for the Prevention of Venous Thromboembolism after Elective Major Knee Surgery**. *N. Engl. J. Med.* 2001, **345**:1305 – 1310.

[119] Eriksson BI, Bauer KA, Lassen MR, Turpie AGG: **Fondaparinux Compared with Enoxaparin for the Prevention of Venous Thromboembolism after Hip-Fracture Surgery**. *N. Engl. J. Med.* 2001, **345**:1298 – 1304.

[120] Lassen MR, Bauer KA, Eriksson BI, Turpie AG: **Postoperative fondaparinux versus preoperative enoxaparin for prevention of venous thromboembolism in elective hip-replacement surgery: a randomised double-blind comparison**. *The Lancet* 2002, **359**:1715 – 1720.

[121] Buller HR, Davidson BL, Decousus H, Gallus A, Gent M, Piovella F, Prins MH, Raskob G, Segers A, Cariou R, Leeuwenkamp O, Lensing AWA: **Fondaparinux or Enoxaparin for the Initial Treatment of Symptomatic Deep Venous Thrombosis: A Randomized Trial**. *Ann. Intern. Med.* 2004, **140**:867 – 873.

[122] Agnelli G, Bergqvist D, Cohen AT, Gallus AS, Gent M, on behalf of the PEGASUS Investigators : **Randomized clinical trial of postoperative fondaparinux versus perioperative dalteparin for prevention of venous thromboembolism in high-risk abdominal surgery**. *Br. J. Surgery* 2005, **92**:1212 – 1226.

[123] Petitou M, Lormeau JC, Choay J: **Chemical Synthesis of Glycosamino-**

glycans: New Approaches to Antithrombotic Drugs. *Nature* 1991, **350**:30 – 33.

[124] Olson S, Bjork I, Sheffer R, Craig PA, Shore JD, Choay J: **Role of the antithrombin-binding pentasaccharide in heparin acceleration of antithrombin-proteinase reactions. Resolution of the antithrombin conformational change contribution to heparin rate enhancement**. *J. Biol. Chem.* 1992, **267**:2528 – 2538.

[125] Walenga JM, Bara L, Petitou M, Samama M, Fareed J, Choay J: **The inhibition of the generation of thrombin and the antithrombotic effect of a pentasaccharide with sole anti-factor Xa activity**. *Thromb. Res.* 1988, **51**:23 – 33.

[126] Lormeau JC, Herault JP: **The effect of the synthetic pentasaccharide SR 90107/ORG 31540 on thrombin generation ex vivo is uniquely due to ATIII-mediated neutralization of factor Xa**. *Thromb. Haemost.* 1995, **74**:1474 – 1477.

[127] Gerotziafas G, Depasse F, Chakroun T, Dreden PV, Samama MM, Elalamy I: **Comparsion of the effect of fondaparinux and enoxaparin on thrombin generation during in-vitro clotting of whole blood and platelet rich plasma**. *Blood Coag. Fibrin.* 2004, **15**:149 – 156.

[128] Herbert JM, Herault JP, Bernat A, van Amsterdam RGM, Vogel GMT, Lormeau JC, Petitou M, Meuleman DG: **Biochemical and Pharmacological Properties of SANORG 32701**. *Circ. Res.* 1996, **79**:590 – 600.

[129] Lorrain J, Lechaire I, Gauffeny C, Masson R, Roome N, Herault JP, O'Connor S, Schaeffer P, Herbert JM: **Effects of SanOrg123781A, a Synthetic Hexadecasaccharide, in a Mouse Model of Electrically Induced Carotid Artery Injury: Synergism with the Antiplatelet Agent Clopidogrel**. *J. Pharmocol. Exp. Ther.* 2004, **309**:235 – 240.

[130] Di Nisio M, Middeldorp S, Büller HR: **Direct Thrombin Inhibitors**. *N. Engl. J. Med.* 2005, **353**:1028 – 1040.

[131] Tulinsky A: **Molecular Interactions of Thrombin**. *Semin. Thromb. Hemost.* 1996, **22**:117 – 124.

[132] Sarich TC, MWolzt, Eriksson UG, CMattsson, Schmidt A, Elg S, Andersson M, Wollbratt M, Gunnar F, Gustafsson D: **Effects of Ximelagatran, an**

Oral Direct Thrombin Inhibitor, r-Hirudin and Enoxaparin on Thrombin Generation and Platelet Activation in Healthy Male Subjects. *J. Am. Coll. Cardiol.* 2003, **41**:557 – 564.

[133] Feuerstein GZ, Patel A, Toomey JR, Bugelski P, Nichols AJ, Church WR, Valocik R, Koster P, Baker A, Blackburn MN: **Antithrombotic Efficacy of a Novel Murine Antihuman Factor IX Antibody in Rats**. *Arterioscler. Thromb. Vasc. Biol.* 1999, **19**:2554 – 2562.

[134] Benedict CR, Ryan J, Wolitzky B, Ramos R, Gerlach M, Tijburg P, Stem D: **Active Site-blocked Factor IXa Prevents Intravascular Thrombus Formation in the Coronary Vasculature without Inhibiting Extravascular Coagulation in a Canine Thrombosis Model**. *J. Clin. Invest.* 1991, **88**:1760 – 1765.

[135] Thompson A: **Structure, function and molecular defects of Factor IX**. *Blood* 1986, **67**:565 – 572.

[136] Lollar P, Fass D: **Inhibition of activated porsine factor IX by dansyl-glutamyl-glycyl-arginyl-chloromethylketone**. *Arch. Biochem. Biophys.* 1984, **233**:673 – 682.

[137] Ahmad S, Rawalah-Sheik R, Walsh P: **Comparative interaction of factor IX and IXa with human platelets**. *J. Biol. Chem.* 1989, **264**:3244 – 3251.

[138] Weiss H, Lages B: **Evidence for tissue-factor-dependent activation of the classic extrinsic coagulation mechanism in blood obtained from bleeding time wounds**. *Blood* 1998, **71**:629 – 635.

[139] Brass S: **Cardiovascular Biology - Small Cells Big Issues**. *Nature* 2001, **409**:145–147.

[140] Enjyoji K, Sévigny J, Lin Y, Frenette PS, Christie PD, II JSAE, Imai M, Edelberg JM, Rayburn H, Lech M, Beeler D, Csizmadia E, Wagner D, Robson S, Rosenberg R: **Targeted Disruption of CD39/ATP Diphosphohydrolase Results in Disordered Hemostasis and Thromboregulation**. *Nature Med* 1999, **5**:1010–1017.

[141] Diamond SL: **Reaction complexity in flowing human blood**. *Biophys. J.* 2001, **80**:1031.

[142] Frojmovic M, Nash G, Diamond SL: **Cell Aggregation and Cell Adhesion in Flow**. *Thromb. Haemost.* 2002, **87**:771.

[143] Goel M, Diamond SL: **Factor VIIa-mediated tenase function on activated platelets under flow**. *J.Thromb. Haem.* 2004, **2**:1402.

[144] Lo K, Diamond SL: **Blood Coagulation Kinetics: High Throughput Method for Realtime Reaction Monitoring**. *Thromb. Haemost.* 2004, **92**:874.

[145] Lo K, Denney WS, Diamond SL: **Stochastic modeling of blood coagulation initiation**. *Pathophysiol. Haemost. Thromb.* 2005, **34**:80 – 90.

[146] Butenas S, Veer C, Mann KG: **'Normal' Thrombin Generation**. *Blood* 1999, **94**:2169–2178.

[147] Spiegel MR: *Statistics: Schaum's Easy Outlines*. McGraw-Hill 2000.

[148] Newsam GN, Ramsdell JD: **Estimation of Sparse Jacobian Matrices**. *Siam J. Alg. Disc. Meth.* 1983, **4**:404 – 418.

[149] Welch BL: **The generalization of students problem when several different population variances are involved**. *Biometrika* 1947, **34**:28 – 35.

[150] Rao BM, Lauffenburger DA, Wittrup KD: **Integrating cell-level kinetic modeling into the design of engineered protein therapeutics**. *Nat. Biotechnol.* 2005, **23**:191 – 194.

[151] Bailey JE: **Complex Biology with no Parameters**. *Nat. Biotechnol.* 2001, **19**:503–504.

[152] Covert M, Knight E, Reed J, Herrgard M, Palsson B: **Integrating high-throughput and computational data elucidates bacterial networks**. *Nature* 2004, **429**:92 – 96.

[153] Reed J, Vo T, Schilling C, Palsson B: **An expanded genome-scale model of *Escherichia coli* K-12 (iJR904 GSM/GPR)**. *Genome Biol.* 2003, **54**:1 – 12.

[154] Price ND, Reed JL, Palsson BO: **Genome-scale Models of Microbial Cells - Evaluating the consequences of constraints.** *Nat. Rev. Microbiol.* 2004, **2**:886 – 897.

[155] Reed JL, Famili I, Thiele I, Palsson BO: **Towards Multidimensional Genome Annotation.** *Nat. Rev. Genetics* 2006, **7**:130 – 141.

[156] Shen-Orr SS, Milo R, Mangan S, Alon U: **Network motifs in the transcriptional regulation network of Escherichia coli.** *Nature* 2002, **31**:64 – 68.

[157] Kashtan N, Alon U: **Spontaneous evolution of modularity and network motifs**. *Proc. Natl. Acad. Sci. USA* 2005, **102**:13773 – 13778.

[158] Csete ME, Doyle JC: **Reverse Engineering of Biological Complexitys**. *Science* 2002, **295**:1664 – 1669.

[159] Kitano H: **Biological robustness**. *Nat. Rev. Genet.* 2004, **5**:826 – 837.

[160] Csete M, Doyle J: **Bow ties, metabolism and disease**. *Trends Biotechnol.* 2004, **22**:446 – 450.

[161] Mahdavi A, Davey RE, Bhola P, Yin T, Zandstra PW: **Sensitivity Analysis of Intracellular Signaling Pathway Kinetics Predicts Targets for Stem Cell Fate Control**. *PLoS Comp. Biol.* 2007, **3**:e130.

[162] Luan D, Zai M, Varner JD: **Computationally Derived Points of Fragility of a Human Cascade Are Consistent with Current Therapeutic Strategies**. *PLOS Comput. Biol.* 2007, **3**(7):1347–1359.

[163] Nayak S, Salim S, Luan D, Zai M, Varner J: **A test of highly optimized tolerance reveals fragile cell-cycle mechanisms are molecular targets in clinical cancer trials**. *PLos ONE* 2008, **in-press**.

[164] Kitano H: **A robustness based approach to systems-oriented drug design**. *Nat. Rev. Drug Discov.* 2007, **6**:202 – 210.

[165] Gutenkunst RN, Waterfall JJ, Casey FP, Brown KS, Myers CR, Sethna JP: **Universally Sloppy Parameter Sensitivities in Systems Biology**. *PLoS Comput. Biol.* 2007, **3**:e198.

[166] Casey FP, Baird D, Feng Q, Gutenkunst RN, Waterfall JJ, Myers CR, Brown KS, Cerione RA, Sethna JP: **Optimal experimental design in an EGFR signaling and down-regulation model**. *IET Syst. Biol.* 2007, **1**:190 – 202.

[167] Hwang JT, Dougherty EP, Rabitz S, Rabitz H: **The Green's function**

method of sensitivtiy analysis in chemical kinetics. *J. Chem. Phys.* 1978, **69**:5180 – 5191.

[168] Dougherty EP, Rabitz H: **A computational algorithm for the Green's function method of sensitvity analysis in chemical kinetics**. *Int. J. Chem. Kinet.* 1979, **11**:1237 – 1248.

[169] Kramer MA, Calo JM, Rabitz H: **An improved computational method for the sensitivity analysis - Green's function method with AIM**. *Appl. Math. Model.* 1981, **5**:432 – 441.

[170] Lojek B: **Sensitivity analysis of systems of differential and algebraic equations**. *IEE Proc.-G Circuits Devices and Systems* 1982, **129**:85 – 88.

[171] Kramer MA, Rabitz H, Calo JM, Kee RJ: **Sensitivity analysis in chemical kinetics: Recent developments and computational comparisons**. *Int. J. Chem. Kinet.* 1984, **16**:559 – 578.

[172] Dunker AM: **The decoupled direct method for calculating sensitivity coefficients in chemical kinetics**. *J. Chem. Phys.* 1984, **81**:2385 – 2393.

[173] Leis JR, Kramer MA: **Sensitivity analysis of systems of differential and algebraic equations**. *Comput. Chem. Eng.* 1985, **9**:93 – 96.

[174] Caracotsios M, Stewart WE: **Sensitivity analysis of initial value problems with mixed ODEs and algebraic equations**. *Comput. Chem. Eng.* 1985, **9**:359 – 365.

[175] Gunawan R, Cao Y, Petzold L, Doyle III FJ: **Sensitivity Analysis of Discrete Stochastic Systems**. *Biophys. J.* 2005, **88**:2530 – 2540.

[176] Kim D, Debusschere BJ, Najm HN: **Spectral Methods for Parametric Sensitivity in Stochastic Dynamical Systems**. *Biophys. J.* 2007, **92**:379 – 393.

[177] McKay MD, Conover WJ, Beckman RJ: **A Comparison of Three Methods for Selecting Values of Input Variables in the Analysis of Output from a Computer Code**. *Technometrics* 1979, **21**:239 – 245.

[178] Matisse Investigators: **Subcutaneous Fondaparinux versus Intravenous Unfractionated Heparin in the Initial Treatement of Pulmonary Embolism**. *N. Engl. J. Med.* 2003, **349**:1695 – 1702.

[179] Wang K, Banerjee N, Margolin A, Nemenman I, Califano A: **Genome-wide discovery of modulators of transcriptional interactions in human B lymphocytes**. *Lecture Notes in Comp. Sci.* 2006, **3909**:348 – 362.

[180] Fields S, Sternglanz R: **The two-hybrid system: an assay for protein-protein interactions.** *Trends Genet.* 1994, **10**:282 – 292.

[181] Cagney G, Uetz P, Fields S: **High-throughput screening for protein-protein interactions using two-hybrid assay**. *Methods Enzymol* 2000, **328**:3 – 14.

[182] You X, Nguyen AW, Jabaiah A, Sheff MA, Thorn KS, Daugherty PS: **Intracellular protein interaction mapping with FRET hybrids**. *Proc. Natl. Acad. Sci. USA* 2006, **103**:18458 – 18463.

[183] Farmer TB, Caprioli RM: **Determination of protein-protein interactions by matrix-assisted laser desorption/ionization mass spectrometry**. *J. Mass Spectrom.* 1998, **33**:697 – 704.

[184] Appella E, Anderson CW: **Identifying protein interactions. Computational Approaches**. *FEBS J.* 2005, **272**:5099 – 5100.

[185] Fields S: **High-throughput two-hybrid analysis. The promise and the peril**. *FEBS J.* 2005, **272**:5391 – 5399.

[186] Mering C, Krause R, Snel B, Cornell M, Oliver SG, Fields S, Bork P: **Comparative assessment of large-scale data sets of protein-protein interactions**. *Nature* 2002, **417**:399 – 403.

[187] Huang H, Jedynak B, Bader J: **Where have all the interactions gone? Estimating the Coverage of Two-Hybrid Protein Interaction Maps**. *PLoS Comp. Biol.* 2007, **3**:e214.

[188] Selvakkumaran N, GKarypis: **Multi-Objective Hypergraph Partitioning Algorithms for Cut and Maximum Subdomain Degree Minimization.** In *IEEE/ACM International Conference on Computer Aided Design (ICCAD)*, IEEE 2003:726 – 733.

[189] **Efficacy in Hemophilia With Inhibitors** [[http://www.novosevenrt.com/novoseven-rt-difference/speed/efficacy-in-hemophilia-with-inhibitors.aspx]].

[190] Berntorp E: **Differential response to bypassing agents complicates treatmment in patients with haemophilia and inhibitors.** *Haemophilia* 2009, **15**:3–10.

[191] Leissinger CA: **Prevention of bleds in hemophilia patients with inhibitors: emerging data and clinical direction.** *Am. J. Hematol.* 2004, **77**(2):558–563.

[192] Dargaud Y, Lienhart A, Meunier S, Hequet O, Chavanne H, Chamouard V, Marin S, Negrier C: **Major surgery in a severe haemophilia A patient with high titre inhibitor: use of the thrombin generation test in the therapeutic decision.** *Haemophilia* 2005, **11**:552–558.

[193] Economou M, Teli A, Tzantzaroudi A, Tsatra I, Zavitsanakis A, Athanassiou-Metaxa M: **Sequential therapy with activated prothrombin complex concentrate (FEIBA) and recombinant factor VIIa in a patient with severe haemophilia A, inhibitor presence and refractory bleeding**. *Haemophilia* 2008, **14**:390–391.

[194] Gomperts ED, Astermark J, Gringeri A, Teitel J: **From Theory to Practice: Applying Current Clinical Knowledge and Treatment Strategies to the Care of Hemophilia A Patients With Inhibitors**. *Blood Reviews* 2008, **22**(Supplement 1):S1–S11.

[195] Schneiderman J, Nugent DJ, Young G: **Sequential therapy with activated prothrombin complex concentrate and recombinant factor VIIa in patients with severe haemophilia and inhibitors.** *Haemophilia* 2004, **10**:347–351.

[196] Komiyama Y, Pedersen AH, Kisiel W: **Proteolytic activation of human factors IX and X by recombinant human factor VIIa: Effects of Calcium, Phospholipids and Tissure Factor**. *Biochemistry* 1990, **29**:9418–9425.

[197] Payne MA, Neuenschwander PF, Johnson AE, Morrissey JH: **Effect of soluble tissue factor on the kinetic mechanism of factor VIIa: Enhancement of p-Guanidinobenzoate substrate hydrolysis**. *Biochemistry* 1996, **35**:7100–7106.

[198] Monroe DM, Hoffman M, Oliver JA, Roberts HR: **Platelet activity of high-dose factor VIIa is independent of tissure factor.** *Br. J. Haematol.* 1997, **99**:542–547.

[199] Hoffman M, Monroe III DM, Roberts HR: **Activated factor VII activates factors IX and X on the surface of activated platelets: thoughts on the mechanism of action of high-dose activated factor VII**. *Blood Coag. Fibrin.* 1998, **9**:S61–S65.

[200] Butenas S, Brummel KE, Branda RF, Paradis SG, Mann KG: **Mechanism of factor VIIa-dependent coagulation in hemophilia blood**. *Blood* 2002, **99**(3):923–930.

[201] Allen GA, Persson E, Campbell RA, Ezban M, Hedner U, Wolberg AS: **A variant of recombinant factor VIIa with enhanced procoagulant and antifibrinolytic activities in an in vitro model of hemophilia**. *Arterioscler. Thromb. Vasc. Biol.* 2007, **27**:683–689.

[202] GOLDHABER SZ, COLMAN RW, CLOWES AW (Eds): *HEMOSTASIS AND THROMBOSIS: BASIC PRINCIPLES AND CLINICAL PRACTICE*. Lippincott Williams and Wilkins 2006.

[203] Brummel KE, Paradis SG, Butenas S, Mann KG: **Thrombin functions during tissue factor-induced blood coagulation**. *Blood* 2002, **100**:148–152.

[204] Carmeliet P: **Clotting Factors Build Blood Vessels**. *Science* 2001, **293**:1602–1604.

[205] Fujikawa K: **Historical perspective of factor XI**. *Thromb. Res.* 2005, **115**:441–450.

[206] Walsh PN, Sinha D, Koshy A, Seaman FS, Bradford H: **Functional Characterization of Platelet-bound Factor XIa: Retention of Factor XIa Activity on the Platelet Surface**. *Blood* 1986, **68**:225–230.

[207] Hemker HC, Giesen P: **The calibrated automated thrombogram (CAT): a universal routine test for hyper- and hypocoagulability.** *Pathophysiol Haemost Thromb* 2002, **32**(5-6):249–53.

[208] Tanaka KA, Szlam F, Rusconi CP, Levy JH: **In-vitro evaluation of anti-factor IXa aptamer on thrombin generation, clotting time, and viscoelastometry.** *Thromb Haemost* 2009, **101**:827–833.

[209] Kanungo T, Mount DM, Netanyahu NS, Piatko CD, Silverman R, Wu AY: **An efficient k-means clustering algorithm: Analysis and implementation**. *IEEE Trans. Pattern. Anal. Mach. Intell.* 2002, **24**(881 - 892).

[210] Gruber A, Hanson SR: **Potential new targets for antithrombotic therapy**. *Current Pharmaceutical Design* 2003, **9**:2367–2374.

[211] Adams TE, Everse SJ, Mann KG: **Predicting the pharmacology of thrombin inhibitors**. *J. Thromb. Haemost.* 2003, **1**:1024–1027.

[212] Gailani D, Renné T: **The intrinsic pathway of coagulation: a target for treating thromboembolic disease?** *J. Thromb. Haemost.* 2007, **5**:1106–1112.

[213] Bolton-Maggs PHB: **The management of factor XI deficiency**. *Haemophilia* 1998, **4**:683–688.

[214] Meijers JCM, Tekelenburg WLH, Bouma BN, Bertina RM, Rosendaal FR: **High levels of coagulation factor XI as a risk factor for venous thrombosis**. *N. Engl. J. Med.* 2000, **342**(10):696–701.

[215] Yang DT, Flanders MM, Kim H, Rodgers GM: **Elevated factor XI activity levels are associated with an increased odds ratio for cerebrovascular events**. *Am. J. Clin. Pathol.* 2006, **126**:411–415.

[216] Allen GA, Wolberg AS, Oliver JA, Hoffman M, Roberts HR, Monroe DM: **Impact of Procoagulant Concentration of Rate, Peak and Total Thrombin Generation in a Model System**. *J. Thromb. Haemost.* 2004, **2**:402–413.

[217] HEMKER HC, Béguin S: **The love of artist for his model of thrombin generation**. *J. Thromb. Haemost.* 2004, **2**:400–401.

[218] Wolberg AS: **Thrombin generation and fibrin clot structure**. *Blood* 2007, **21**:131–142.

[219] Baird TR, Gailani D, Furie B, Furie BC: **Factor XI deficient mice have reduced platelet accumulation and fibrin deposition after laser injury**. *Blood* 2004, **104**:218.

[220] Renné T, Nieswandt B, Gailani D: **The intrinsic pathway of coagulation is essential for thrombus stability in mice**. *Blood Cells, Molecules and Diseases* 2006, **36**:148–151.

[221] Furie B, Furie BC: **Thrombus formation *in vivo***. *J. Clin. Invest.* 2005, **115**(12):3355–3362.

[222] Rosen ED, Gailani D, Castellino FJ, Keck WM: **FXI is essential for thrombus formation following FeCl3-induced injury of the carotid artery in the mouse**. *Thromb. Haemost.* 2002, **87**:774–776.

[223] Yamashita A, Nishihira K, Kitazawa T, Yoshihashi K, Soeda T, Esaki K, Imamura T, Hattori K, Asada Y: **Factor XI contributes to thrombus propagation on injured neointima of the rabbit iliac artery**. *J. Thromb. Haemost.* 2006, **4**:1496–1501.

[224] Gruber A, Hanson SR: **Factor XI-dependence of surface- and tissue factor-initiated thrombus propagation in primates**. *Blood* 2003, **102**:953–955.

[225] Wang X, Cheng Q, Xu L, Feuerstein GZ, Hsu MY, Smith PL, Seiffert DA, Schumacher WA, Ogletree ML, Gailani D: **Effects of factor IX or factor XI deficiency on ferric chloride-induced carotid artery occlusion in mice**. *J. Thromb. Haemost.* 2005, **3**:695–702.

[226] Lin J, Deng H, Jin J, Pandey P, Quinn J, Cantin S, Rynkiewicz MJ, Gorga JC, Bibbins F, Celatka CA, Nagafuji P, Bannister TD, Meyers HV, Babine RE, Hayward NJ, Weaver D, Benjamin H, Stassen F, Abdel-Meguid SS, Strickler JE: **Design, synthesis, and biological evaluation of peptidomimetic inhibitors of facter XIa as novel anticoagulants**. *J. Med. Chem.* 2006, **49**:7781–7791.

[227] Hathcock JJ: **Flow effects on coagulation and thrombosis**. *Arterioscler. Thromb. Vasc. Biol.* 2006, **26**:1729–1737.

[228] Italiano JE, Shivdasani RA: **Megakaryocytes and beyond: the birth of platelets**. *J. Thromb. Haemost.* 2003, **1**:1174 – 1182.

[229] Jin J, Daniel JL, Kunapuli SP: **Molecular Basis of ADP-induced Platelet Activation II: The P2Yi Receptor Mediates ADP-induced Intracellular Calcium Mobilzation and Shape Change in Platelets**. *J. Biol. Chem.* 1998, **273**:2030–2034.

[230] Schroer K: **Antiplatelet Drugs: A Comparative Review**. *Drugs* 1995, **50**:7–28.

[231] Bhatt DL, Topol EJ: **Scientific and Therapeutic Advances in Antiplatelet Therapy**. *Nature Rev. Drug Discovery* 2003, **2**:15–28.

[232] Eisenberg PR: **The role of thrombin in coronary artery thrombosis**. *Coronary Artery Desease* 1996, **7**:400–408.

[233] Yamamota J, Taka T, Nakajima S, Ueda M, Sugimoto E, Sasaki Y, Muraki T, Seki J, Watanabe S: **A shear-induced in vitro platelet function test can assess clinically relevant anti-thrombotic effects**. *Platelets* 1999, **10**:178–184.

[234] Ruef J, Bode C, Runge MS: **Effects of fluild shear stress on atherogenesis and hemostasis.** *Fibrinolysis and Proteolysis* 1997, **11**:159–164.

[235] Giddens DP, Zarins CK, Glagov S: **The role of fluid mechanics in the localization and detection of atherosclerosis**. *J. Biomech. Eng.* 1993, **115**:588–594.

[236] Nagel T, Resnick N, Dewey CF, Gimbrone MA: **Vascular endothelial cells respond to spatial gradients in fluid shear stress by enhanced activation of transcription factors**. *Arterioscler. Thromb. Vasc. Biol.* 1999, **19**:1825–1834.

[237] Chatzizisis YS, Jonas M, Coskun AU, Beigel R, Stone BV, Maynard C, Gerrity RG, Daley W, Rogers C, Edelman ER, Feldman CL, Stone PH: **Prediction of the localization of high-risk coronary atherosclerotic plaques on the basis of low endothelial shear stress: An intravascular ultrasound and histopathology natural history study.** *Circulation* 2008, **117**:993–1002.

[238] Caro CG: **Discovery of the role of wall shear in atherosclerosis.** *Arterioscler. Thromb. Vasc. Biol.* 2009, **29**:158–161.

[239] Yamamota J, Kovacs IB: **Shear-induced in-vitro hasmostasis/thrombosis tests: The benifit of using native blood**. *Blood Coagulation and Fibrinolysis* 2003, **14**:697–702.

[240] Chow TW, Hellums JD, Moake JL, Kroll MH: **Shear stress-indced van Willebrand factor binding to platelet glycoprotein Ib initiates calcium influx associated with aggregation.** *Blood* 1992, **80**:113–120.

[241] Alevriadou BR, Moake JL, Turner NA, Ruggeri ZM, Folie BJ, Philips MD, Schreiber AB, Hrinda ME, Mclntire LV: **Real-time analysis of shear-dependent thrombus formation and its blockade by inhibitors of von Willebrand factor binding to platelets.** *Blood* 1993, **81**(5):1263–1276.

[242] Schulz-Heik K, Ramachandran J, Bluestein D, Jesty J: **The extent of platelet activation under shear depends on platelet count: Differential expression of of anionic phoppholipid and factor Va**. *Pathophysiol. Haemost. Thromb.* 2005, **34**:255–262.

[243] Fallon AM, Marzec UM, Hanson SR, Yoganathan AP: **Thrombin formation in vitro in response to shear-induced activation of platelets.** *Thromb. Res.* 2007, **121**:397–406.

[244] Brown CH, Leverett LB, Lewis CW, Alfrey CP, Hellums JD: **Morphological, biochemical and functional changes in human platelets subjected to shear stress**. *J. Lab. Clin. Med.* 1975, **86**:462–471.

[245] Ramstack JM, Zuckerman L, Mockros LF: **Shear-induced activation of platelets**. *J. Biomechanics* 1978, **12**:113–125.

[246] Anderson GH, Hellums JD, Moake J, Alfrey GP: **Platelet response to shearstress: changes in serotonin uptake, serotonin release, and ADP induced aggregation**. *Thromb. Res.* 1978, **13**:1039–1047.

[247] O'Brien JR: **Shear-induced platelet aggregation**. *The Lancet* 1990, **335**:711–712.

[248] Konstantopoulos K, Wu KK, Udden MM, Banez EI, Shattil SJ, Hellums JD: **Flow cytometric studies of platelet responses to shear stress in whole blood**. *Biorheology* 1995, **32**:73–93.

[249] Kroll MH, Hellums JD, Mclntire LV, Schafer AI, Moake JL: **Platelets and shear stress**. *Blood* 1996, **88**:1525–1541.

[250] Hellums JD, Petersion DM, Stathopoulos NA, Moake JL, Giorgio TD: **Studies on the mechanisms of shear-induced platelet activaion**. In *Cerebral Ischemia and Hemorheology*. Edited by Hartmann A, Kuschinsky W, Springer-Verlag Berlin Heidelberg 1987:80–89.

[251] Boreda R, Fatemi RS, Rittgers SE: **Potential for platelet stimulation in critically stenosed carotic and coronary arteries**. *J. Vascular Invest.* 1995, **1**:26–37.

[252] Jesty J, Yin W, Perrotta P, Bluestein D: **Platelet activation in a circulating flow loop: combined effects of shear stress and exposure time**. *Platelets* 2003, **14**:143–149.

[253] Raz S, Einav S, Alemu Y, Bluestein D: **DPIV prediction of flow induced platelet activation-Comparison to numerical prediction**. *Ann. Biomed. Eng*. 2007, **35**(4):493–504.

[254] Kastrup CJ, Runyon MT, Shen F, Ismagilov RF: **Modular chemical mechanism predicts spatiotemporal dynamics of initiation in the complex network of hemostasis**. *PNAS* 2006, **103**(43):15747–15752.

[255] Kastrup CJ, Shen F, Ismagilov RF: **Response to shape emerges in a complex biochemical network and its simple chemical analogue**. *Angew. Chem. Int. Ed.* 2007, **46**:3660–3662.

[256] Shen F, Kastrup CJ, Liu Y, Ismagilov RF: **Threshold response of initiation of blood coagulation by tissue factor in patterned microfluidic capillaries is controled by shear rate.** *Arterioscler. Thromb. Vasc. Biol.* 2008, **28**:2035–2041.

[257] Scheefers-Borchel U, Muller-Berghaus G, Fuhge P, Eberle R, Heimburger N: **Discrimination between fibrin and fibrinogen by a monoclonal antibody against a synthetic peptide**. *Proc. Natl. Acad. Sci. USA* 1985, **82**:7091–7095.

[258] Mutch NJ, Moore NR, Wang E, Booth NA: **Thrombus lysis by uPA, scuPA and tPA is regulated by plasma TAFI**. *J. Thromb. Haemost.* 2003, **1**:2000–2007.

[259] Lerche D, Vlastos G, Koch B, Pohl M, Affeld K: **Viscoelastic behaviour of human blood and polyacrylamide model fluids for heart valve testing**. *J. Phys. III France* 1993, **3**:1283–1289.

[260] Jesty J, Beltrami E: **Positive feedbacks of coagulation: their role in threshold regulation**. *Arterioscler. Thromb. Vasc. Biol.* 2005, **25**:2463–2469.

[261] Okorie UM, Denney WS, Chatterjee MS, Neeves KB, Diamond SL: **Determination of surface tissue factor thresholds that trigger coagulation at venous and araterial shear rates: amplification of 100 fM circulating tissue factor requires flow.** *Blood* 2008, **111**:3507–3513.

[262] Billy D, Willems GM, Cahalan PT, Lindhout T: **Prothrombin activation by prothrombinase in a tubular flow reactor**. *J. Biol. Chem.* 1995, **270**(3):1029–1034.

[263] Blezer R, Willems GM, Cahalan PT, Lindhout T: **Initiation and propagation of blood coagulation at artificial surfaces studied in a capillary flow reactor**. *Thromb. Haemost.* 1998, **79**(2):296–301.

[264] Fogelson AL, Tania N: **Coagulation under flow: The influence of flow-mediated transport on the initiation and inhibition of coagulation**. *Pathophysiol. Haemost. Thromb.* 2005, **34**:91–108.

[265] Runyon MK, Johnson-Kerner BL, Kastrup CJ, Van Ha TG, Ismagilov RF: **Propagation of blood clotting in the complex biochemical network of hemostasis is described by a simple mechanism**. *J. Am. Chem. Soc.* 2007, **129**:7014–7015.

[266] Murray CD: **The physiological principle of minimum work I. The vascular system and the cost of blood volume.** *Proc. Natl. Acad. Sci. USA* 1926, **12**:207–214.

[267] Goto S, Sakai H, Goto M, Ono M, Ikeda Y, Handa S, Ruggeri ZM: **Enhanced shear-induced platelet aggregation in acute mycardial infarction.** *Circulation* 1999, **99**:608–613.

[268] Krasotkina YV, Sinauridze EI, Ataullakhanov FI: **Spatiotemporal dynamics of fibrin formation and spreading of active thrombin entering non-recalcified plasma by diffusion**. *Biochim Biophys Acta* 2000, **1474**:337–345.

[269] Frojmovic MM, Longmire K, van de Ven T: **Long-range interactions in mammalian platelet aggregation II: The role of platelet pseudopod number and length**. *Biophys. J.* 1990, **58**:309–318.

[270] Singer MA, Pope SB: **Exploiting ISAT to solve the reaction-diffusion equation**. *Combust. Theory Modelling* 2004, **8**:361–383.

[271] Hamdi S, Schiesser WE, Griffiths GW: **Method of lines**. *Scholarpedia* 2007, **2**(7):2859.

[272] Dellas C, Loskutoff DJ: **Historical analysis of PAI-1 from its discovery to its potential role in cell motility and disease**. *Thromb. Haemost.* 2005, **93**:631–640.

[273] Rijken DC, Hoegee-De Nobel E, Jie AFH, Atsma DE, Schalij MJ, Nieuwenhuizen W: **Development of a new test for the global fibrinolytic capacity in whole blood**. *J. Thromb. Haemost.* 2008, **6**:151–157.

[274] Bjorquist P, Brohlin M, Ehnebom J, Ericsson M, Kristiansen C, Pohl G, Deinum J: **Plasminogen activator inhibitor type-i interascs exclusively with the proteinase domain of tissue plasminogen activator**. *Biochimica et Biophysica Acta (BBA) - Protein Structure and Molecular Enzymology* 1994, **1209**(2):191–202.

[275] Thelwell C, Longstaff C: **The regulation by fibrinogen and fibrin of tissue plasminogen activator kinetics and inhibition by plasminogen activator inhibitor 1**. *J. Thromb. Haemost.* 2007, **5**:804–811.

[276] Ranby M: **Studies on the kinetics of plasminogen activation by tissure plasminogen activator**. *Biochimica et Biophysica Acta (BBA) - Protein Structure and Molecular Enzymology* 1982, **704**(3):461–469.

[277] Madison EL, Coombs GS, Corey DR: **Substrate specificity of tissure type plasminogen activator**. *J. Biol. Chem.* 1995, **270**(13):7558–7562.

[278] Ellis V, Behrendt N, Dano K: **Plasminogen activation by receptor-bound urokinase**. *J. Biol. Chem.* 1991, **266**(19):12752–12758.

[279] Wiman B, Collen D: **On the kinetics of the reaction between human antiplasmin and plasmin**. *Eur. J. Biochem.* 1978, **84**:573–578.

[280] Christensen U, Bangert K, Thorsen S: **Reaction of human a2-antiplasmin and plasmin stopped-flow fluorescence kinetics**. *Biochem. J.* 1995, **305**:97–102.

[281] Ries M, Easton RL, Longstaff C, Zenker M, Morris HR, Dell A, Gaffney PJ: **Differences between neonates and adults in carbohydrate sequences and reaction kinetics of plasmin and a2-antiplasmin**. *Thromb. Res.* 2002, **15**:247–256.

[282] Ries M, Zenker M: **Influence of soluble fibrin on reaction kinetics of plasmin type 1 and type 2 with a2-antiplasmin**. *Blood Coagulation and Fibrinolysis* 2003, **14**:203–209.

[283] Kolev K, Lerant I, Tenekejiev K, Machovich R: **Regulation of fibrinolytic activity of neutrophil leukocyte elastase, plasmin, and miniplasmin by plasma protease inhibitors**. *J. Biol. Chem.* 1994, **269**(25):17030–17034.

[284] Hall SW, Humphries JE, Gonias SL: **Inhibition of cell surface receptor-**

bound plasmin by a2-antiplasmin and a2-macroglobulin. *J. Biol. Chem.* 1991, **266**(19):12329–12336.

[285] De Boer JP, Creasey AA, Chang A, Abbink JJ, Roem D, Eerenberg AJM, Hack CE, Taylor FB: **Alpha-2-macroglobulin fuctions as an inhibitor of fibrinolytic, clotting, and neutrophilic proteinases in sepsis: Studies using a baboon model**. *Infection and Immunity* 1993, **61**(12):5035–5043.

[286] Schneider M, Nesheim M: **A study of the protection of plasmin from antiplasmin inhibition within an intact fibrin clot during the course of clot lysis**. *J. Biol. Chem.* 2004, **279**(14):13333–13339.

[287] Schneider M, Brufatto N, Neill E, Nesheim M: **Activated thrombin-activatable fibrinolysis inhibitor reduces the ability of high molecular weight fibrin degradation procuctions to protect plasmin from antiplasmin**. *J. Biol. Chem.* 2004, **279**(14):13340–13345.

[288] Boffa MB, Wang W, Bajzar L, Nesheim ME: **Plasma and recombinant TAFI and activated TAFI compared with respect to Glycosylation, thrombin/thrombomodulin-depent activation**. *J. Biol. Chem.* 1998, **273**(4):2121–2135.

[289] Ansani NT: **Fondaparinux: The first pentasaccharide anticoagulant**. *PT* 2002, **27**(6):310–315.

[290] Parry MA, Maraganore JM, Stone SR: **Kinetic mechamism for the interaction of Hirulog with thrombin**. *Biochemistry* 1994, **33**:14807–14814.

[291] Elg M, Gustafsson D, Deinum J: **The importance of enzyme inhibition kinetics for the effect of thrombin inhibitors in a rat model of arterial thrombosis**. *Thromb. Haemost.* 1997, **78**:1286–1292.

[292] Tanaka KA, Szlam F, Vinten-Johansen J, Cardin AD, Levy JH: **Effects of antithrombin and heparin cofactor II levels on anticoagulation wiht Intimatan**. *Thromb. Haemost.* 2005, **94**:1–6.

[293] Lawson JH, Butenas S, Ribarik N, Mann KG: **Complex-dependent inhibition of factor VIIa by antithrombin III and heparin**. *J. Biol. Chem.* 1993, **268**(2):767–770.

[294] Espana F, Berrettini M, Griffin JH: **Purification and characterization of plasma protein C inhibitor**. *Thromb. Res.* 1989, **55**:369–384.